NOVA SCHOOL OF SCIENCE & TECHNOLOGY

DEPARTMENT OF CHEMISTRY

SOFIA ALEXANDRA DE ALBUQUERQUE MARTINS

BSc in Cell and Molecular Biology

HIV-BASED VIRUS-LIKE PARTICLES: THE NEXT STEP IN TARGETED THERAPY

MASTER IN BIOTECHNOLOGY

NOVA University Lisbon

November, 2022

NOVA SCHOOL OF SCIENCE & TECHNOLOGY

DEPARTMENT OF CHEMISTRY

HIV-BASED VIRUS-LIKE PARTICLES: THE NEXT STEP IN TARGETED THERAPY

SOFIA ALEXANDRA DE ALBUQUERQUE MARTINS

BSc in Cell and Molecular Biology

Supervisor: Doctor Rita Lourenço Paiva de Melo
Researcher, Center for Nuclear Sciences and Technologies, Instituto Superior Técnico, University of Lisbon

Co-Supervisor: Doctor João Domingos Galamba Correia
Principal Researcher, DECN, Instituto Superior Técnico, University of Lisbon

Examination Committee:

Chair: Doctor Ana Rita Cruz Duarte,
Associate Professor, NOVA School of Science and Technology

Rapporteur: Doctor Frederico Aires da Silva,
Assistant Professor, Faculty of Veterinary Medicine, University of Lisbon

Supervisor: Doctor Rita Lourenço Paiva de Melo,
Researcher, Center for Nuclear Sciences and Technologies, Instituto Superior Técnico, University of Lisbon

MASTER IN BIOTECHNOLOGY

NOVA University Lisbon
November, 2022

HIV-Based Virus-Like Particles: The Next Step in Targeted Therapy

To everyone who has been a part of this journey.

ACKNOWLEDGMENTS

This past year was very challenging but incredibly fulfilling, and I could not have done it without any of the people I will now mention:

First, I would like to express my deepest and most sincere gratitude to my supervisor, Dr. Rita Melo, for taking me in as a master student and for teaching me so much. I was able to grow a lot, both as a scientist and as a person. Everything I've learned will stay with me forever. Thank you for all the opportunities, support, and kindness. It was truly a pleasure to work with you.

I would also like to thank my co-supervisor, Dr. João Galamba Correia, for the opportunity to integrate the Radiopharmaceutical Sciences group and for all the help and advice provided for this project.

A very special thank you to Dr. Sandra Cabo Verde for allowing me to conduct the experiments at her laboratory, teaching me everything I needed to know to develop this project and advising me on how to proceed whenever things did not go according to plan.

To everyone that works at LETAL, in particular to Joana Madureira, Helena Marcos and Bárbara Pinheiro, thank you for all the help provided during this year.

To the Electron Microscopy Facility at Instituto Gulbenkian de Ciência (IGC), in particular to Dr. Erin Tranfield, Maria João Almeida, Sofia Pacheco, Ana Sousa, and Beatriz Tomaz, thank you for the TEM analyses, which were a very important contribution to this project.

To Miguel Cardoso and Dr. Vera Ferreira from the Molecular Microbiology and Biotechnology lab at iMed.ULisboa, thank you for all the assistance provided in the construction and bacterial transformation of our plasmid of interest.

I would also like to thank Dr. Filipa Mendes, Dr. Lurdes Gano, Elisabete Correia, Catarina Pinto, Rúben Silva, and Denise Rosário for all the assistance provided during this year, as well as all the other researchers from the Radiopharmaceutical Sciences group, for always being available to help.

I would also like to acknowledge the facilities of the Radiation, Elements and Isotopes group, the Radiopharmaceutical Sciences group, the Molecular Microbiology and Biotechnology lab at iMed.ULisboa and the Electron Microscopy Unit at IGC for all the provided materials and equipment.

To all the friends I made at the Radiopharmaceutical Sciences group. Each one of you deserves to be mentioned, as you were such a big part of my life in the past year. To Catarina Pinto, thank you for being the very first student to speak to me when I arrived at C^2TN. Thank you for your sweetness and kindness, and for all the help you gave me. This work would not have been possible without you. To my sweet Catarina Pedrosa, my office mate, thank you for getting me out of my comfort zone and for pushing me to talk to you. I gained a wonderful friend because of that. To Joana Santos, my social anxiety partner, thank you for being who you are and for understanding what it's like to be shy and socially anxious. And thank you for providing some of the funniest moments our group has experienced. To Miguel "Origamita", thank you for being our child, for always making us laugh, for all the origami you did for us instead of *cough, cough* writing, and for all the beers. To Afonso Belchior, aka "Tio mais bacano", thank you for being so random and laid-back. You became a legend at C^2TN. To Rúben Silva, thank you for all the help provided with the radiolabelling experiments and for all the jokes. To Rafael Travassos, thank you for taking an interest in VLPs, for helping me with my experiments during the final weeks, and for adapting to our group so effortlessly. To Joana Duarte, for worrying about us and always laughing with us, and for all the coffee. To Marco Sá, Margarida Sobral, Maria Beatriz, Kyle Gonçalves and Joana Santos, for spending time with us and participating in our jokes. And lastly, to João Franco-Machado. You were the biggest (and best) surprise of my stay at C^2TN, and I'm beyond grateful for having you in my life. Thank you for being by my side and for always encouraging me, even whilst dealing with problems of your own. You're my favourite person and I'm beyond proud of you and all your achievements.

To my wonderful friends. To Sofia Duarte, thank you for always listening to me and for all the words of support and encouragement, which were essential for the development of this thesis. And thank you for always making plans with me, no matter how busy your schedule is. To Silvia Almeida, for being my partner in trying new restaurants and for always being by my side, no matter what. To all my high school friends, Teresa Nobre, Sofia Falcão, Luisa Bastos, Pablo Sanz, and Enrique Martínez, thank you for all the lunches, dinners, and nights out that we had throughout the past year. I had so much fun with all of you and was able to forget about the thesis-related stress, at least for a while. To the friends I made at the Master's Program in Biotechnology, in particular to Sara Nascimento, Inês Cardoso, Ana Dias and Miguel Graça, thank you for all the help, for sharing your struggles with me and for always being ready to meet up for a drink. Lastly, to Alexandre Afonso, thank you for being my best and most dedicated friend. Your support and help were pivotal during this past year. Thank you for always being just a text or call away, and for always reassuring me that everything will be fine in the end. I'm so unbelievably proud of you and everything you have accomplished thus far.

Most importantly, I would like to thank my family, in particular my parents. If I am here today, it's because of you. Thank you for your patience, for always listening to my rants, for believing in me and for never allowing me to give up, even when that seems like the easiest route. This work is as yours as it is mine.

“It is our choices that show what we truly are, far more than our abilities.”

(J. K. Rowling, *Harry Potter and the Chamber of Secrets*)

LIST OF COMMUNICATIONS

Poster Presentations

Martins, S. A., Cabo Verde, S., Correia, J. D. G., & Melo, R. HIV-1-Based Virus-Like Particles: The Next Step in Targeted Therapy. *2nd Chem & Biochem Students Meeting*, 15th July 2022, Faculty of Sciences of the University of Lisbon.

Publications

Martins, S. A., Santos, J., Silva, R. D., Rosa, C., Cabo Verde, S., Correia, J. D. G., & Melo, R. (2022). How Promising Are HIV-1-Based Virus-Like Particles for Medical Applications? *Frontiers in Cellular and Infection Microbiology* 12, 1526. https://doi.org/10.3389/fcimb.2022.997875.

Martins, S. A., Santos, J., Cabo Verde, S., Correia, J. D. G., & Melo, R. (2022). Construction of HER2-Specific HIV-1-Based Virus-Like Particles. *Bioengineering*, *9*(11), 713. https://doi.org/10.3390/bioengineering9110713.

ABSTRACT

Nanomedicine has emerged in recent years as a field aimed at surpassing the shortcomings of standard medicine. Among the different types of nanoparticles (NPs), virus-like particles (VLPs) arise as promising nanostructures comprised of assembled viral proteins that take structural cues from viruses whilst lacking viral genetic material. Production of these platforms can be carried out in a myriad of expression systems, namely insect cells and mammalian cells. VLPs are characterized by being modifiable, biocompatible, capable of self-assembly, immunogenic, and able to cross cell membranes, and can therefore be harnessed as vaccines, delivery platforms and carriers of imaging molecules. Antibody fragments, such as single-chain variable fragments (scFv), have been widely studied as targeting moieties.

This thesis aimed to construct and characterize human immunodeficiency virus type 1 (HIV-1) VLPs that were modified with a scFv derived from trastuzumab, an antibody against the human epidermal growth factor receptor 2 (HER2), and thus provide a proof-of-concept approach for targeted delivery. HEK-293T, a mammalian cell line, was selected for VLP production through transient transfection. Characterization of the VLPs was performed by Western Blot and transmission electron microscopy. The constructed VLPs display the protein of interest and the described morphology. Next, cytotoxicity assays to ascertain the antiproliferative activity of the developed VLPs were conducted in two breast cancer cell lines, an HER2-overexpressing cell line (SK-BR-3) and a cell line that lacks HER2 overexpression (MDA-MB-231). The VLPs do not appear to be cytotoxic, which is an important feature for targeted delivery tools. Lastly, histidine-tagged VLPs were successfully radiolabelled with technetium-99m tricarbonyl and can be used for further *in vitro* and *in vivo* studies. Overall, this project set up a novel protocol for the production of a modified HIV-1-based VLP that can potentially be used as a targeted delivery platform for various targets in multiple diseases.

Keywords: Human Immunodeficiency Virus Type 1 (HIV-1)-Based Virus-Like-Particles, Human Epidermal Growth Factor Receptor 2 (HER2), Single-Chain Variable Fragment (scFv), Targeted Therapy

RESUMO

A nanomedicina surgiu recentemente como uma área que visa ultrapassar as lacunas apresentadas pela medicina tradicional. Entre os diferentes tipos de nanopartículas (NPs), as partículas semelhantes a vírus (VLPs) surgem como plataformas promissoras que se assemelham a vírus naturais, mas sem material genético. A produção destas estruturas pode ser feita em células de insetos e células de mamíferos, entre outras. As VLPs são modificáveis, biocompatíveis, imunogénicas, capazes de se auto-montarem e de atravessar membranas celulares, o que permite que possam ser exploradas como vacinas e sistemas de entrega de fármacos e/ou de agentes de imagem. Fragmentos de anticorpos, tais como os fragmentos variáveis de cadeia simples (scFv), têm sido amplamente explorados como forma de adquirir especificidade para um determinado alvo.

Este trabalho teve como objetivo a construção e caracterização de VLPs baseadas em vírus da imunodeficiência humana tipo 1 (VIH-1) que foram modificadas com um scFv contra o recetor do fator de crescimento epidérmico humano tipo 2 (HER2). Para tal, a linha celular HEK-293T foi escolhida para a produção de VLPs através de transfecção transitória. A caracterização das VLPs foi realizada através de Western Blot e microscopia eletrónica de transmissão. Os resultados revelaram que as VLPs expressam a proteína de interesse e apresentam a morfologia descrita. De seguida, ensaios de citotoxicidade foram realizados em duas linhas celulares, uma linha celular que sobreexpressa o HER2 (SK-BR-3) e outra que carece dessa sobreexpressão (MDA-MB-231), com o intuito de precisar o efeito citotóxico das VLPs. Estas não aparentam ser citotóxicas. Por último, as VLPs foram marcadas com tecnécio-99m tricarbonilo, e, por conseguinte, podem ser avaliadas em estudos *in vitro* e *in vivo*. De forma geral, este projeto estabeleceu um novo protocolo para a produção de uma VLP modificada que poderá eventualmente ser explorada como sistema de entrega para diferentes alvos em múltiplas patologias.

Palavras-Chave: Partículas Semelhantes a Vírus Baseadas no Vírus da Imunodeficiência Humana Tipo 1 (VIH-1), Recetor do Fator de Crescimento Epidérmico Humano Tipo 2 (HER2), Fragmento de Anticorpo de Cadeia Simples (scFv), Terapêutica Dirigida

TABLE OF CONTENTS

LIST OF FIGURES

LIST OF TABLES

LIST OF ABBREVIATIONS, ACRONYMS AND SYMBOLS

%	Percentage
°C	Degree Celsius
µCi	Microcurie
µg	Microgram
µL	Microliter
µM	Micromolar
ADC	Antibody-drug conjugate
AIDS	Acquired immunodeficiency syndrome
Akt	Protein kinase B
ANOVA	Analysis of variance
APC	Antigen-presenting cell
ATP	Adenosine triphosphate
bNAb	Broad neutralizing antibody
CA	Capsid
CAP	CEVEC'S Amniocyte Production
Cas9	Clustered regularly short palindromic repeats associated protein 9
CCR5	C-C motif chemokine receptor 5
CD4	Cluster of differentiation 4
CFPS	Cell-free protein synthesis
CRISPR	Clustered regularly short palindromic repeats

CT	Cytoplasmic tail
CTD	C-terminal domain
CXCR4	C-X-C motif chemokine receptor 4
DMEM	Dulbecco's Modified Eagle Medium
DNA	Deoxyribonucleic acid
ECD	Extracellular domain
ELISA	Enzyme-linked immunosorbent assay
Env	Envelope
ESCRT	Endosomal sorting complexes required for transport
et al.	Et alia
Fab	Fragment antigen-binding
FBS	Fetal bovine serum
Fc	Fragment crystallizable
FDA	Food and Drug Administration
g	G-force
Gag	Group-specific antigen
h	Hours
HA	Hemagglutinin
HEK-293	Human embryonic kidney 293
HER2	Human epidermal growth factor receptor 2
HIV	Human immunodeficiency virus
HPV	Human papillomavirus
HRP	Horseradish peroxidase
IgG	Immunoglobulin G
ITLC-SG	Instant thin layer chromatography by silica gel
kb	Kilobase
LB	Luria-Bertani
MA	Matrix
mAb	Monoclonal antibody

MAPK	Mitogen-activated protein kinase
MBq	Megabecquerel
mg	Milligram
MHC	Major histocompatibility complex
min	Minutes
mL	Millilitre
mM	Millimolar
MOI	Multiplicity of infection
MRI	Magnetic resonance imaging
mRNA	Messenger ribonucleic acid
NC	Nucleocapsid
nM	Nanomolar
nm	Nanometre
NP	Nanoparticle
NTD	N-terminal domain
PBS	Phosphate buffered saline
PBS-T	Phosphate buffered saline with Tween 20
PEG	Polyethylene glycol
PET	Positron emission tomography
pg	Picogram
PI3K	Phosphatidylinositol 3-kinase
PM	Precision medicine
pM	Picomolar
Pol	Polymerase
PR	Protease
PTM	Post-translational modification
RNA	Ribonucleic acid
rpm	Revolutions per minute
RT	Reverse transcriptase

RTK	Receptor tyrosine kinase
RRE	Rev-response element
SARS-CoV-2	Severe acute respiratory syndrome coronavirus 2
scFv	Single-chain fragment variable
SDS-PAGE	Sodium dodecyl sulphate polyacrylamide gel electrophoresis
siRNA	Small interfering ribonucleic acid
SPECT	Single photon emission computed tomography
SV40	Simian virus 40
T-DM1	Trastuzumab emtansine
TEM	Transmission electron microscopy
TSB	Tryptic soy broth
VLP	Virus-like particle
vs	Versus
WST-1	(4-[3-(4-iodophenyl)-2-(4-nitrophenyl)-2H-5-tetrazolio] -1,3-benzene disulfonate)

1

INTRODUCTION

1.1 Precision Medicine and Targeted Therapy

1.1.1 Precision Medicine

Global life expectancy has significantly increased over the past decades, largely due to advances in the medical field[1]. Notwithstanding, most medical treatments rely on a "one-size-fits-all" strategy, disregarding patient heterogeneity[2]. This prompted the development of precision medicine (PM), which was first introduced by Francis Collins in 1999, fuelled by the progress in the Human Genome Project[3]. PM is defined as an individualized approach based on the genetic, phenotypic, lifestyle and psychosocial features of each patient (Figure 1.1)[4]. The sequencing of the human genome, together with powerful characterizing tools such as genomics, proteomics and metabolomics, and computational methods, hastened the progress toward a novel era of tailored healthcare[5].

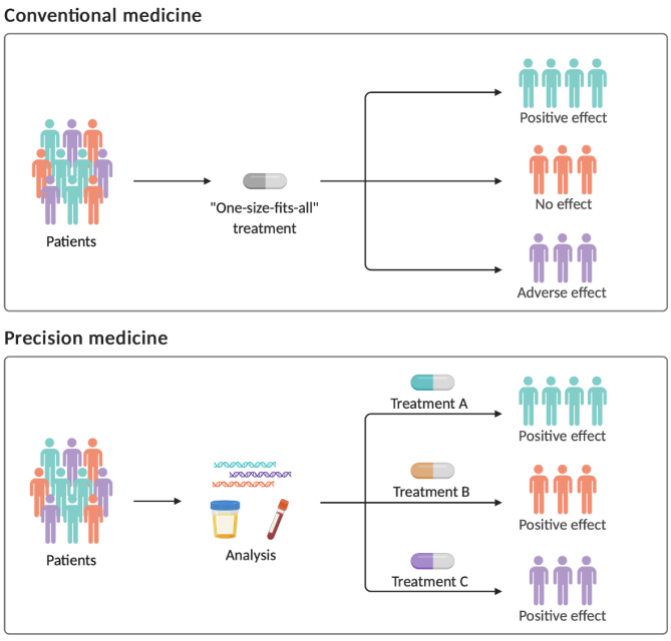

Figure 1.1 – **Conventional medicine vs precision medicine.** Conventional medicine is based on a "one-size-fits-all" strategy, whereas precision medicine relies on an individualized approach. Adapted from "Precision Cancer Medicine", by BioRender.com (2022). Retrieved from https://app.biorender.com/biorender-templates.

PM is often employed interchangeably with personalized medicine, albeit different[6]. Personalized medicine is centred on the individualization of a patient from diagnosis to treatment without resorting to population-based strategies, whereas PM relies on large data sets to categorize patients into subpopulations according to predisposition to certain disorders, prognosis, and response to treatment[2,6]. Individual genetic variability is strongly associated with disease causation, and the increasing accessibility to genomic information has given rise to novel therapeutic interventions[7,8]. Genetic therapies, for instance, have emerged as attractive alternatives for inherited disorders[8]. Programmable nucleases have also been harnessed for genome engineering, with the aim of correcting mutations responsible for various pathologies[8]. The genetic profile of each individual also plays a pivotal role in drug metabolism, influencing drug dosage and therapeutic effect[8]. Furthermore, the discovery of specific biomarkers has spurred the development of genetic tests and the approval of targeted therapies[8]. Therefore, some of the most promising applications for precision medicine include pharmacogenomics and genetic diseases such as cystic fibrosis and cancer[7,9,10].

1.1.2 Targeted Therapy

Cancer is established as one of the primary causes of death in every country in the world, with 19.3 million novel cases and 10 million cancer deaths reported in 2020[11]. The standard therapeutic modalities for cancer include surgery, radiotherapy and chemotherapy, the latter being the cornerstone treatment for most malignancies[12]. This therapeutic strategy uses cytotoxic drugs that hamper the proliferation and growth of cancer cells[12,13]. The lack of selectivity for tumour cells is one of the main hindrances of chemotherapy, resulting in off-target effects and systemic toxicity[12,13]. PM prompted a shift in anticancer therapy, from wide-spectrum cytotoxic drugs to targeted strategies[13]. Targeted therapy is designed to deliver agents to particular genes and proteins that partake in cancer growth, progression and migration[12,14]. This approach acts specifically on cancerous cells, reducing off-target effects and consequently displaying low toxicity and high efficacy[13]. Targeted therapies are typically aimed at different molecular targets, including overexpressed, anomalous and altered proteins, as well as genomic abnormalities[14-16]. The mechanisms of action of targeted drugs include the blockage of chemical signals involved in cell growth and division, the alteration of proteins, the interference in angiogenesis, the stimulation of the immune system and the transport of toxic agents to tumour cells[15,16].

1.2 Nanomedicine

The innate limitations of conventional therapeutic approaches have spurred the development of novel strategies[17]. There has been a growing interest in nanotechnology and its applicability in the clinical field[17]. Nanotechnology is depicted as the construction, assembly and characterization of platforms aimed at the nanoscale range (1-100 nm)[18,19]. Unlike their bulk counterparts, nanoparticles (NPs) are characterized by displaying an increased surface-to-volume proportion and high surface energy, together with adaptable magnetic, mechanical, electrical and biologic features, deeming them fitting for a myriad of applications, spanning from electronics to medicine[18-20]. The latter gave rise to a

novel field termed nanomedicine, which strives to circumvent the shortcomings of standard medicine, namely systemic toxicity, inadequate specificity and poor bioavailability[20]. Indeed, NPs can stimulate the transport of payloads across the cell membrane, heighten the solubility and stability of packaged drugs and extend circulation periods to increase effectiveness and safety[17]. Moreover, NPs can effectively bear and deliver therapeutic cargoes, imaging agents, or biological substances to specific targets, opening new avenues for more efficient theragnostic strategies[20]. This propelled both *in vitro* and *in vivo* studies, which originated auspicious results[17]. Nonetheless, the translational gap between animal tests and clinical trials and the biological barriers that hamper delivery have curtailed the implementation of nanoplatforms in the medical setting[17]. Further NP designs are thus required to attain more efficacious treatments[17].

NPs can be broadly assorted into three different classes: polymeric NPs, inorganic NPs and lipid-based NPs[17]. Polymeric NPs can be manufactured with natural or synthetic components, along with monomers and polymers, which permits the development of varied structures[17]. Their applicability as delivery vehicles derives from features such as biodegradability and biocompatibility[17]. Inorganic NPs are mostly based on gold, silica or iron, among others[17]. Their physical, optical, electrical and magnetic properties, together with the capacity to alter their size and architecture through engineering, make them adequate nanoplatforms for imaging, diagnostics and thermal therapy[17]. Lipid-based NPs are normally composed of at least one lipid bilayer enclosing at least one aqueous core and present properties such as self-assembly, biocompatibility, high bioavailability, simple production and ability to encapsulate large cargoes[17,19].

Despite the potential exhibited by NPs, they reveal several shortcomings[21,22]. Lipid-based NPs display instability, short drug retention following *in vivo* administration, and fusion with the membrane of off-target cells[21,22]. Polymeric NPs are unstable, structurally heterogeneous, potentially immunogenic and release their cargo in a slow and non-uniform manner[23,24]. Inorganic NPs, namely metal particles, can be highly toxic and nonspecific[25,26]. Furthermore, the majority of NPs undergo fast clearance mediated by phagocytic and dendritic cells[27]. This drawback can be surpassed by covering NPs with polyethylene glycol (PEG) polymers, but PEGylation can prompt immune reactions and reduce NP uptake by the target cells[27].

1.3 Virus-Like Particles

Virus-like particles (VLPs) emerge as a promising option among the several types of NPs[28-31]. VLPs are nanoplatforms composed of assembled viral proteins that take structural cues from viruses but lack viral genetic material, being therefore non-infectious[28-31]. These particles are typically manufactured with proteins from a single virus. Structural proteins from diverse viruses can also be employed for chimeric VLP assembly, and can acquire helical, spherical or icosahedral structures, depending on the type of virus from which they originate[28,31,32]. VLPs were originally detected in the sera of individuals with leukaemia, Down's syndrome and hepatitis[33]. Their character was unidentified, but

antigenic sites were observed at their surface[33]. It was later established that viral proteins can assemble and form VLP structures[28].

VLPs range from 20 to 200 nm in size and are characterized by being modifiable, easy to manufacture, capable of self-assembly, biocompatible, immunogenic and able to cross cell membranes releasing the desired cargo into the cytoplasm[28,30,34]. Furthermore, their production can be performed in a wide range of expression platforms, namely prokaryotic systems, yeast, insect cells, plant cells and mammalian cells[28,30]. Such features confer VLPs the suitability for a myriad of biomedical applications, namely vaccines and delivery vectors of therapeutic and imaging agents[28,29]. Notwithstanding, VLPs display several shortcomings that need to be taken into consideration[29]. VLPs may undergo phagocyte-mediated clearance and induce strong immune responses, which can hamper their use as therapeutic platforms[28,29]. These limitations can be tackled through alteration of the VLP surface with different functional ligands[29].

1.3.1 Classification of VLPs

VLPs can be categorized into different classes (Figure 1.2)[28,35]. Concerning the existence or lack of a lipidic envelope, these nanostructures can be categorised as enveloped or non-enveloped, respectively[28]. The lipid membrane of enveloped VLPs is acquired from the expression host during assembly and budding[28]. Enveloped VLPs are subclassified as single- or double-layered VLPs, regarding the inner structures placed beneath the lipid envelope[28]. Glycoproteins can be integrated into the lipidic membrane of these VLPs and stimulate the production of neutralizing antibodies[28,35]. Enveloped VLPs derive from viruses such as influenza, Ebola, and human immunodeficiency virus (HIV), among others[36-38]. These VLPs display a more complex structure and are more sensitive to the environment than non-enveloped VLPs, and therefore entail expression in eukaryotic hosts[36-38]. Contrarily, non-enveloped VLPs comprise single- or multiple-capsid proteins, and can be single-layered, double-layered and triple-layered[28,35]. Single-layered VLPs contain a single capsid protein and are structurally simple, which permits assembly in multiple expression platforms[39-41]. Human papillomavirus (HPV) VLPs and Norwalk VLPs are included in this group[39,40]. Multi-capsid protein VLPs, such as rotavirus VLPs, present a more complex structure and therefore require eukaryotic expression platforms[42].

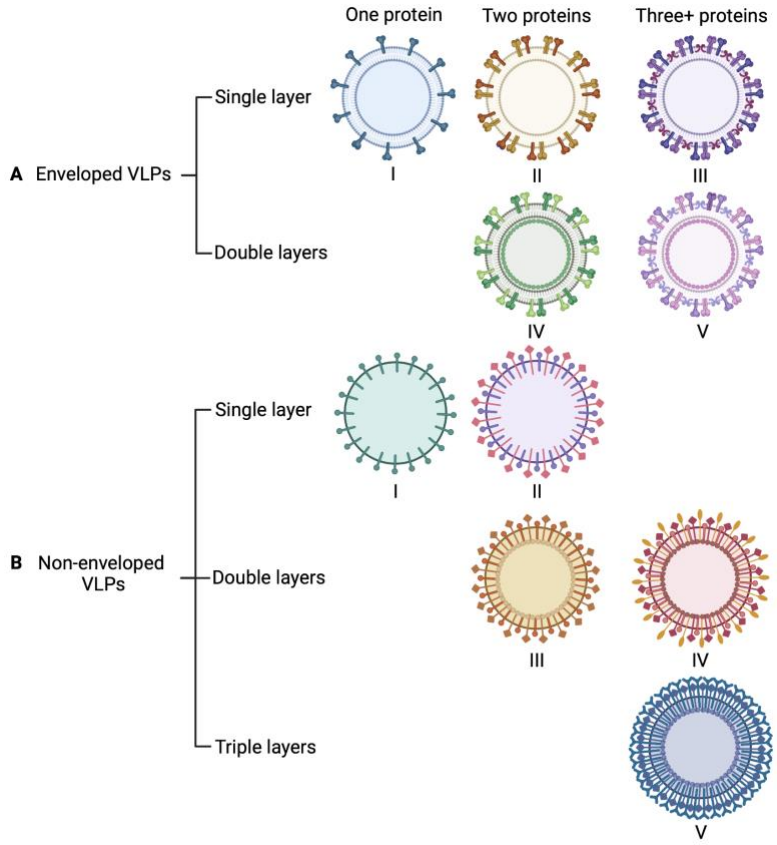

Figure 1.2 – Classification of VLPs. (**A**) Enveloped VLPs can be categorized into single-layered or double-layered VLPs. Expression of one (I), two (II), three or more (III) glycoproteins can form single-layered VLPs. Double-layered VLPs can display two (IV) or more (V) types of glycoproteins on their surface. (**B**) Non-enveloped VLPs can comprise single- or multiple-capsid proteins, and can be single-layered, double-layered, and triple-layered. VLPs with a single layer can be formed with one (I) or two (II) proteins. VLPs with double layers can assemble with two (III), three or more (IV) proteins. VLPs with triple layers are constructed with three or more (V) proteins. Adapted from *Nooraei, S. et al*.[28]**.** Created with BioRender.com.

1.3.2 VLP Production

The construction of VLPs entails cloning of the required structural genes, expression of the corresponding structural proteins in host systems, and purification to remove cellular debris[28,30]. The selection of an adequate expression host system is pivotal to achieve appropriate protein folding and post-translational modifications (PTMs)[28]. Expression platforms include prokaryotic (bacteria), eukaryotic (yeast, mammalian cells, insect cells and plant cells) and cell-free systems[28,30].

Recombinant proteins are typically produced in prokaryotic systems, and these platforms can also be harnessed for VLP assembly[28,30,43]. The incapacity to confer PTMs and to form complete disulphide bonds, together with protein solubility issues, impair their suitability for the production of enveloped VLPs[28,30,43]. Nonetheless, bacteria can be used for the assembly of simple non-enveloped VLPs[28,30,43]. The standard prokaryotic expression platform for VLP assembly is *Escherichia coli*, due to its swift cell growth, high protein expression yields, cost-effective production and simple scale-up[28,35,43].

Yeast host platforms, namely *Saccharomyces cerevisiae* and *Pichia pastoris*, have also been employed for VLP production as a consequence of their fast cell growth, high protein expression yields,

ability to provide certain PTMs like phosphorylation and glycosylation, low production cost and scalability[28,30,35,43,44]. Strikingly, yeast expression systems were utilized for the development of two Food and Drug Administration (FDA)-approved VLP vaccines, Gardasil® (HPV vaccine) and Engerix-B® (hepatitis B vaccine)[45,46]. In spite of the achieved success, the incapacity to bestow complex PTMs hinders the use of yeast expression systems for VLP production[28,43].

Insect cells, together with baculovirus-based vectors, are widely explored for the manufacture of both enveloped and non-enveloped VLPs, owing to rapid growth rates, high protein expression levels, ability to form multi-protein VLPs, capacity to provide complex PTMs akin to those conferred by mammalian cells, and easy scale-up [28,30,35,43]. Insect cell lines that stem from *Spodoptera frugiperda* and *Trichoplusia ni* are the most frequently used insect expression systems for VLP assembly[28,30]. Nevertheless, baculovirus-related contamination can thwart the relevance of these systems for VLP production[47].

Plant expression systems display high yields of recombinant protein expression, low maintenance cost, adequate machinery for PTMs and protein assembly and reduced risk of incorporation of extrinsic pathogens[28,43,48]. Accordingly, plant biomass production and upstream processing are simple and cost-effective[48]. Several VLPs have been successfully constructed in plant cells[49,50].

The gold standard for the synthesis of recombinant proteins in the pharmaceutical industry is the mammalian expression system[28,30,43]. Mammalian cells are the most proficient expression hosts due to their faculty to perform complex PTMs that are crucial for correct protein folding and their capacity to produce more elaborate VLPs[28,30,43]. Chinese hamster ovary, CAP-T (CEVEC'S Amniocyte Production expressing the large T antigen of simian virus 40 (SV40)), which originates from human amniocytes, human embryonic kidney 293 (HEK-293) and Vero 9 are the most utilized mammalian cell lines for VLP assembly[28]. However, these host systems display low production yields, prolonged expression times, elevated production costs, potential contamination from host cell debris and limited scalability, which can hinder their use for development of VLPs for medical purposes[28,43].

Lastly, cell-free protein synthesis systems (CFPS) arise as a further possibility for VLP production[28,30]. These platforms incorporate prokaryotic or yeast cells for the production of viral capsid proteins, and cell-free conditions for VLP assembly[28,30]. CFPS display several advantages over cell-based expression platforms, in particular high protein expression yields, cost-effective production and scarce contamination risks[28,51]. Shortcomings of this type of system include elevated production costs and restricted scalability[28].

Following expression, VLPs must undergo purification to assure safety and efficacy[28,30]. Typically, this process includes the following steps: (i) cell lysis for efficient VLP release; (ii) clarification to eliminate debris and aggregates; (iii) concentration; and (iv) enhancing to clear away residual contaminants[28,30]. Cell lysis is performed through mechanical treatment or treatment with detergent-containing solutions in expression systems that do not secret the VLPs into the culture supernatant[28,30]. Methods for clarification include depth filtration, cell sedimentation and microfiltration tangential flow

filtration[28]. Further VLP purification can be attained through ultracentrifugation or chromatographic processes[30]. In certain cases, disassembly and reassembly may be required to improve the functionality of the constructed VLPs[28,30].

Lastly, characterization is required to ascertain the stability and functionality of the purified VLPs[28]. The biochemical characterization of VLPs comprises the assessment of molecular mass, linear amino acid sequence, purity and isoelectric point, and can be carried out through mass spectrometry, liquid chromatography, reverse phase-high performance liquid chromatography and sodium dodecyl sulphate polyacrylamide gel electrophoresis (SDS-PAGE)[28,30]. Characteristics such as size and morphology can be determined through transmission electron microscopy (TEM), cryo-electron microscopy and atomic force microscopy[28]. The biological aspects of VLPs are related to the binding affinity of their functional epitopes to specific antibodies against the native virus from which they derive, and this can be analysed through enzyme-linked immunosorbent assays (ELISA) and surface plasmon resonance[28].

1.3.3 VLP Applications

Owing to their structural characteristics, VLPs can prompt strong immune reactions, be engineered to enclose various molecules, and be functionalized to present targeting motifs on the outer surface to achieve target specificity[28,29,51]. These properties enable VLPs to have numerous applications, namely vaccine development, drug delivery and imaging[28,29,31,34].

1.3.3.1 Vaccines

VLPs are capable of eliciting potent immune reactions due to their dense repetitive surface structure[32,43,52]. This highly organized structure forms a powerful pathogen-associated structural pattern that can be detected by immune cells and molecules[52]. Components of the innate humoral immune system interact with VLPs, which in turn are opsonized and taken up by antigen-presenting cells (APCs)[52]. Following uptake, processed VLPs are displayed on major histocompatibility complex (MHC) proteins and elicit immune cell activation[52]. After presentation through MHC II proteins and stimulation of T helper cells, VLP vaccines prompt strong antibody responses and are therefore typically aimed at B cells[32]. Notwithstanding, VLP peptides can be cross-presented on MHC class I proteins, which is attributable to the structure of VLPs and poses an advantage for VLP vaccine candidates[32]. Moreover, genetic modification and co-expression of proteins from diverse viruses can be employed to incorporate foreign epitopes into VLPs[53].

Several VLP-based vaccines are currently in use, such as vaccines against HPV infections (Gardasil® and Cervarix™), hepatitis B (Engerix-B® and Recombivax®), hepatitis E (Hecolin®) and malaria (Mosquirix™)[45,46,54,55]. VLP vaccines aimed at various infectious agents, including HIV, influenza virus and the most recent severe acute respiratory syndrome coronavirus 2 (SARS-CoV-2), are under development[56-58]. Furthermore, the ability to engineer VLPs can also be explored for the elaboration of

vaccines aimed at non-infectious diseases, namely cancer, neurodegenerative diseases, and autoimmune disorders[59-61].

1.3.3.2 Therapeutic Delivery

Besides their immunogenic properties, VLPs can be decorated with targeting moieties and enclose nucleic acids, proteins, peptides or other small molecules[28,31]. Surface modification can be achieved through covalent or noncovalent interactions[29,43,53]. Native or nonnatural amino acid residues present on the VLP surface can be harnessed for covalent attachment, although genetic fusion of the gene coding the ligand of interest to the gene for the VLP coat protein can also be carried out[29,43]. Noncovalent modifications rely on the use of linkers to attach ligands to the VLP surface[29,43]. Encapsulation can also occur via covalent or noncovalent approaches analogous to those employed for surface modification[29]. Moreover, the self-assembly process through which viruses encapsulate their genetic material can be exploited for packaging of other molecules[62]. VLPs can disassemble through changes in pH, buffer conditions, and ionic strength, and reassemble with the desired cargo through buffer exchange approaches[62].

Uptake of VLPs by cells takes place by receptor-mediated endocytosis[28,31]. VLPs are engulfed by the plasma membrane and then bud off as vesicles in the interior of the cells[28]. The vesicles then enter the cytosol and transit through the cytoskeleton to fuse with early endosomes[28,31]. The endosomal vesicles eventually dissociate from the early endosomes, develop into late endosomes and merge with pre-lysosomal vesicles to give rise to lysosomes[28,31]. The exogenous material is thus fragmented and released for cell use[28,31]. In spite of that, lysosomal degradation hampers proper drug delivery[28,31]. VLPs can bypass lysosomal degradation and discharge their cargo in response to variations in the biological environment, such as temperature, pH, osmotic pressure, oxidative stress, or other stimuli, and are therefore ideal for drug delivery[28,31,63]. Additionally, VLPs sometimes display a natural tropism to certain tissues, which can be tackled for drug delivery[28]. Lastly, VLPs can deliver molecules intracellularly to specific targets, enhance the bioavailability of certain drugs, curtail the required drug dose and boost treatment effects[28].

Several studies have explored VLPs as delivery vehicles[64-68]. VLPs can be engineered to display targeting moieties on their surface and explored for drug delivery to cancer cells, protein delivery, gene therapy, among other applications[64-68].

1.3.3.3 Imaging

Molecular imaging is a medical field focused on the comprehensive visualization and characterization of biological processes that occur at cellular and molecular levels[69]. Different imaging modalities can be employed for molecular imaging, including optical imaging and magnetic resonance imaging (MRI), as well as more sensitive techniques like single photon emission computed tomography (SPECT) and positron emission tomography (PET)[62,69]. Unlike synthetic NPs, VLPs are more valuable for molecular imaging given their short retention period and half-life, which can reduce potential side

effects[62]. VLPs can be tailored to bear imaging moieties of different nature through multiple approaches[62]. Such moieties can be incorporated by conjugation to the external layer or by encapsulation[62]. The latter approach allows the VLP to carry the imaging moieties within its hollow core, improving *in vivo* stability while leaving the outer surface free for further modification, namely with cell-targeting ligands[62].

In vivo fluorescent imaging was achieved through encapsulation of organic fluorophores in simian virus 40 (SV40) VLPs[70]. Magnetic NPs were enclosed in hepatitis B core protein VLPs for MRI[71]. Green-fluorescence VLPs were loaded with a chemotherapy drug, modified with a cell-penetrating peptide, and labelled with a PET tracer[72].

1.4 HIV-1-Based Virus-Like Particles

Among the variety of VLPs under development, HIV-1-based VLPs have emerged as pertinent nanostructures due to their simple self-assembly, which entails only one polyprotein, their stability, and their recognized applicability as vaccine candidates[73,74].

1.4.1 HIV Biology

HIV-1 is the most prevalent and pathogenic subtype of HIV, a primate-derived virus that affects the human immune system and thus provokes the acquired immunodeficiency syndrome (AIDS)[75]. HIV is categorized as an enveloped retrovirus with a small ribonucleic acid (RNA) genome of 9.7 kilobases (kb) comprised of nine functional genes[73,76]. The three main genes are *gag* (group-specific antigen), *pol* (polymerase) and *env* (envelope glycoprotein)[73,76]. The *gag* gene codes for Pr55Gag, a polyprotein precursor that is cleaved by the viral protease (PR), generating the proteins matrix (known as p17 or MA), capsid (p24 or CA), nucleocapsid (p7 or NC), and p6, together with two small spacer peptides, p2 and p1[73,76]. The *pol* gene originates Pr160GagPol, a polyprotein that is also cleaved by PR to originate three enzymes: PR, reverse transcriptase (RT) and integrase (IN)[73,76]. The *env* gene encodes gp120, a surface Env glycoprotein that facilitates HIV entry into the host cell through binding to the cluster of differentiation 4 (CD4) receptor and the C-C motif chemokine receptor 5 (CCR5) and C-X-C motif chemokine receptor 4 (CXCR4) and is therefore responsible for viral infection, and gp41, a transmembrane glycoprotein that intervenes in the fusion of the cell membrane and the viral envelope and therefore prompts viral core entry[73,76]. The HIV genome also includes genes that code for several regulatory proteins, such as Tat, which is required for transcription, and Rev, which participates in the transport of viral RNAs to the cytoplasm through binding to the Rev-response element (RRE)[76]. Further elements include the accessory proteins Vpu, Vif, Vpr and Nef (Figure 1.3)[73,76].

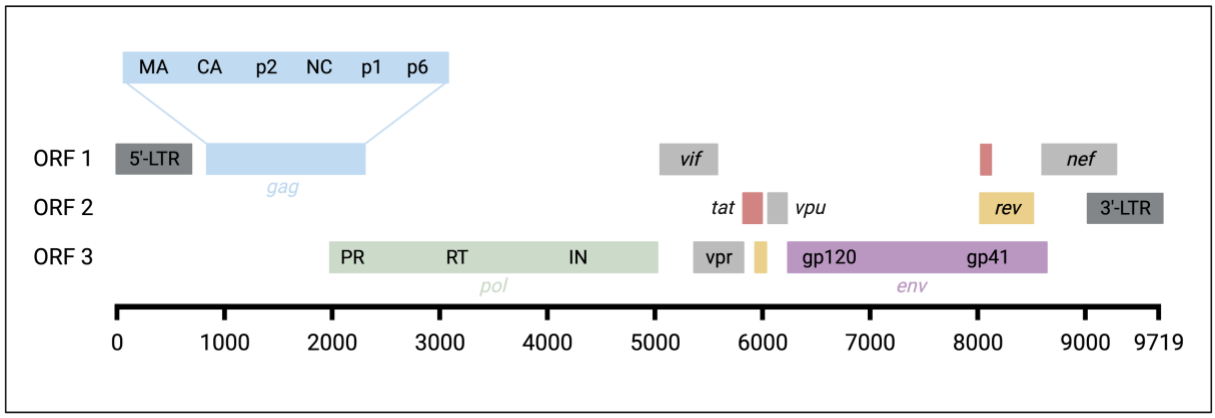

Figure 1.3 – HIV genome map. The HIV genome is composed of nine genes: three structural genes (*gag* in blue, *pol* in green, *env* in purple), two regulatory genes (*tat* in red, *rev* in yellow) and four accessory genes in grey (*vif*, *vpr*, *vpu*, *nef*). The *gag* gene encodes the Pr55Gag polyprotein precursor, which can be further processed into MA, CA, NC, p6 and the small spacer peptides p2 and p1. The *pol* gene originates the Pr160GagPol polyprotein that is further cleaved to give rise to PR, RT and IN enzymes. The *env* gene originates the surface glycoprotein gp120 and the transmembrane glycoprotein gp41. Adapted from *Cervera et al.*[73]. Created with BioRender.com.

HIV-1 mostly targets CD4+ T cells, and its replication leads to progressive CD4+ T cell loss, which culminates in immune abnormalities that make the host prone to several diseases[75]. HIV infection initiates with the interaction of the viral envelope proteins to the CD4 receptor and the CCR5 or CXCR4 co-receptors present at the target cell surface[73,75]. This interaction elicits the merging of the viral envelope with the target cell membrane and subsequent viral core entry[73,75]. The viral constituents transit to the cytoplasm and the viral genetic material undergoes reverse transcription into DNA and is incorporated into the host cell genome[73,75]. The cellular machinery is then hijacked for transcription of structural and regulatory genes required for assembly of more HIV-1 virions (Figure 1.4)[73,75].

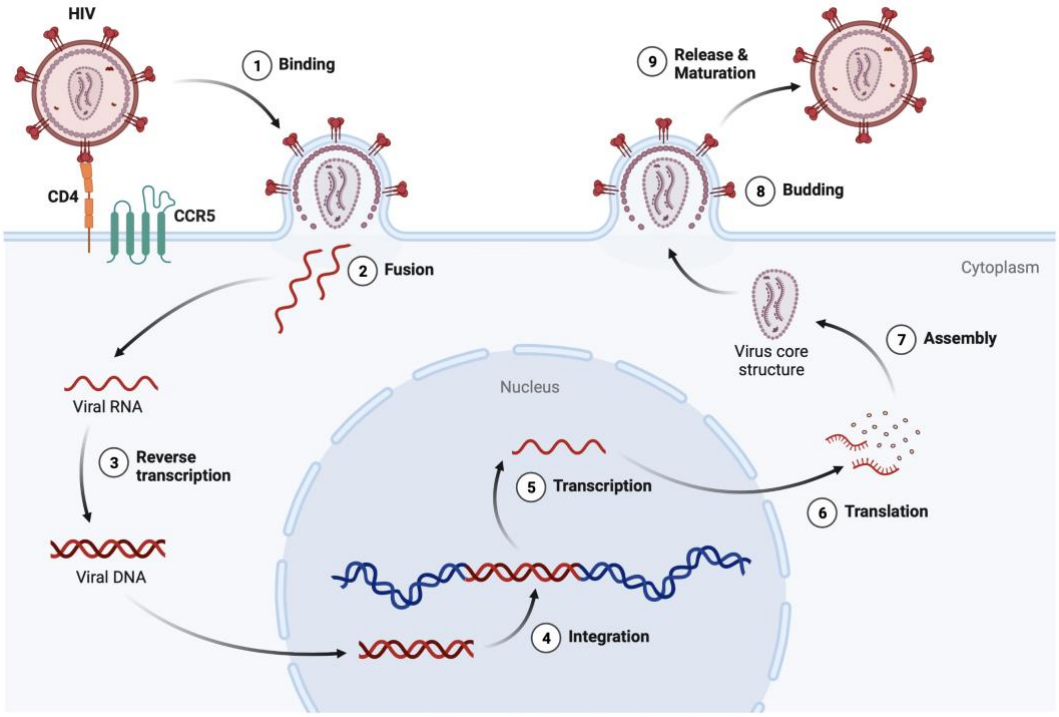

Figure 1.4 – Schematic illustration of the HIV replication cycle in CD4+ T cells. The HIV replication process initiates with the binding (1) of the surface envelope proteins to the CD4 receptor and CCR5 co-receptor. This contact elicits membrane fusion (2), genetic material release and consequent reverse transcription into DNA (3). The viral DNA is incorporated into the CD4+ T cell genome (4) and subsequently transcribed (5) and translated (6) into viral structural proteins. The viral core structure is then assembled (7), recruiting other proteins to bud from the CD4+ T cell (8), before maturing and becoming infectious (9)[73]. Adapted from "HIV Replication Cycle", by BioRender.com (2022). Retrieved from https://app.biorender.com/biorender-templates.

1.4.2 HIV-1-Based VLP Assembly and Budding

HIV-1-based VLPs vary from 100 to 200 nm in size and are typically composed of a core of Gag polyproteins circumscribed by a lipidic membrane derived from the host cell membrane[74,77,78]. There are two categories of HIV-1-based VLPs that can be constructed: HIV-1 Gag VLPs and HIV-1 Env-Gag VLPs (Figure 1.5)[47,74,79]. Expression of the *gag* gene in the host cell originates HIV-1 Gag VLPs (Figure 1.5 - A), whereas co-expression of *env* and *gag* generates HIV-1 Env-Gag VLPs (Figure 1.5 - B)[47,74,79].

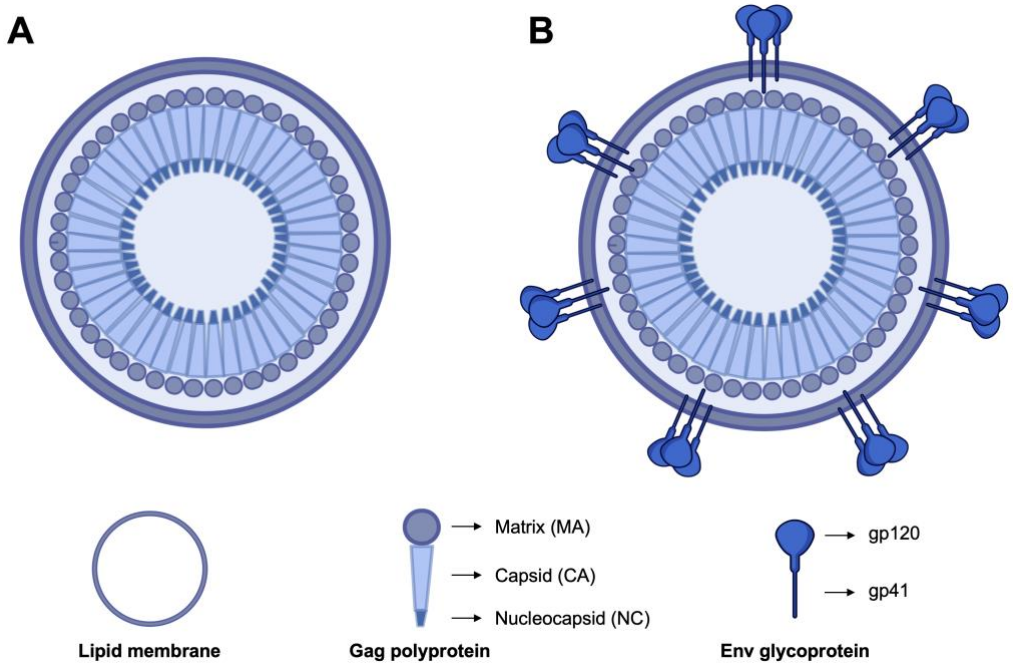

Figure 1.5 – Schematic depiction of HIV-1-based VLPs. (A) HIV-1 Gag VLP. (B) HIV-1 Env-Gag VLP. Created with BioRender.com.

HIV-1 VLP assembly can occur with just the Gag polyprotein, and no additional viral genetic material and factors[74,80]. Coordinated interactions between the diverse domains of the Gag polyprotein are necessary for this to occur[73,74]. The matrix (MA) domain is positioned at the amino-terminal section of Gag and includes an N-terminal glycine residue, which undergoes myristoylation and is therefore responsible for VLP formation and interaction of the Gag polyprotein precursor with the inner leaflet of the cell membrane[73,74,78]. Moreover, MA partakes in the incorporation of the Env glycoprotein at the VLP surface[74,78]. Capsid (CA) is located at the central section of Gag and is comprised of two domains: N-terminal domain (NTD) and C-terminal domain (CTD)[73,74]. NTD is involved in core formation, whereas

CTD partakes in particle assembly[73,74]. The small spacer peptide p2 links CA to NC and is key for maturation[73,74]. NC is involved in the encapsulation of the viral genetic material and p6 is necessary for VLP separation from the cell, integration of the accessory protein Vpr and particle size control[73,74].

The Gag polyproteins are produced in cytosolic ribosomes and then transit to the plasma membrane through the endosomal sorting complexes required for transport (ESCRT)[73,74,78]. Furthermore, this machinery coordinates the association and oligomerization of Gag monomers and succeeding budding and membrane scission[73,74,81]. In HIV-1 mature particles, Gag undergoes a maturation process based on proteolytic cleavage of its components following budding[74,77]. This originates the typical cone-shaped capsid that encloses the viral genome and leaves MA subunits underneath the inner leaflet of the membrane[74,77]. VLPs, on the other hand, comprise around 3000 unprocessed Gag monomers[77].

HIV Gag captures two copies of the viral RNA that harbour an HIV packaging signal termed the ψ-site[74,82]. Packaging of viral genetic material is hindered by mutations in this locus, but encapsulation of cellular RNA derived from the host cell remains unaffected[74,82]. Packaging occurs due to RNA binding to residues located at distinct Gag domains, specifically the NC domain, and alterations in these residues appear to thwart RNA packaging and particle assembly[74,82]. It has thus been described that RNA operates as a scaffold for particle assembly, with nucleotides ranging from 20 to 40 bases being capable of supporting VLP formation[74,82]. Gag molecules, when attached to RNA, bind to akin molecules, which prompts VLP assembly[74,82]. This suggests that oligomerization is pivotal in this process[74,82]. The assembly of HIV-1 Gag VLPs in different host systems may thus incite cellular RNA encapsulation, which is particularly unfavourable for therapeutic applications[83]. However, it has been reported that the replacement of NC domains with extrinsic sequences in Gag polyproteins permits VLP assembly with neglectable viral RNA encapsulation, which indicates that protein engineering could be explored to preclude host-derived RNA from being enclosed in VLPs[84].

Co-expression of *gag* and *env* in the host platform generates HIV-1 Env-Gag VLPs[79]. Translation of the Env glycoprotein occurs in the endoplasmic reticulum, with consequent migration through the Golgi complex to the plasma membrane[73,74].

The incorporation of Env glycoproteins into HIV-1-based VLPs can be explained through four different models[74,85]. A passive mechanism through which HIV-1 virions bud from the cell membrane and incorporate the Env glycoproteins that were placed at the assembly site comprises the first model[74,85]. The second model entails co-targeting of Gag and Env to lipid rafts in the cell membrane, which could heighten the packaging of Env glycoproteins[74,85]. The remaining models are related to direct or indirect protein-protein interactions[74,85]. The former proposes that integration of Env glycoproteins into the virions requires a direct interaction between MA and the cytoplasmic tail (CT) of gp41[74,85]. Conversely, the indirect interaction model is based on the existence of a cellular bridging co-factor that binds to Env and Gag[74,85]. The Rab11 family interacting protein 1c has been described as an Env incorporation co-factor[86].

1.4.3 HIV-1-Based VLP Production

Given that HIV-1-based VLPs are enveloped VLPs, eukaryotic platforms are the most adequate expression host systems[73]. HIV-1-based VLP assembly is achieved through transfection techniques and should be scalable, cost-effective and confer the adequate structure and immunogenicity[73]. Moreover, the selected expression platform determines the production yield and the glycosylation profile[74,87]. The latter is critical for the solubility, stability, efficacy and safety of biopharmaceutical compounds, and influences the downstream processing, as it defines the purification and separation approaches needed for elimination of inadequate glycoforms[74,87].

Yeasts can be employed as expression platforms given their simple scalability, high production yield and ability to confer PTMs[73]. Notwithstanding, the PTMs conferred by yeast are not identical to human-derived PTMs, which limits their applicability for HIV-1-based VLP production[73].

Insect cell lines are defined by their high productivity and easy scalability, and are therefore frequently used for vaccine production[73,74]. They can also perform several PTMs akin to those performed by mammalian cells[73,74]. Consequently, the baculovirus system and stable insect cell lines are widely used in the construction of HIV-1-based VLPs[73,74]. The main shortcoming of this host platform is the incorporation of glycans that differ considerably from human glycoforms, which affects the immunogenicity of the constructed VLPs[74,88]. The assembly of HIV-1-based VLPs in the insect cell-baculovirus system is influenced by several factors, including cell line, multiplicity of infection (MOI), cell density and time of infection[73,74].

Out of all the available expression systems, mammalian cells are the most commonly used platforms for the assembly of enveloped VLPs, given their ability to confer complex PTMs[73,74]. The HEK-293 cell line is the most prevalent mammalian platform due to its rapid growth and simple handling[73,74]. Furthermore, this cell line can confer modifications such as N-myristoylation, which partakes in the transport of Gag molecules to the plasma membrane for budding[74,89]. The main limitations of this system include the low production yields and the high probability of contamination, namely with extracellular vesicles[73,74,87]. Moreover, this cell line is mostly used in adherent cell culture at a reduced scale, which precludes the production of bigger yields[73,74]. The production yield can be further increased through methods such as extended gene expression and the inclusion of chemical additives[74,90]. Notwithstanding, the modifications and contaminants derived from this cell line can affect assembly and VLP function and must there be taken into consideration in downstream processing[74,87]. The CAP-T mammalian cell line is also utilized in the construction of HIV-1-based VLPs[74,91,92]. This cell line is characterized by rapid cell growth and ability to perform human PTMs, and can be cultured in suspension and in serum-free medium[74,91,92]. The main advantage of this cell line is its suitability for large-scale production[74,91,92]. Despite its potential, further tests are necessary to assess the capability of this cell line to accurately manufacture engineered HIV-1 based VLPs.

Lastly, plant cells can be explored for HIV-1-based VLP production, since they display easy scalability, are capable of performing human PTMs and are not likely to be affected by human infectious

agents[73]. Shortcomings of this host platform include time-consuming growth and low production levels[73]. Soybean, rice and tobacco plants could be used as host platforms for VLP assembly, and expression can occur in stable and transient expression systems[73].

1.4.4 HIV-1-Based VLP Applications

The major assets of HIV-1 VLPs when compared with other VLP types include their capacity to self-assemble with only one polyprotein, their enveloped nature, which can be harnessed for the presentation of membrane proteins, and their ability to present HIV-1 epitopes on the surface[37,74,93,94]. Additionally, as VLPs, they can prompt strong immune reactions, display targeting moieties on their surface and encapsulate molecules in their hollow core[31,74]. Albeit promising, these VLPs also display several limitations[37,74]. Expression of only the *gag* gene results in the formation of immature particles given the lack of PR, which cleaves the Gag polyprotein precursor and generates mature virions[74,76]. Without this enzyme, high levels of HIV-1 VLP production can be achieved with integration of Env glycoproteins into the viral envelope[74,95]. Notwithstanding, the immature virion structure precludes the clustering and lateral movement of the Env glycoproteins in the membrane, which can affect the immunogenicity of the VLPs[74,95]. Contrarily, HIV-1 VLPs that resemble mature particles may incorporate the viral genetic material and inactivation steps may be required, which hinders the production process[37,74]. In addition, contamination with host proteins, exosomes, microvesicles and RNA can occur[37,74,96]. Consequently, these limitations need to be considered when producing HIV-1-based VLPs and strategies to circumvent them need to be implemented. HIV-1-based VLP applications include vaccination and delivery[56,65,74].

1.4.4.1 Vaccines

HIV-1 VLPs can elicit strong cellular and humoral immune reactions as a consequence of their capability to integrate Env trimeric glycoproteins on their surface, which stimulates the production of broad neutralizing antibodies (bNAbs), and their structure, which prompts APC uptake and subsequent robust cellular response[73,74]. For these reasons, HIV-1-based VLPs can be exploited as vaccines.

One of the most burdensome infectious agents in the vaccination field is in fact HIV, due to the lack of effective prevention approaches for AIDS[97]. Antiretrovirals therapies have decreased HIV-associated mortality, but resistance and long-term side effects may arise[97]. Pre-exposure prophylaxis, on the other hand, is a preventive procedure, but is not accessible for most countries with high HIV prevalence, and can also provoke undesirable effects[97]. Several HIV vaccine candidates have been developed and evaluated in clinical trials, but without success[98]. This spurs the design of novel vaccine candidates that are capable of inducing bNAbs and cellular immune responses[97]. The first HIV-1-based VLP that was tested in clinical trials as an HIV vaccine candidate was the recombinant p24/p17 VLP[99,100]. This VLP was produced in *Saccharomyces cerevisiae* and its immunogenicity was assessed in healthy volunteers and HIV-1-infected individuals[99,100]. The obtained results revealed that this VLP is a safe vaccine candidate without significant side effects, although its immunogenicity was low[99,100]. A Pr55Gag

VLP was also assembled in a baculovirus expression platform and its immunogenicity was assessed in mice, stimulating a humoral immune response[101]. The incorporation of stimulatory molecules, namely CD40 ligand and glycoproteins, in HIV-1 Gag VLPs has also been tested[56,102,103].

HIV-1 VLPs have also been investigated as vaccines for other viruses besides HIV, such as dengue virus, West Nile virus, influenza virus, foot-and-mouth disease virus and the most recent SARS-CoV-2[94,104-106]. Furthermore, HIV-1-based VLPs can be modified to improve the immune defence against tumours and therefore function as anti-cancer vaccines[107].

1.4.4.2 Therapeutic Delivery

HIV-1-based VLPs are versatile nanostructures that can be modified to encapsulate and deliver a wide range of molecules of biologic or synthetic origin[62,74]. One study reported the fusion of *gag* to genes encoding green fluorescent protein, a natural transcription factor and a synthetic transcription factor[108]. Protein delivery was achieved in human cells, and protein engineering was used to modify their location within cells[108]. Genome editing enzymes, like clustered regularly interspaced short palindromic repeats (CRISPR) associated protein 9 (Cas9), can also be packaged into HIV-1-based VLPs[65,109,110].

Besides enclosing active molecules, VLPs can also be modified to display targeting moieties on their surface[31]. Since the viral structures that are harnessed for VLP production are well characterized, it is possible to select the most adequate sequences for genetic modification[31]. Protein fusion of targeting peptides or small proteins can be performed on the VLP surface[31]. Larger peptides may affect VLP assembly, and are therefore incorporated through direct conjugation[43]. Functionalization of HIV-1-based VLPs has been mostly performed in different vaccine candidates[94,103,106].

1.5 Human Epidermal Growth Factor Receptor 2 (HER2)

The human epidermal growth factor receptor 2 (HER2) is a 185 kilodalton (kDa) glycoprotein and member of the epidermal growth factor receptor (EGFR) family, a group of receptor tyrosine kinases (RTKs) that partake in the signalling pathways that regulate cell proliferation, differentiation and survival[111]. This family comprises four members: ErbB1/HER1, ErbB2/HER2, ErbB3/HER3 and ErbB4/HER4[111]. These receptors are composed of three domains: the extracellular cysteine-rich binding domain, the transmembrane domain and the intracellular tyrosine kinase domain[111]. They are present as monomers on the cell membrane but undergo dimerization following binding of the corresponding ligands, which in turn provokes transphosphorylation of their tyrosine kinase domains[111]. HER2 does not have any identified ligands and thus depends on homodimerization, when expressed in high levels, or heterodimerization with other family receptors for activation[111]. HER3 has impaired tyrosine kinase activity and thus requires heterodimerization for activation[112]. Upon dimerization, signalling pathways such as phosphatidylinositol 3-kinase-protein kinase B (PI3K/Akt) and mitogen-activated protein kinase

(MAPK) are triggered[111]. These pathways regulate cell growth, survival, differentiation, angiogenesis and migration[111].

Consequently, amplification of the *HER2* gene and/or overexpression of the corresponding protein dysregulate the downstream signalling pathways which, in turn, spurs cancer development (Figure 1.6)[111].

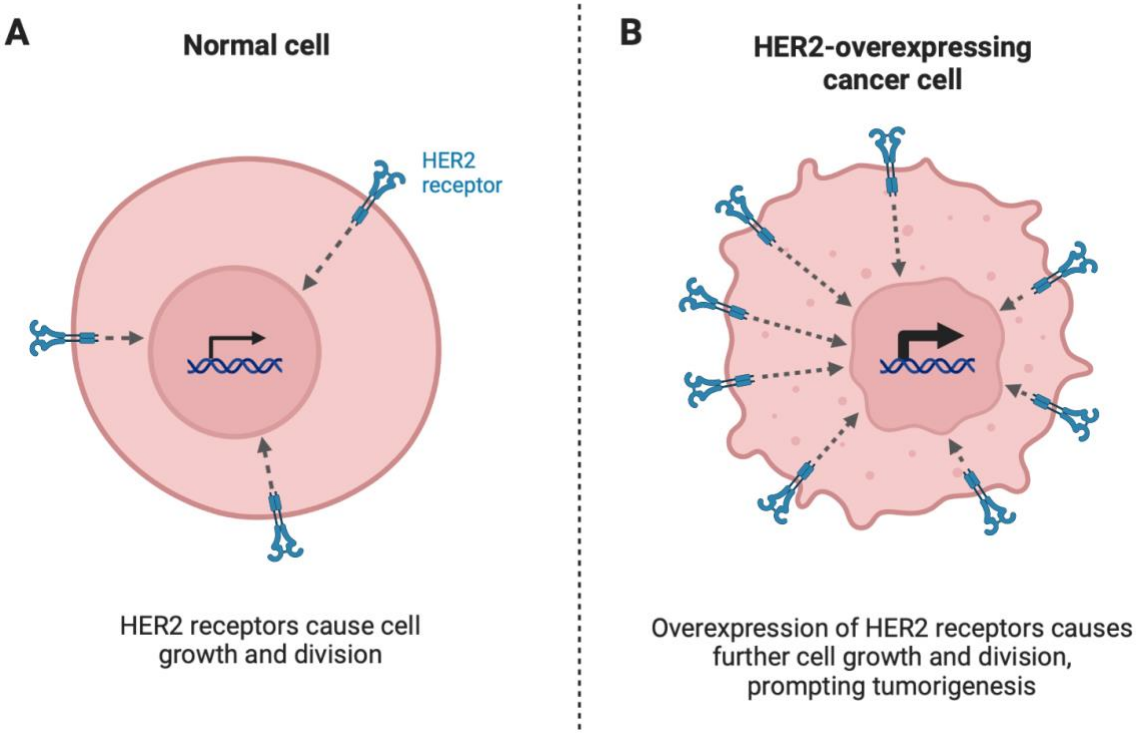

Figure 1.6 – HER2 in normal and cancer cells. (A) In normal cells, HER2 receptors are involved in cell growth and division. (B) Overexpression of HER2 receptors occurs when there is an amplification of the *HER2* gene, and this is involved in tumorigenesis. Adapted from "HER2+ Cancer Cell", by BioRender.com (2022). Retrieved from https://app.biorender.com/biorender-templates.

1.5.1 HER2-Associated Malignancies

HER2 overexpression has been described in breast, gastric, ovarian and endometrial cancers, among others (Table 1.1)[111].

Table 1.1 – HER2-overexpressing cancers and their characteristics.

Cancer	HER2-overexpressing cases	Characteristics	Therapeutic strategies
Breast cancer	20-25%	Short disease-free and overall survival. Aggressive breast cancer subtype with poor prognosis[111-113]. Associated with lymph node metastases and resistance to endocrine therapy[112,113].	The standard therapeutic strategies for this cancer include chemotherapy in combination with targeted therapy[113].
Gastric cancer	10-30%	Associated with an aggressive phenotype and poor outcome[111]. The correlation between HER2 status and gastric cancer prognosis is not yet established[114].	Targeted therapy, together with chemotherapy, is the cornerstone treatment for HER2-overexpressing gastric cancers[115].
Ovarian cancer	20-30%	HER2 overexpression is typically observed in more advanced stages and is concomitant with poor survival and resistance to chemotherapy[111].	HER2-targeted therapies have a limited effect on this type of malignancy given the low frequency of HER2 strong expression[111].
Endometrial cancer	17-30%	HER2 overexpression correlates with more advanced stages, lymph node involvement and worse survival outcomes[116].	HER2-directed therapy was shown to be inefficient in the treatment of HER2-overexpressing endometrial cancer, likely due to intrinsic or acquired resistance pathways[116].

1.5.2 Targeting HER2

The role of HER2 in tumorigenesis has prompted the development of several therapeutic modalities to hinder its signalling, including antibodies that block the extracellular domain, tyrosine kinase inhibitors and oligonucleotides that silence *HER2* expression (Figure 1.7)[112,117]. Moreover, HER2 can be explored as a target for drug delivery[117].

1.5.2.1 Antibodies

Trastuzumab is a humanized murine monoclonal antibody aimed at the subdomain IV of the extracellular domain (ECD) of HER2, which occurs in an open configuration and is therefore constitutively accessible for dimerization with other members of the EGFR family[112,117]. The possible mechanisms of action of trastuzumab include obstruction of ligand-independent HER2 dimerization, hindrance of HER2 ECD shedding, inhibition of downstream signalling pathways, induction of apoptosis, antibody-dependent cellular cytotoxicity and inhibition of angiogenesis[111,112]. This antibody is approved

as targeted therapy for HER2-overexpressing breast and gastric cancers in combination with cytotoxic agents[111,112].

Pertuzumab is a humanized recombinant monoclonal antibody that precludes HER2 dimerization with other HER receptors through binding to the subdomain II of the HER2 ECD[111,117]. Given that pertuzumab and trastuzumab bind to different ECD subdomains, they can be explored in combinational therapy, together with docetaxel, a chemotherapy agent[111,112,117]. This regimen has been approved for metastatic HER2-overexpressing breast cancer[111,112,117].

1.5.2.2 Tyrosine Kinase Inhibitors

The tyrosine kinase domain of HER2 can also be targeted for therapeutic purposes[112,117]. Small molecules, such as lapatinib, afatinib, neratinib and pyrotinib have been designed to impede the phosphorylation of the HER2 tyrosine kinase domain (Figure 1.7)[112,117].

Lapatinib is a dual reversible tyrosine kinase inhibitor, capable of targeting both EGFR and HER2 pathways[111,112]. It hampers signal transduction through competition with adenosine triphosphate (ATP) in the ATP-binding site of the EGFR and HER2 tyrosine kinase domains[117]. Since its mechanism of action differs from the one presented by trastuzumab, they can be used in combination for HER2-overexpressing malignancies[117]. Lapatinib also appears to be efficient in tumours that are resistant to trastuzumab[112,117]. It can also be used with capecitabine in metastatic settings[112]. Furthermore, lapatinib is capable of crossing the blood brain barrier and can thus prevent progression to the central nervous system[112,117].

Afatinib is an oral irreversible small molecule that targets EGFR, HER2 and HER4[111,112]. It has been mostly tested in trastuzumab-resistant metastatic breast cancer, and displayed partial response, indicating that further studies assessing its efficacy are required[111,112].

Neratinib is an oral irreversible tyrosine kinase inhibitor aimed at EGFR, HER2 and HER4[111,112]. This small molecule could be used synergistically with trastuzumab and has displayed inhibitory effects in trastuzumab-resistant malignancies[112].

Lastly, pyrotinib is an irreversible pan-HER receptor tyrosine kinase inhibitor, that binds to ATP-binding sites in the tyrosine kinase domains of EGFR, HER2 and HER4[112]. Several studies have reported that pyrotinib is efficient in individuals with HER2-overexpressing metastatic breast cancer when in combination with capecitabine[118,119].

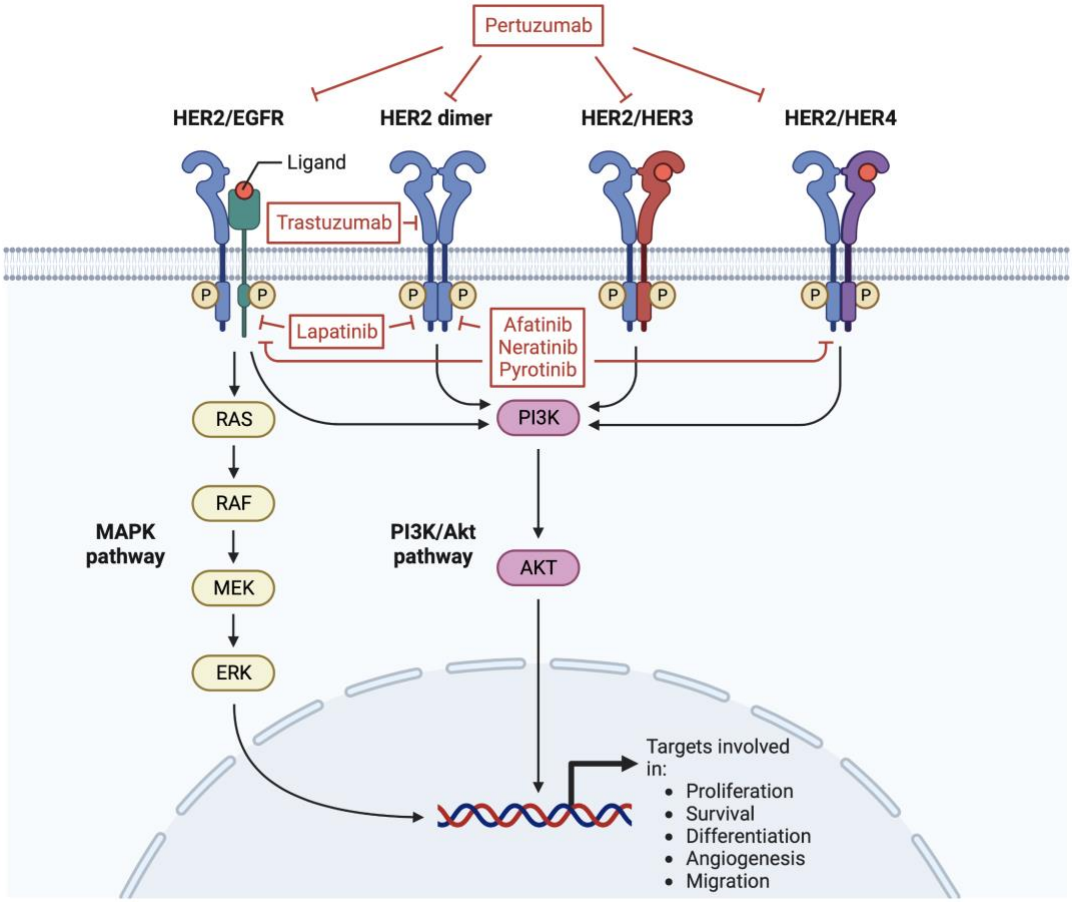

Figure 1.7 – Downstream signalling pathways of HER2 and HER2-targeted therapies. HER2 (blue) undergoes homodimerization, when expressed in high levels, or heterodimerization with other family receptors (EGFR, green; HER3, red; HER4, purple). This leads to transphosphorylation of the tyrosine kinase domains, which in turn activates the MAPK (depicted in yellow) and PI3K/Akt (depicted in pink) pathways. These pathways partake in cell proliferation, survival, differentiation, angiogenesis and migration[111]. HER2-targeted therapies include monoclonal antibodies (trastuzumab and pertuzumab) and tyrosine kinase inhibitors (lapatinib, afatinib, neratinib and pyrotinib). Trastuzumab hinders ligand-independent HER2 dimerization, whereas pertuzumab blocks HER2 homo- and heterodimerization with other HER receptors. Lapatinib targets EGFR and HER2, whereas afatinib, neratinib and pyrotinib are pan-HER family inhibitors, and target EGFR, HER2 and HER4[112]. Adapted from "HER2 Signaling Pathway", by BioRender.com (2022). Retrieved from https://app.biorender.com/biorender-templates.

1.5.2.3 Oligonucleotides

Silencing of *HER2* gene expression arises as another strategy to hamper HER2 signalling[117]. This can be achieved with antisense oligonucleotides and small interfering RNA (siRNA)[117]. Antisense oligonucleotides act through binding to the complementary messenger RNA (mRNA) sequence of *HER2*, which prompts its degradation[117]. These oligonucleotides can act in a dose-dependent manner and consequently hinder the proliferation of HER2-overexpressing tumour cells[117]. This strategy has been employed in combination with chemotherapy in HER2-overexpressing breast cancer cells, and has proven to be effective[117]. siRNA prompts *HER2* mRNA degradation through the RNA interference mechanism, in which the antisense strand of siRNA binds to the complementary mRNA sequence and elicits its degradation[117]. This strategy induces apoptosis and inhibits proliferation in HER2-overexpressing cancer cells[117].

1.5.2.4 Targeted Drug Delivery

The accessibility of the ECD of HER2 makes it a relevant target for drug delivery[117]. Antibody fragments, affibodies and peptides against HER2 have thus been designed for targeted drug delivery[117].

The most widely used systems for HER2 targeted drug delivery are antibody-conjugated nanoplatforms[117]. These structures can be engineered with anti-HER2 antibodies or its fragments (fragment antigen-binding (Fab) and single-chain fragment variable (scFv)), and can bear drugs or nucleic acids[117].

The immunoglobulin G (IgG) is the most explored antibody in the therapeutic setting[117,120]. It is a large protein of around 150 kDa that comprises two heavy chains and two light chains linked by disulphide bridges[117,120]. Antibody-drug conjugates (ADCs) have thus been developed to overcome the limitations of using an antibody as a single agent[117]. One example of ADC is the trastuzumab emtansine (T-DM1), which comprises trastuzumab linked to the cytotoxic agent DM1 (derived from maytansine)[117]. This ADC has revealed potent activity in trastuzumab-refractory HER2-overexpressing tumour cells[117]. Despite their successful application, ADCs also display several shortcomings, including the reduced reproducibility of the chemical conjugation given the various coupling sites present in a single antibody, and the increased propensity to aggregate[117].

Fab fragments have a molecular weight of around 50 kDa and comprise a light chain linked to a heavy chain by a disulphate bond[117,121]. Fab fragments retain the native antibody's ability to bind to its antigen with high specificity[121]. Furthermore, Fab fragments lack the fragment crystallizable (Fc) region, diminishing bystander activation of immune cells and facilitating production[121]. Notwithstanding, they display a reduced half-life, which prompts rapid degradation and consequently hinders their applicability[121]. This limitation can be overcome by fusion to PEG or albumin-binding domains[121]. Fab fragments have been employed for targeted delivery of nucleic acids[117].

scFv fragments are only composed of the variable domains linked by a flexible peptide and are therefore the smallest antibody fragments (27 kDa)[121]. The main advantages of scFv fragments include their small size, which permits large-scale production with high yields and enhanced tissue penetration, and their lack of an Fc domain, which decreases the risk of host's immune system activation[121]. Nevertheless, the lack of an Fc region also brings various disadvantages, namely a reduced half-life, low thermostability and a higher propensity for aggregation[121]. The half-life can be increased by PEGylation or fusion to albumin[121]. Anti-HER2 scFv fragments have been fused to molecules capable of inducing tumour cell death[117].

Affibody molecules are small fragments of 58 amino acids that derive from the IgG binding regions of staphylococcal protein A[117]. Their binding domain contains 13 amino acids that can be randomized for specific targeting[117]. Affibodies are characterized by their small molecular weight (6 kDa), which facilitates tissue penetration, availability of functional end groups for conjugation, and robust structure[117]. Disadvantages include rapid clearance and short half-life, which can be circumvented with fusion to the

albumin-binding domain[117]. Anti-HER2 affibodies have been explored as targeting moieties for NP-mediated drug delivery to HER2-overexpressing cancer cells[117].

Finally, peptides arise as relevant targeting moieties due to their small size (around 1 kDa), high tissue penetration, easy production and adaptable chemical conjugation[117]. Anti-HER2 peptides can be fused to cell-penetrating peptides, transcriptional factors or proapoptotic peptides to target HER2-overexpressing malignancies[117].

Table 1.2 – Properties of different anti-HER2 targeting moieties. The depicted half-life refers to blood of nude mice. Adapted from *Tai et al.*[117].

Properties	Antibody	Fab	scFv	Affibody	Peptide
Molecular Weight	150 kDa	50 kDa	27 kDa	5 kDa	1 kDa
Immunogenicity	Yes	No	No	No	No
Ligand affinity (Kd)	pM-nM	nM	nM	nM-μM	μM
Half-life	2-3 days	4 hours	30-60 minutes	10-60 minutes	5 minutes
Tissue Penetrability	Poor	Moderate	Moderate	Good	Excellent

1.6 Motivation and Aim

Precision medicine has emerged as a tailored form of healthcare, with cancer as one of its applications[9]. Cancer is classified as a leading cause of death worldwide, with 19.3 million novel cases and 10 million deaths reported in 2020 and with breast cancer as the most commonly diagnosed malignancy[11]. HER2-overexpressing breast cancer accounts for 20-25% of all breast cancer cases and is a particularly aggressive malignancy, with a poor prognosis, short overall survival and resistance to endocrine therapy[113]. HER2 is therefore a relevant target for targeted therapy[117].

NPs are being studied as targeted therapy platforms due to their ability to improve the transport, solubility, stability and efficiency of packaged drugs[17]. VLPs are composed of assembled viral proteins but lack the viral genome and display features such as flexibility, biocompatibility, simple production, self-assembly, immunogenicity, and capacity to cross cell membranes to deliver the desired agents at the cytoplasm[28]. These features, together with the ability to modify their surface with targeting moieties, make VLPs promising nanoplatforms for targeted drug delivery[28]. HIV-1-based VLPs arise as particularly appealing nanoplatforms, given their ability to employ just one polyprotein for self-assembly[73]. HIV-1-based VLPs can thus be harnessed as targeted delivery systems for different targets, namely HER2.

Previous studies reported the design and construction of a targeting motif that combines an anti-HER2 scFv derived from trastuzumab with the HIV-1 protein gp41[122]. Firstly, docking studies were conducted to determine the most adequate gp41 residue for fusion with the scFv, which led to the design

of a plasmid comprising the scFv-HER2_gp41 sequence for transfection in a mammalian platform[122]. This plasmid was then expressed in HEK-293T cells (HEK-293 cells expressing the SV40 large T antigen) and validated through the Western Blot method[122].

The goal of this thesis was to construct and characterize HIV-1-based VLPs modified with an anti-HER2 scFv derived from trastuzumab, and to evaluate their binding to HER2-overexpressing cancer cells. These nanoplatforms could then be employed for targeted delivery of therapeutic drugs and imaging molecules to HER2-overexpressing cancer cells (Figure 1.8). The overarching aim of this work is to establish the proof of concept of this approach for targeted therapy by using HER2 as a target, since it is a well-characterized receptor that plays a pivotal role in different types of cancer.

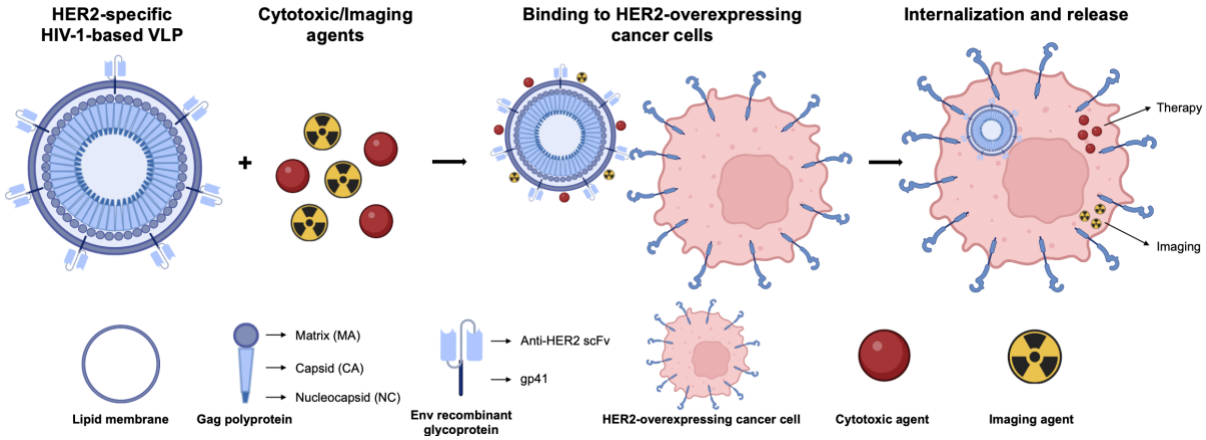

Figure 1.8 – Schematic illustration of the overarching goal of this thesis. Created with BioRender.com.

In order to achieve the main objective, the work of this thesis included a step-by-step protocol with the following goals:

1. Production of HER2-specific HIV-1-based VLPs:
   - Transient transfection assays in HEK-293T cells using the previously constructed plasmid harbouring the scFv-HER2_gp41 sequence, together with a plasmid containing Gag-Pol and a plasmid containing Rev.
2. Characterization of HER2-specific HIV-1-based VLPs:
   - ELISA to validate the produced VLPs.
   - Western Blot assays to confirm the incorporation of the anti-HER2 scFv into the VLPs.
   - TEM assays to characterize the morphology of the produced VLPs.
3. Cytotoxic evaluation of HER2-specific HIV-1-based VLPs:
   - Cytotoxicity assays using HER2-positive and HER2-negative breast cancer cell lines treated with VLPs.
4. Radiolabelling of HER2-specific HIV-1-based VLPs for downstream uptake assays.

1.7 Thesis Outline

This thesis is divided into five chapters. The first chapter provided the background to the work developed in this thesis and presented the motivation and aim. The second chapter describes the materials and experimental procedures. The third chapter reports the obtained results and their discussion. The fourth chapter contains the conclusions of the work herein developed. The fifth chapter depicts the future perspectives of this work.

2

MATERIALS AND METHODS

2.1 Plasmids

The X1665+pcDNA3.1+ plasmid (which will be referred as pX1665 from hereon) encodes the protein sequence harbouring the anti-HER2 scFv fused to the HIV protein gp41 and was synthesized by Synbio Tech (USA). The X1665+His+G plasmid (which will be referred as pX1665+His from hereon) encodes the same protein sequence with a polyhistidine tag (His-Tag) and was synthesized by Synbio Tech (USA). The pMDLg/pRRE plasmid codes for Gag-Pol and RRE (Addgene plasmid #12251; http://n2t.net/addgene:12251; RRID:Addgene_12251). The pRSV-REV plasmid codes for Rev (Addgene plasmid #12253; http://n2t.net/addgene:12253; RRID:Addgene_12253). All plasmid maps are depicted in Annexes (Figures A1 – A4).

2.2 Bacterial Transformation

NEB® 10-beta Electrocompetent *Escherichia coli* cells (New England Biolabs, Inc., USA) were used for transformation and isolation of plasmid clones. The cells were briefly thawed on ice. The plasmid DNA (50 ng/µL) was then incubated with 50 µL of cells on ice for 5 min. Transformation was then carried out through electroporation on a Bio-Rad Gene Pulser at 200 Ω, 25 µF and 1.8 kV. Following electroporation, 950 µL of S.O.C medium (Thermo Fisher Scientific Inc., USA) were added to the cells for recovery, and the cells were incubated for 1 hour at 37 °C and 220 rpm. Cells that underwent transformation were plated on Luria-Bertani (LB)-agar plates with 100 µg/mL of ampicillin (NZYTech, Portugal) and incubated at 37 °C overnight. Then, an isolated colony was selected, cultured in 5 mL of LB containing 100 µg/mL of ampicillin and incubated at 37 °C for 6 h at 220 rpm. The pre-inoculum was then added to 100 mL of LB supplemented with 100 µg/mL of ampicillin and incubated at 37 °C and 220 rpm overnight. The cells were centrifuged at 6,000 × *g* (Centrifuge 5804 R, Eppendorf, Germany) for 15 min at 4 °C, and the supernatant was discarded. The pellet was stored at -80°C until use.

2.3 DNA Extraction

DNA extraction and purification were conducted with the GF-1 Bacterial DNA Extraction Kit (Vivantis, Malaysia) as per the manufacturer's instructions. DNA concentration and purity were assessed with the Varioskan™ Lux multimode microplate reader (Thermo Fisher Scientific Inc., USA).

2.4 Cell Lines

The HEK-293T (American Type Culture Collection, USA, CRL-3216™), SK-BR-3 (breast cancer cell line that displays HER2 overexpression, American Type Culture Collection, USA, HTB-30™) and MDA-MB-231 (triple-negative breast cancer cell line that lacks HER2 overexpression, American Type Culture Collection, USA, HTB-26™) cell lines were used in this study. All cell lines were evaluated for mycoplasma with the LookOut® Mycoplasma PCR Detection Kit (Sigma-Aldrich, Inc., USA) as per the manufacturer's indications, and were mycoplasma-free.

2.5 Cell Culture

Cells were cultured in Dulbecco's Modified Eagle's Medium (DMEM)/High Glucose supplemented with 10% (v/v) fetal bovine serum (FBS), 10 mM HEPES, 1x MEM Non-Essential Amino Acids, 1 mM sodium pyruvate and 1x penicillin-streptomycin (which will be referred from hereon as complete medium) (all reagents were attained from Cytiva, USA). 75 cm^3 disposable polycarbonate cell culture flasks (Thermo Fisher Scientific, Inc., USA) were used to maintain the cells at 37 °C in a humidified incubator (CelCulture® (CCL-O50) CO_2 incubator, Esco Lifesciences, Singapore) with 5% CO_2.

Upon reaching confluence, culture medium was removed from the flasks and cells were washed with phosphate buffered saline (PBS) (Cytiva, USA). Trypsin (Cytiva, USA) was then added, and cells were incubated for 5 min at room temperature to achieve detachment. Culture medium was then added to block trypsin action. Cells were then transferred to a new flask, where fresh pre-warmed complete medium was added.

The trypan blue exclusion assay was conducted to determine cell viability and concentration. Briefly, cells were diluted at 1:2 with trypan blue dye (Merck, Germany) and counted on a Neubauer chamber.

2.6 Transient Transfection

The Lipofectamine™ 3000 Transfection Reagent (Invitrogen, Thermo Fisher Scientific, USA) was used for transient transfection to produce VLPs (Figure 2.1).

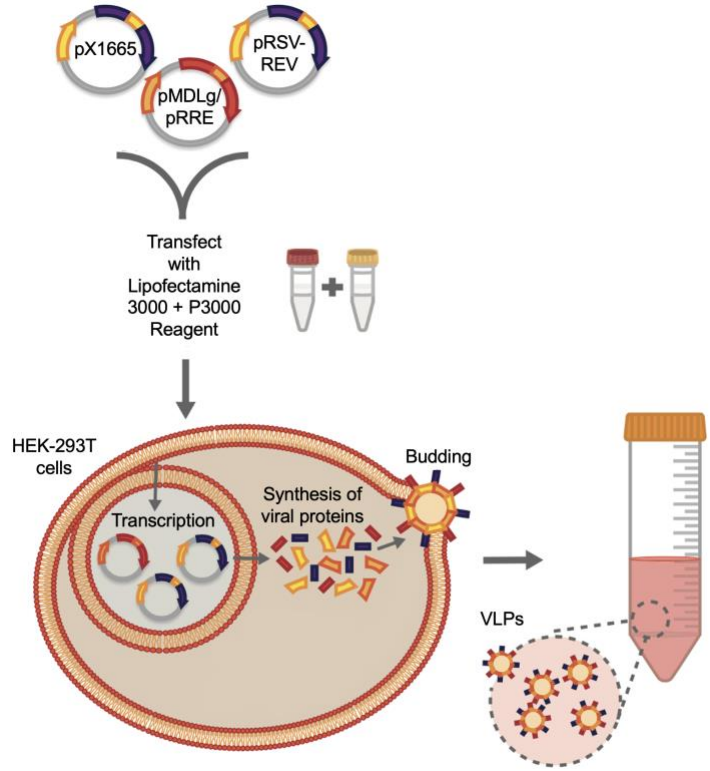

Figure 2.1 – Schematic illustration of the transfection protocol for HER2-specific VLP production using Lipofectamine™ 3000. Adapted from the 'Improve lentiviral production using Lipofectamine 3000 reagent' application note.

2.6.1 HIV-1-Based VLP Production

HIV-1-based VLPs were constructed as controls, according to the following protocol:

HEK-293T cells were plated in 6-well plates at a density of 1.0 x 10^6 cells/well and incubated with complete medium at 37 °C and 5% CO_2 overnight. Cells were then transfected with Lipofectamine™ 3000 Transfection Reagent (Invitrogen, Thermo Fisher Scientific, USA) in accordance with the manufacturer's procedure using 2.041 µg of pMDLg/pRRE and 0.959 µg of pRSV-REV (1:1 ratio). Briefly, the plasmid DNA was diluted in DMEM supplemented with 2% (v/v) FBS, 10 mM HEPES, 1x MEM Non-Essential Amino Acids, 1 nM sodium pyruvate and 1% (v/v) penicillin-streptomycin. The P3000 Reagent was then added to the plasmid DNA solution. Lipofectamine™ 3000 Transfection Reagent was also diluted in the same medium. The plasmid DNA solution was then added to the Lipofectamine™ solution and incubated for 12 min at room temperature. Cells were then incubated with the DNA-Lipofectamine™ mix for 6 h at 37 ºC and 5% CO_2. Following incubation, the medium was disposed of, and fresh complete medium was added. The supernatant was recovered 48 h post-transfection and centrifuged at 2,000 rpm for 10 min at room temperature (Beckman, J2-21M, Beckman Coulter, Inc., USA). The VLP-containing supernatant was collected and stored in single use aliquots at -80 °C (Figure 2.2).

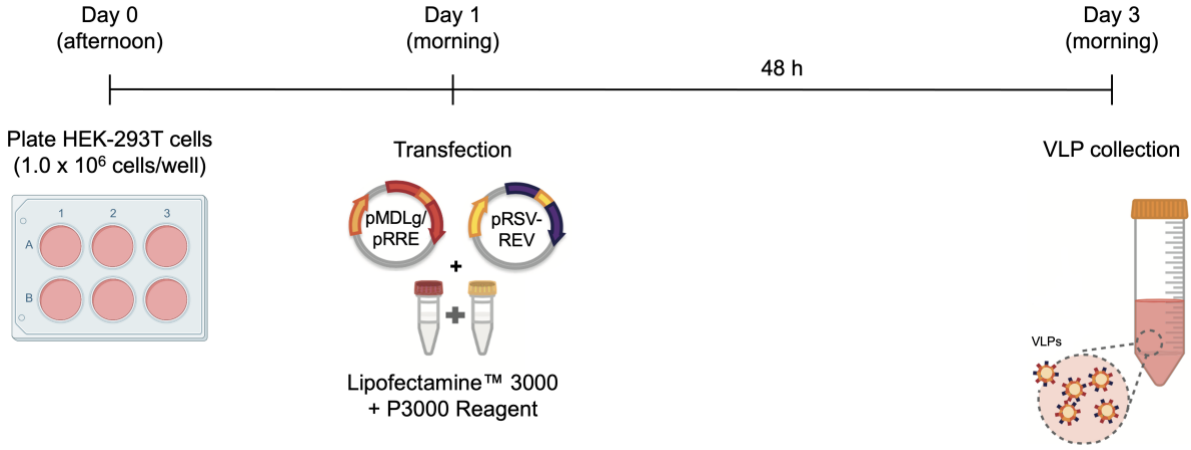

Figure 2.2 – Scheme of the transfection protocol for HIV-1-based VLP production.

2.6.2 HER2-Specific VLP Production

HER2-specific VLPs were constructed according to the ensuing protocol:

HEK-293T cells were plated at a density of 1.0 x 10^6 cells/well in 6-well plates and incubated with complete medium at 37 °C and 5% CO_2 overnight. Cells were then transfected with Lipofectamine™ 3000 Transfection Reagent (Invitrogen, Thermo Fisher Scientific, USA) according to the manufacturer's instructions using 1.016 µg of pX1665, 1.350 µg of pMDLg/pRRE and 0.635 µg of pRSV-REV (Figure 2.3).

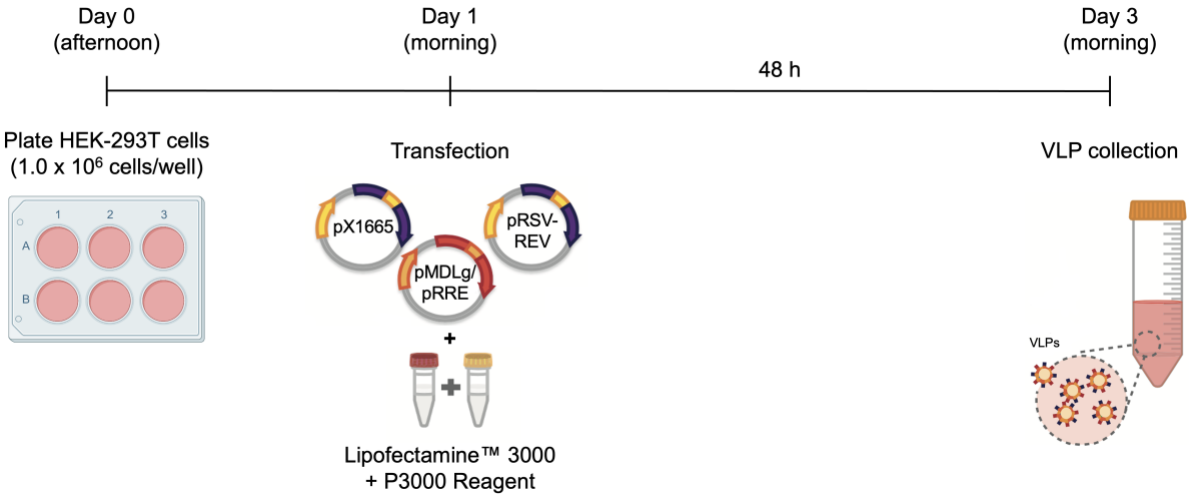

Figure 2.3 – Scheme of the transfection protocol for HER2-specific VLP production.

2.6.3 HER2-Specific VLP Production for Radiolabelling

HER2-specific VLPs for radiolabelling were manufactured as per the following protocol:

HEK-293T cells were plated at a density of 1.0 x 10^6 cells/well in 6-well plates and incubated with complete medium at 37 °C and 5% CO_2 overnight. Cells were then transfected with Lipofectamine™

3000 Transfection Reagent (Invitrogen, Thermo Fisher Scientific, USA) according to the manufacturer's instructions using 1.018 µg of pX1665+His, 1.348 µg of pMDLg/pRRE and 0.634 µg of pRSV-REV (Figure 2.4).

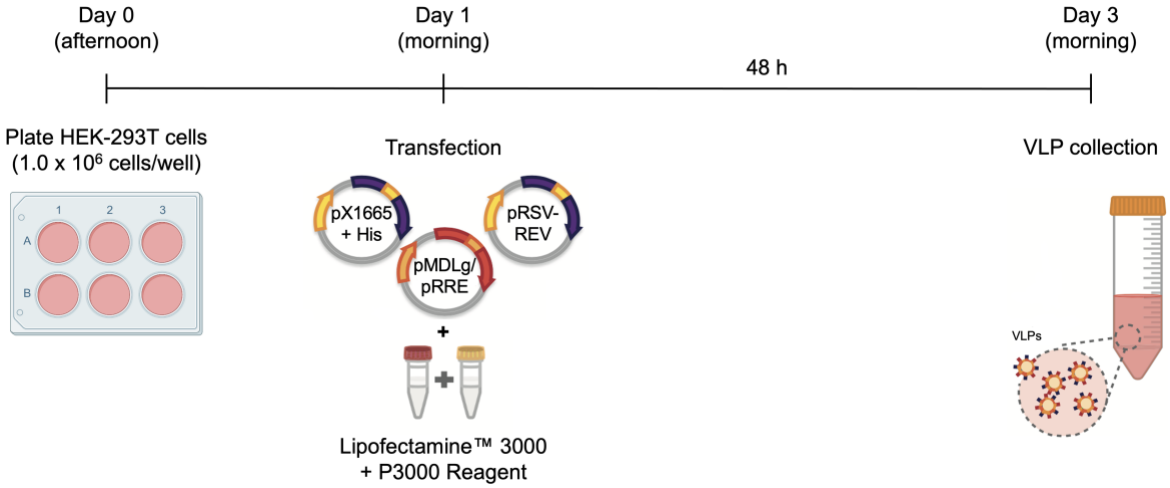

Figure 2.4 – Scheme of the transfection protocol for HER2-specific VLP production for radiolabelling.

2.7 VLP Concentration

Three protocols were tested for VLP concentration:

1) Amicon® Ultra centrifugal ultrafiltration

500 µL of VLP-containing supernatant were added to Amicon® centrifugal filters with a molecular weight cut-off of 50 kDa (Merck, Germany) and centrifuged at 8,000 rpm for 40 min at room temperature. The flow-through was discarded and the retentate was eluted with 5 mL of pre-warmed PBS and centrifuged at 8,000 rpm for 30 min at room temperature twice. The obtained VLP suspension was recovered and stored in single use aliquots at -80 °C.

2) Lenti-X™ Concentrator

One volume of Lenti-X™ Concentrator (Takara Bio, Japan) was combined with three volumes of VLP-containing supernatant, mixed by gentle inversion, incubated at 4 ºC for 30 min and then centrifuged at 1,500 × *g* for 45 min at 4 ºC. The supernatant was discarded, and the pellet was resuspended in 1/10 of the original sample volume of PBS and stored at -80 °C.

3) Sucrose cushion

A 30% (w/v) sucrose solution was prepared in PBS. 500 µL of VLP-containing supernatant were added to 83 µL of the 30% sucrose solution and centrifuged at 20,000 rpm for 4 h at 11 °C. The supernatant was disposed of, and the pellet was resuspended in 100 µL of PBS.

2.8 Enzyme-Linked Immunosorbent Assay

Quantification of the different HIV-1-based VLP batches was performed with the INNOTEST® HIV Antigen mAb (Fujirebio, Japan), a sandwich ELISA test aimed at HIV p24 antigen in plasma, serum, and cell culture supernatant, in accordance with the manufacturer's instructions. The wells of the polystyrene microtiter plates had been treated with human polyclonal antibodies against HIV. 100 µL of either VLP-containing cell culture supernatants or controls were incubated with 100 µL of a mixture of biotinylated anti-p24 monoclonal antibodies in each well for 1 h at 37 °C. Washing of the wells was carried out with washing solution 5 times. Then, 200 µL of peroxidase-conjugated streptavidin, which displays affinity for biotin, were added and incubated for 30 min at 37 °C. The wells were washed 5 times with washing solution. 200 µL of peroxidase substrate and chromogen were then added and incubated for 30 min at room temperature. This produced a blue colour, which turned yellow after stopping the reaction with 50 µL of sulfuric acid. To determine VLP concentration, the absorbance at 450 nm was read on an EZ Read 800 Microplate Reader (Biochrom, USA) and a standard p24 curve was used for quantification.

2.9 Western Blot

The collected samples and positive control (cell extracts containing hemagglutinin (HA)) were mixed with either 1/6 of 6X or 1/2 of 2X SDS sample loading buffer and heated at 95 °C for 10 min. Samples and positive controls were loaded onto a 12.5% SDS-polyacrylamide gel for separation through electrophoresis, using the Mini-PROTEAN Tetra cell (BioRad, USA). Following electrophoresis, transference of the samples onto a nitrocellulose membrane (BioRad, USA) using the Tetra Blotting Module (BioRad, USA) was performed. Blockage of the membranes was carried out in 5% (w/v) non-fat dried milk in PBS containing 0.2% (v/v) Tween 20 (PBS-T) at 4 °C overnight. The membranes were then washed with PBS-T, and were either incubated with the horseradish peroxidase (HRP)-conjugated anti-HA polyclonal antibody (Fisher Scientific, USA) diluted 1:10000 in 1% (w/v) non-fat dried milk in PBS-T at room temperature for 90 min with gentle agitation, or with an anti-HA monoclonal antibody (BioLegend, USA) diluted 1:2000 in 1% (w/v) non-fat dried milk in PBS-T at room temperature for 60 min with gentle agitation and washed with PBS-T, followed by incubation with an anti-mouse secondary antibody (BioRad, USA) diluted 1:3000 in 1% (w/v) non-fat dried milk in PBS-T at room temperature for 1 h with gentle agitation. The membranes were washed with PBS-T and the proteins were detected using the ECL® reagent (GE Lifesciences, USA) following the manufacturer's protocol.

2.10 Transmission Electron Microscopy (TEM)

TEM of the collected VLPs was performed by Maria João Almeida, Sofia Pacheco, Ana Sousa, and Beatriz Tomaz from the Electron Microscopy Facility at Instituto Gulbenkian da Ciência (IGC). Morphology of the constructed VLPs was analysed through the negative staining method as follows: briefly, 3 µL of different HIV-1-based VLP suspensions were absorbed for 5 min onto formvar/carbon-

coated glow-discharged copper EM grids. Distilled water was employed to wash the grids 10 times, and staining with a drop of 2% uranyl acetate for 5 min ensued. TEM analysis was performed with a FEI Tecnai G^2 Spirit BioTWIN transmission electron microscope at 120 keV. An Olympus-SIS Veleta CCD Camera was used at 16.5K, 43K and 60K to capture TEM images, which were then processed in the ImageJ software[123].

2.11 Cytotoxicity Assay

Cell viability was assessed through the tetrazolium salt WST-1 (4-[3-(4-iodophenyl)-2-(4-nitrophenyl)-2H-5-tetrazolio] -1,3-benzene disulfonate) assay. SK-BR-3 and MDA-MB-231 cells were plated at a density of 1.0 x 10^5 cells/well in 96-well plates and incubated with complete medium at 37 °C and 5% CO_2 overnight. Sample dilutions were prepared in PBS. The complete medium was aspirated, and the cellular monolayers were washed with PBS by gentle agitation. The cells were then incubated with 100 µL of the prepared sample dilutions and 100 µL of 2x Minimum Essential Medium Eagle (MEM) (prepared with MEM AutoMod™ (Sigma-Aldrich, Inc., USA) and ultrapure water) supplemented with 2% (v/v) FBS, 0.225% $NaHCO_3$, 30 mM HEPES, 4 nM L-glutamine, 0.2 mM non-essential amino acids, 2x penicillin-streptomycin and 2 mM sodium pyruvate for 24 h at 37 °C and 5% CO_2. The inoculum was then removed and replaced with 100 µL of fresh complete medium, together with 10 µL of the WST-1 reagent (Roche, Switzerland). Incubation at 37 °C for 6 h ensued, and the absorbance at 450 nm was read on an EZ Read 800 Microplate Reader (Biochrom, USA), using 620 nm as a reference wavelength. Untreated cells in complete medium, sample dilutions in complete medium and fresh complete medium were used as controls. The results were presented as percentages of cell viability of treated cells in reference to untreated cells. The values were depicted as the mean of the triplicates with error bars indicating the 95% confidence interval for the mean. Data underwent statistical analysis through one-way analysis of variance (ANOVA), at a significance level of $p < 0.05$.

2.12 Radiolabelling HER2-Specific VLPs with Technetium-99m

2.12.1 Preparation of Technetium-99m

Manipulation of all radioactive elements was carried out in adequate laboratory facilities in accordance with the radiation protection regulation. Preparation was performed by Denise Rosário from the Radiopharmaceutical Sciences group at Centre for Nuclear Sciences and Technologies (C^2TN). Pertechnetate ($[^{99m}TcO_4]^-$) was eluted with a solution of 0.9% (w/v) NaCl from a $^{99}Mo/^{99}Tc$ generator. Around 1 mL of the eluate was added to a glass vial purged with N_2 containing 2.80 mg of sodium tetraborate decahydrate, 4.50 mg of sodium boranocarbonate, 7.15 mg of sodium carbonate and 8.50 mg of sodium tartrate dihydrate, and incubated at 100 °C for 30 min in a dry block heater (Tembloc, J.P. Selecta, Spain). The solution was then neutralized with 1 M HCl. Radiochemical purity was evaluated by instant thin layer chromatography by silica gel (ITLC-SG) (Agilent Technologies, USA), with 0.1 M sodium citrate buffer as a mobile phase.

2.12.2 VLP Labelling with Technetium-99m

Radiolabelling was conducted by Rúben Silva from the Radiopharmaceutical Sciences group at C^2TN. For radiolabelling, 12.5 µL of His-tagged HER2-specific HIV-1-based VLPs suspended in PBS were added to 12.5 µL of $^{99m}Tc(I)$-tricarbonyl (*fac*-$[^{99m}Tc(CO)_3(H_2O)_3]^+$) at 41.6 µCi (1:1 ratio) , and the mixture was incubated at 37 °C for 30, 60 and 90 min. Radiolabelling efficiency was determined through ITLC-SG, with 0.1 M sodium citrate buffer as a mobile phase. Strips were dried before being counted on a gamma BGO-V-Detector coupled to a miniGITA system (Elysia-raytest, Germany).

3

RESULTS AND DISCUSSION

The main aim of this thesis was the construction and characterization of HIV-1-based VLPs that possess an anti-HER2 scFv derived from trastuzumab. To achieve this objective, both HIV-1-based VLPs and HER2-specific VLPs were produced through transient transfection of HEK-293T cells. HIV-1-based VLPs were constructed as a control, to unveil whether there is a morphological difference between wild-type HIV-1 Gag VLPs and modified HIV-1-based VLPs. HER2-specific VLPs were constructed with and without His-tags, the former for radiolabelling with technetium-99m. Characterization of the manufactured VLPs ensued. Western Blot analyses were carried out to ascertain the presence of the protein of interest, whereas TEM analyses were performed to visualize the assembled VLPs and uncover their size. The antiproliferative effect of HER2-specific VLPs was then verified in HER2-overexpressing cells and cells that do not possess HER2 overexpression, through a cell viability assay. Lastly, His-tagged VLPs were radiolabelled with technetium-99m for downstream uptake assays.

3.1 HER2-Specific VLP Production and Quantification

VLP production requires cloning of the needed structural genes, expression of the corresponding structural proteins in expression platforms, and purification to remove cellular debris[28,30]. The selection of the expression system is essential for adequate protein folding and post-translational modifications[28]. Following production, VLPs can be retrieved from the cells or the cell culture supernatant.

Considering that HIV-1-based VLPs are enveloped VLPs, they require an eukaryotic expression system for production[73]. The HEK-293 cell line is one of the most frequently employed eukaryotic systems for VLP production due to its rapid growth and simple handling[73]. It also displays several shortcomings, namely low production yields and the high risk of contamination[73,87]. HEK-293T is a variation of the HEK-293 cell line that was modified with a temperature-sensitive version of the SV40 large T antigen, which enables the amplification of vectors that contain the SV40 origin of replication and thus augments the expression yields obtained through transient transfection[124]. Despite the

challenges posed by these cell lines, the HEK-293T cell line was chosen to produce HIV-1-based VLPs in this work, given that it is a proof-of-concept approach to establish a novel targeted therapy tool.

Twenty-five batches of HER2-specific VLPs were produced through transient transfection of HEK-293T cells using the previously constructed biomimetic vector, pX1665[122], together with pMDLg/RRE and pRSV-REV, at a 1:1:1 ratio (Section 2.6.2). The protein concentration of the produced HER2-specific VLPs was determined through p24 ELISA (Section 2.8). p24 derives from the precursor Pr55Gag polyprotein and is one of the constituents of the HIV-1 capsid.

Serial dilutions of standard solutions were analysed by ELISA at 450 nm. Figure 3.1 shows the calibration curve for batches 1 and 2.

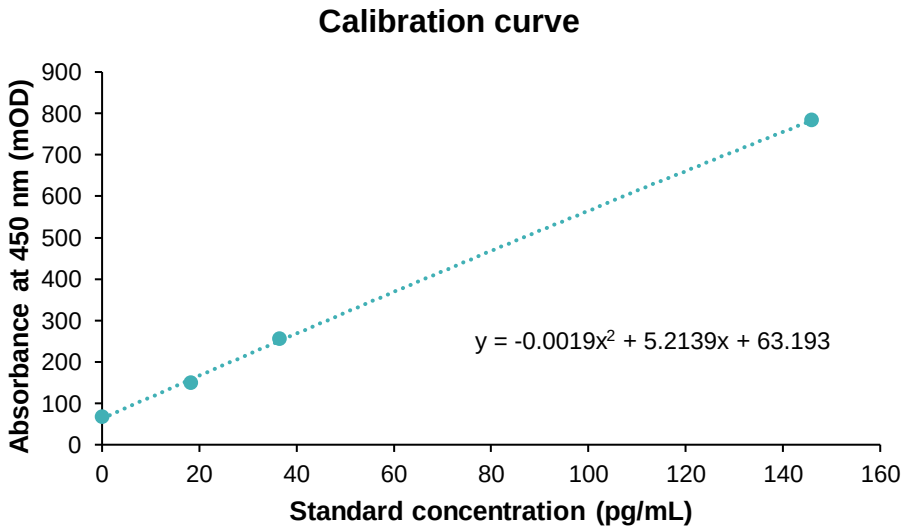

Figure 3.1 – INNOTEST® HIV Antigen mAb calibration curve for batches 1 and 2 of HER2-specific VLPs.

The obtained equation was:

$$y = -0.0019x^2 + 5.2139x + 63.193 \qquad (1)$$

Equation 1 was used to calculate the concentration of p24 (x) of batches 1 and 2 of HER2-specific VLPs through the obtained absorbances (y). The obtained concentrations are depicted in Table 3.1.

Table 3.1 – Quantification of p24 protein of batches 1 and 2 of HER2-specific VLPs.

Batches	p24 (pg/mL)
1	63.78
2	155.28

The concentrations for batches 1 and 2 of HER2-specific VLPs were lower than expected[37], which could be attributed to confluence and morphology. The HEK-293T cells used to produce batches 1 and

2 were at passage 17 and displayed around 60% confluency at the time of transfection. Moreover, cells did not display their typical morphology, which could affect VLP production.

3.2 Characterization of HER2-Specific VLPs

3.2.1 Presence of the Anti-HER2 scFv in HER2-Specific VLPs

After VLP production, it is important to assess whether the protein of interest is expressed in the VLPs. The previously constructed plasmid containing the scFv-HER2_gp41 sequence included an N-terminal HA-tag for protein detection (Section A.1 – Figure A.1). Western Blot analysis with anti-HA antibodies can thus be performed to assess the presence of the anti-HER2 scFv in the constructed VLPs. Despite the low concentrations obtained for batches 1 and 2, they still underwent Western Blot analysis to validate the transfection of the constructed plasmid comprising the scFv-HER2_gp41 sequence.

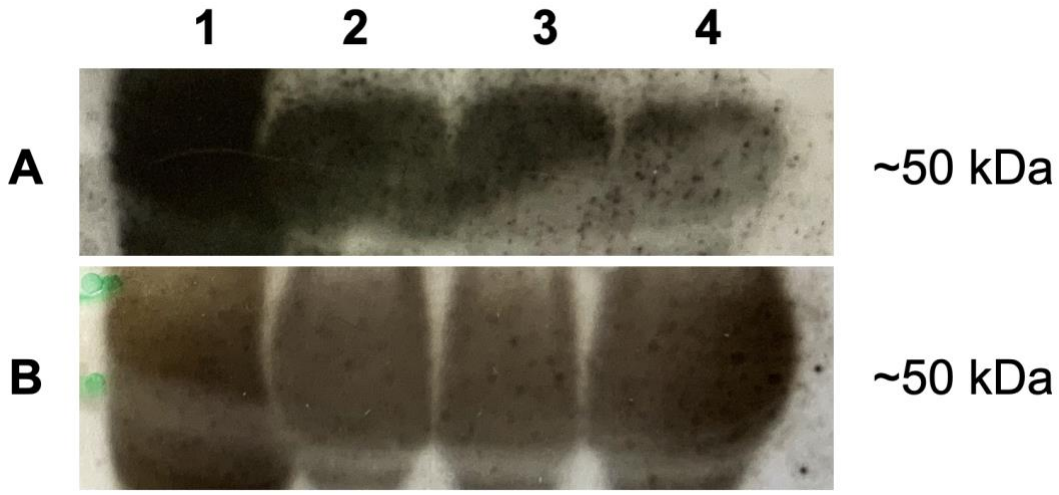

Figure 3.2 – Western Blot analysis of batches 1 and 2. (A) Western Blot detection conducted with a HRP-conjugated anti-HA polyclonal antibody (1:10000). (B) Western Blot detection conducted with an anti-HA monoclonal antibody (1:2000) and an anti-mouse secondary antibody (1:3000). Lanes 1 and 2: positive controls (cell extracts containing HA); lane 3: batch 1; lane 4: batch 2. Visualization of the bands was performed with the ECL® reagent.

The presence of the anti-HER2 scFv was first evaluated with a HRP-conjugated anti-HA polyclonal antibody. Cell extracts containing HA were used as positive controls. The estimated molecular weight of the protein of interest was previously ascertained, and is 47.1 kDa[122]. The molecular weight of the protein present in the VLPs of batches 1 and 2 is around 50 kDa (Figure 3.2 - A), which is analogous to the established value. These results indicate that the scFv-HER2_gp41 recombinant protein is present in the VLPs of batches 1 and 2. To validate the presence of the anti-HER2 scFv in the VLPs, a new Western Blot analysis was carried out with an anti-HA monoclonal antibody. The attained molecular weight around 50 kDa (Figure 3.2 - B) coincides with the first Western Blot analysis. These results confirm the presence of the anti-HER2 fragment in the VLPs of batches 1 and 2. Moreover, it

indicates that the transfection protocol with pX1665 was successfully performed and can therefore be reproduced for novel batches.

3.3 HER2-Specific VLP Production Optimization and Quantification

A new transfection protocol was performed with cells at a higher passage to determine whether cell conditions influence VLP assembly. The obtained concentrations are depicted in Table 3.2.

Table 3.2 – Quantification of p24 protein of batches 3 to 8 of HER2-specific VLPs.

Batches	p24 (pg/mL)
3	311.53
4	216.43
5	214.53
6	233.40
7	217.06
8	174.45

The obtained concentrations for batches 3 to 8 are 2 to 3 times higher than the ones obtained for batches 1 and 2. The cells that were employed to produce these batches were at passage 26, had an adequate morphology and displayed around 80% confluency at the time of transfection, which suggests that confluence and morphology are indeed limiting factors for the development of HIV-1-based VLPs. It is therefore important to consider these factors when constructing these VLPs through transient transfection in HEK-293T cells.

3.4 Characterization of Optimized HER2-Specific VLPs

3.4.1 Presence of the Anti-HER2 scFv in Optimized HER2-Specific VLPs

After the production step, evaluation of the presence of the protein of interest ensued.

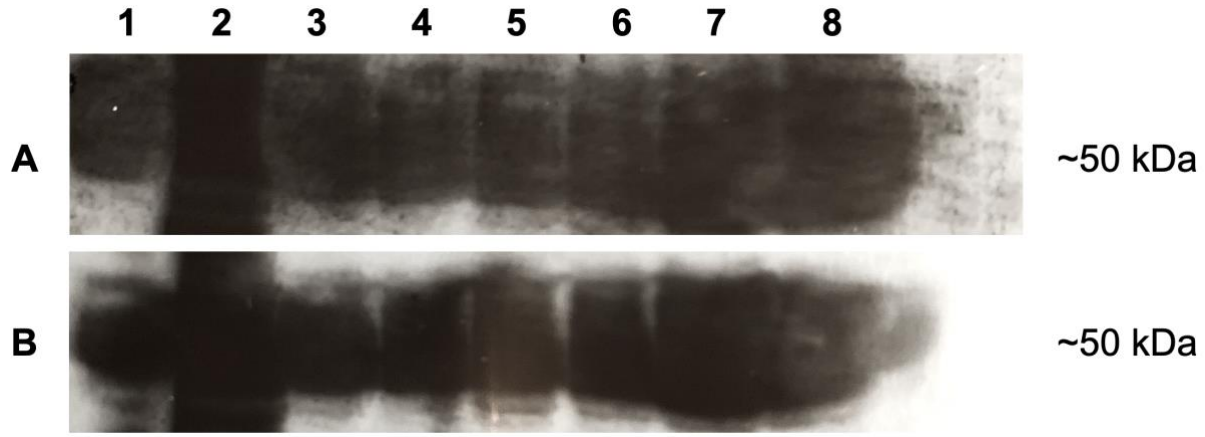

Figure 3.3 – Western Blot analysis of batches 3 to 8. (A) Western Blot detection conducted with a HRP-conjugated anti-HA polyclonal antibody (1:10000). (B) Western Blot detection conducted with an anti-HA monoclonal antibody (1:2000) and an anti-mouse secondary antibody (1:3000). Lanes 1 and 2: positive controls (cell extracts containing HA); lane 3: batch 3; lane 4: batch 4; lane 5: batch 5; lane 6: batch 6; lane 7: batch 7; lane 8: batch 8. Visualization of the bands was performed with the ECL® reagent.

The presence of the anti-HER2 scFv was first evaluated with a HRP-conjugated anti-HA polyclonal antibody. The molecular weight of the protein present in the VLPs of batches 3 to 8 is around 50 kDa (Figure 3.3 - A), which is similar to the theoretical value and coincides with the value obtained for batches 1 and 2. These results indicate that the scFv-HER2_gp41 recombinant protein was incorporated in the VLPs of batches 3 to 8. An anti-HA monoclonal antibody was then employed for a novel Western Blot analysis, to confirm the presence of the anti-HER2 scFv. The molecular weight of the protein present in the VLPs of batches 3 to 8 is around 50 kDa (Figure 3.3 - B). This corroborates the results obtained with the polyclonal antibody and confirms the presence of the protein of interest.

3.4.2 Morphological Characterization of the Optimized HER2-Specific VLPs

After evaluating the presence of the anti-HER2 scFv in the constructed VLPs, their morphological characterization was performed by TEM analysis. This analysis aimed to determine whether the transfection protocol permits the formation of VLPs and therefore assess if HER2-specific HIV-1-based VLPs display the morphology described for HIV-1 VLPs[96].

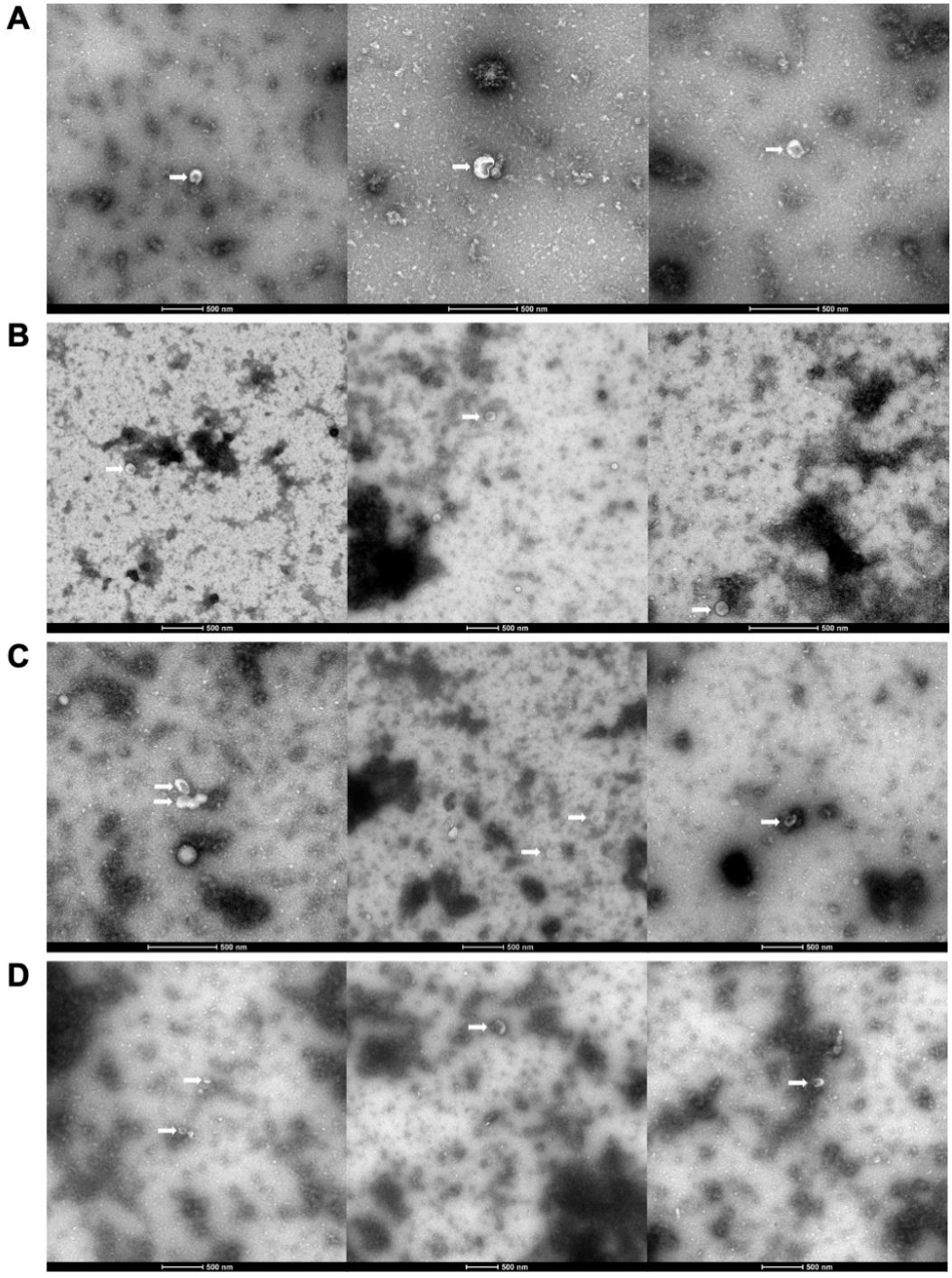

Figure 3.4 – TEM analysis of batches 3, 4, 6 and 7. (A) Batch 3. Scale bar = 500 nm. (B) Batch 4. Scale bar = 500 nm. (C) Batch 6. Scale bar = 500 nm. (D) Batch 7. Scale bar = 500 nm. Images taken at 43K.

Batches 3, 4, 6 and 7 were selected for the first TEM analysis, as they displayed the highest concentrations out of the six batches that were produced in the same protocol (Table 3.2). The TEM images (Figure 3.4) show spherical structures (indicated by white arrows) that display the morphology associated with negative stained HIV-1-based VLPs[96,125-127]. Their size was determined by ImageJ[123] (Table 3.3), and is in accordance with the size range of HIV-1-based VLPs described in the literature

(100-200 nm)[37,128]. This indicates that HER2-specific HIV-1-based VLP assembly occurred, and the transfection protocol is adequate for VLP formation. Notwithstanding, the images show that there are not many VLPs and that the samples contain several impurities. This could be because VLPs were collected from the cell culture supernatant and, despite the centrifugation step to remove cell debris, several proteins and impurities remain in the supernatant. This prompted concentration and purification steps to obtain higher concentrations and cleaner samples.

Table 3.3 – Size characterization of batches 3, 4, 6 and 7 of HER2-specific VLPs. SD stands for standard deviation. Size determined by ImageJ.

Batches	Size ± SD (nm)
3	155.67 ± 11.14
4	145.57 ± 32.86
6	117.12 ± 14.22
7	145.18 ± 52.27

3.4.3 Evaluation of VLP Concentration Methods

After establishing the protocol to produce HER2-specific VLPs, different methods were assessed regarding their potential to concentrate these VLPs. Three methods were tested: 1) Amicon® Ultra centrifugal ultrafiltration with a molecular weight cut-off of 50 kDa, 2) Lenti-X™ Concentrator and 3) sucrose cushion (Section 2.7).

Since batch 3 presented the highest concentration, it was selected to test the different concentration protocols. The three methods were performed, and protein concentration of the obtained HER2-specific VLPs was determined through p24 ELISA (Section 2.8). The obtained concentrations for each method are displayed in Table 3.4.

Table 3.4 – Quantification of p24 protein of batch 3 of HER2-specific VLPs concentrated through three methods.

Concentration method	p24 (pg/mL)	Increase in relation to original batch
Amicon	0.0	-
Lenti-X	491.63	1.58
Sucrose	384.58	1.23

The concentration for batch 3 concentrated through Amicon® Ultra centrifugal ultrafiltration was 0, which likely occurred because the retentate was eluted with 5 mL of PBS twice, and therefore the

obtained VLP suspension was too diluted. Elution with smaller volumes should thus be tested. Other methods of VLP recovery, namely reverse spinning, and removal of VLPs directly from the membrane, could also be performed to assess whether Amicon® Ultra centrifugal ultrafiltration can concentrate HIV-1-based VLPs. The obtained concentrations for batch 3 concentrated through the Lenti-X™ Concentrator and through sucrose cushion were 491.63 and 384.58 pg/mL, respectively. These results suggest that the Lenti-X™ Concentrator might be the best concentration method for HIV-1-based VLPs, although Amicon® Ultra centrifugal ultrafiltration should be repeated to confirm these results.

3.4.4 Morphological Characterization of the Concentrated HER2-Specific VLPs

After VLP concentration, a new TEM analysis was performed. Batch 3 concentrated through Amicon® Ultra centrifugal ultrafiltration was evaluated but no VLPs were observed (results not shown), which is in accordance with the quantification results (Table 3.4). Batch 3 concentrated with the other methods was analysed through TEM (Figure 3.5).

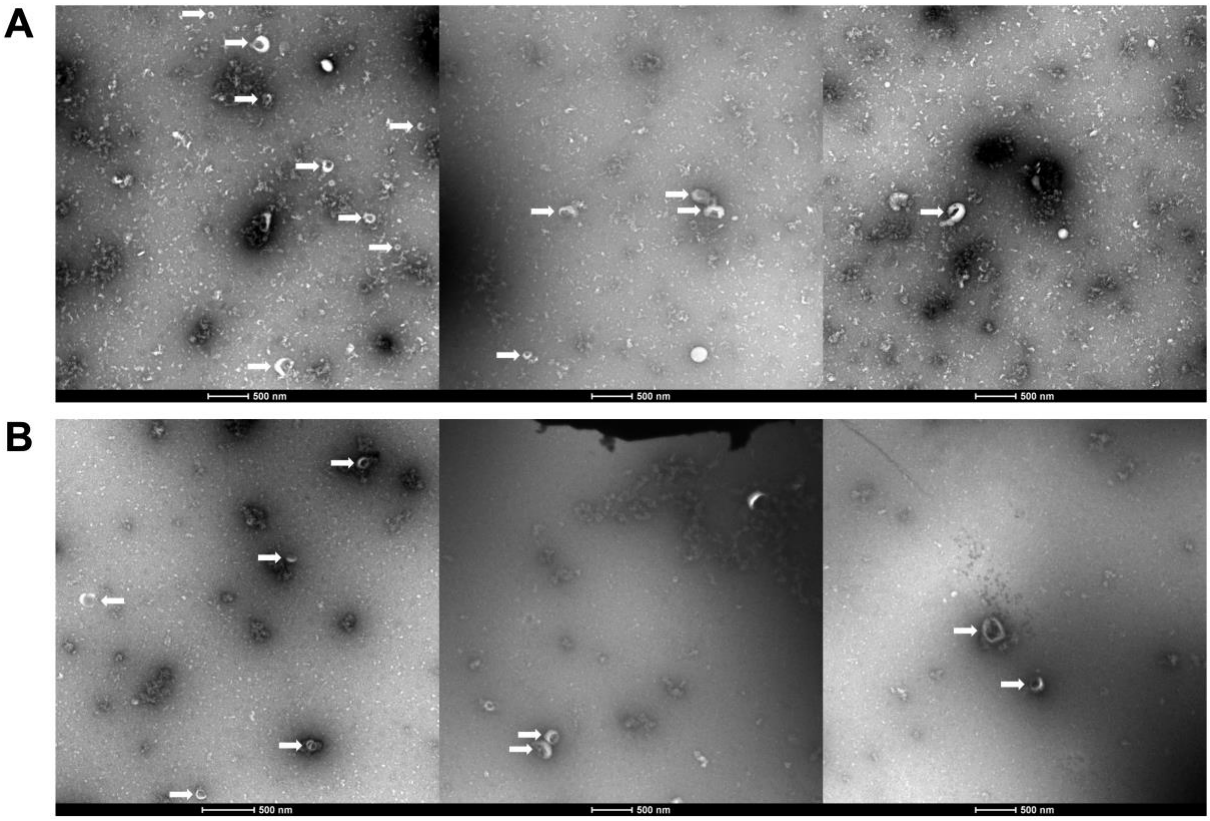

Figure 3.5 – TEM analysis of batch 3 concentrated through different methods. (A) TEM images of batch 3 concentrated through the Lenti-X™ Concentrator. (B) TEM images of batch 3 concentrated through sucrose cushion. Scale bar = 500 nm. Images taken at 43K.

Regarding concentration with the Lenti-X™ Concentrator, several VLPs can be found in the images (Figure 3.5 - A), all of which were in a size range of 163.15 ± 32.52 nm. There is a considerable increase in the number of VLPs and there are less impurities in comparison with the first TEM analysis, which confirms that the concentration protocol was successful. Regarding concentration through

sucrose cushion, HIV-1-based VLPs can also be detected (Figure 3.5 - B), with their size in the range of 146.27 ± 46.68 nm. Moreover, the images are much cleaner than the ones obtained for batch 3 concentrated through the Lenti-X™ Concentrator, which reveals that sucrose cushion is an adequate method for VLP concentration and purification. Notwithstanding, more VLPs can be visualized in the images obtained for batch 3 concentrated through the Lenti-X™ Concentrator, which is attributable to its higher concentration (Table 3.4).

3.5 Further HER2-Specific VLP Production and Characterization

Six new batches of HER2-specific HIV-1-based VLPs were produced (Section 2.6.2) and concentrated through the Lenti-X™ Concentrator method (Section 2.7). These batches were developed for further evaluation of HER2-specific VLPs, namely their antiproliferative effect on HER2-overexpressing cells and cells that lack such overexpression. The protein concentration of the obtained HER2-specific VLPs was determined through p24 ELISA (Section 2.8). The obtained concentrations are depicted in Table 3.5.

Table 3.5 – Quantification of p24 protein of batches 9 to 14 of HER2-specific VLPs.

Batches	[VLP] (pg/mL)
9	706.68
10	703.69
11	969.71
12	610.73
13	737.44
14	405.35

The obtained concentrations for batches 9 to 14 following concentration with the Lenti-X™ Concentrator are considerably higher than the one obtained for batch 3 following concentration with the same method. Given that only one concentration method was used, the starting volume was higher and therefore it was possible to attain more concentrated suspensions. Moreover, the cells that were employed to produce these batches displayed the adequate morphology and were extremely confluent at the time of transfection, which likely affected HIV-1-based VLP production.

3.6 Characterization of Novel HER2-Specific VLP Batches

3.6.1 Presence of the Anti-HER2 scFv in Novel HER2-Specific VLP Batches

The novel VLP batches underwent Western Blot analysis to evaluate the presence of the anti-HER2 scFv.

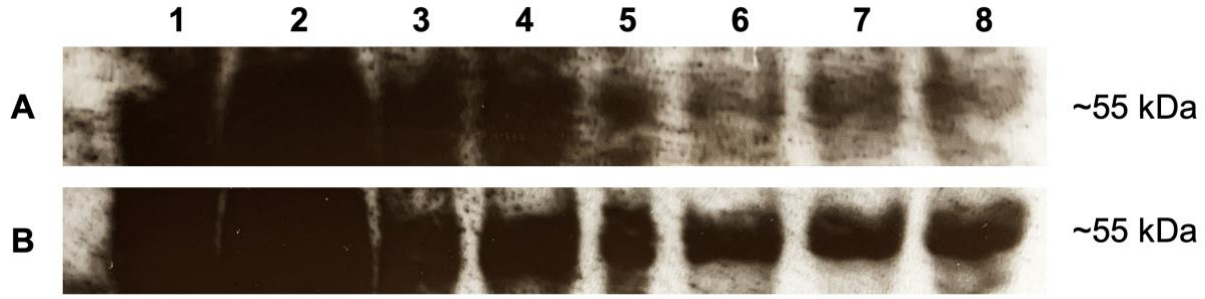

Figure 3.6 – Western Blot analysis of batches 9 to 14. (A) Western Blot detection conducted with a HRP-conjugated anti-HA polyclonal antibody (1:10000). (B) Western Blot detection conducted with an anti-HA monoclonal antibody (1:2000) and an anti-mouse secondary antibody (1:3000). Lanes 1 and 2: positive controls (cell extracts containing HA); lane 3: batch 9; lane 4: batch 10; lane 5: batch 11; lane 6: batch 12; lane 7: batch 13; lane 8: batch 14. Visualization of the bands was performed with the ECL® reagent.

Western Blot analysis was first carried out with a HRP-conjugated anti-HA polyclonal antibody. The molecular weight of the protein present in the VLPs of batches 9 to 14 is around 55 kDa (Figure 3.6 - A), which is marginally higher than the postulated value. This suggests that the scFv-HER2_gp41 recombinant protein is present in the VLPs of batches 9 to 14. To corroborate the obtained results, a novel Western Blot analysis was performed with an anti-HA monoclonal antibody. The attained molecular weight was around 55 kDa (Figure 3.6 - B), which is in accordance with the results obtained with the anti-HA polyclonal antibody. This indicates that the scFv-HER2_gp41 recombinant protein is present in the VLPs of batches 9 to 14.

3.6.2 Morphological Characterization of Novel HER2-Specific VLP Batches

Subsequently, the novel batches were characterized through TEM analysis. Batches 9, 11 and 13 were selected for TEM owing to their high concentrations (Table 3.5).

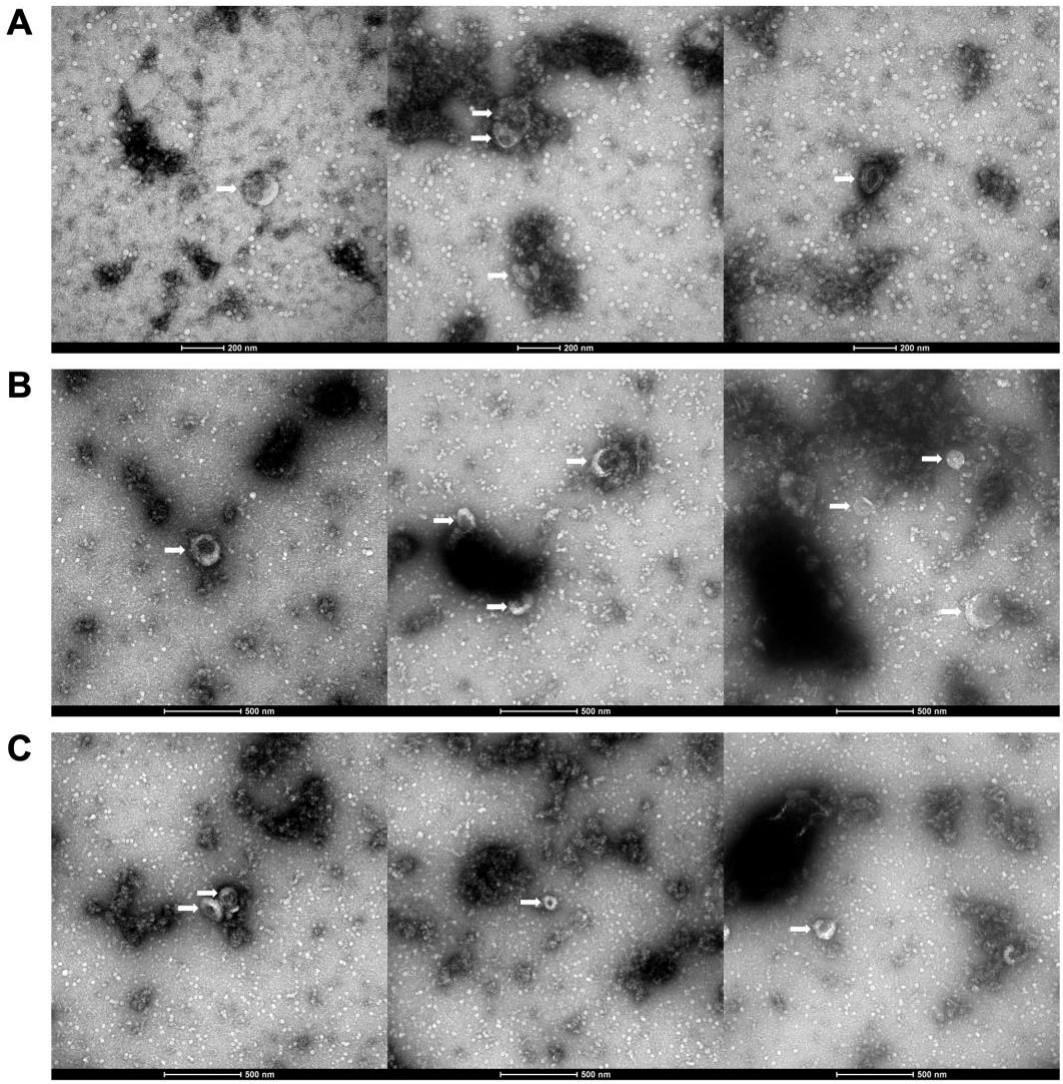

Figure 3.7 – TEM analysis of batches 9, 11 and 13. (A) TEM images of batch 9. Scale bar = 200 nm. Images taken at 60K. (B) TEM images of batch 11. Scale bar = 500 nm. Images taken at 43K. (C) TEM images of batch 13. Scale bar = 500 nm. Images taken at 43K.

Some VLPs can be observed in the TEM images of batches 9 (Figure 3.7 - A), 11 (Figure 3.7 - B) and 13 (Figure 3.7 - C), with the described HIV-1 VLP size[37,128], which validates VLP assembly. The size range is presented in Table 3.6. Nevertheless, the images that were taken did not show many VLPs, despite the obtained concentration, which could be ascribable to sample preparation.

Table 3.6 – Size characterization of batches 9, 11 and 13 of HER2-specific VLPs. SD stands for standard deviation. Size determined by ImageJ.

Batches	Size ± SD (nm)
9	128.38 ± 22.19
11	166.43 ± 31.06
13	131.22 ± 20.86

3.7 Cytotoxic Evaluation of Novel HER2-Specific VLP Batches

A relevant aspect that needs to be considered when developing novel therapeutic delivery tools is their cytotoxic effect on the target cells. For this reason, a cytotoxicity assay that relies on the water-soluble tetrazolium salt WST-1 was conducted. This assay is based on the cleavage of WST-1 to formazan by cellular mitochondrial dehydrogenases[129]. An increase in mitochondrial dehydrogenase activity occurs following cell proliferation, which in turn prompts an increase of formazan dye formed that can be quantified through measurement of the absorbance at 450 nm[129]. This assay permits to measure cell proliferation.

Two cell lines were chosen for this assay: MDA-MB-231 and SK-BR-3. MDA-MB-231 is a breast adenocarcinoma cell line that expresses epidermal growth factor and transforming growth factor alpha but lacks HER2 overexpression[130]. SK-BR-3, on the other hand, is a breast adenocarcinoma cell line that displays HER2 overexpression[131]. Cell proliferation of these two cell lines can thus be compared following treatment with HER2-specific VLPs to determine the cytotoxic effects of the constructed VLPs and assess whether they have a specific effect on HER2-overexpressing cells, when in comparison with cells that do not possess HER2 overexpression.

The most concentrated batches (9, 10, 11 and 13) were chosen for the cytotoxicity assay (Table 3.5). They were diluted at 1/10 in PBS and their cytotoxic effect was tested on MDA-MB-231 and SK-BR-3 cells in triplicate. Cell proliferation of cells treated with HER2-specific VLPs was compared with cell proliferation of untreated cells. VLPs in PBS and cell culture medium were also used as controls.

Cell viability was calculated through Equation 2 and the results are presented in Table 3.7.

$$\%\ Cell\ Viability = \frac{Absorbance_{Treated\ Cells} - Absorbance_{VLPs}}{Absorbance_{Untreated\ Cells} - Absorbance_{Culture\ Medium}} \times 100 \qquad (2)$$

Table 3.7 – Cell viability of MDA-MB-231 and SK-BR-3 cells treated with HER2-specific VLPs.

Samples	% Cell viability	
	MDA-MB-231	SK-BR-3
Batch 9 1/10	86.679	88.506
Batch 10 1/10	93.167	90.887
Batch 11 1/10	93.308	92.904
Batch 13 1/10	90.786	90.833

The obtained results for MDA-MB-231 cells are represented in Figure 3.8, and the obtained results for SK-BR-3 cells are represented in Figure 3.9.

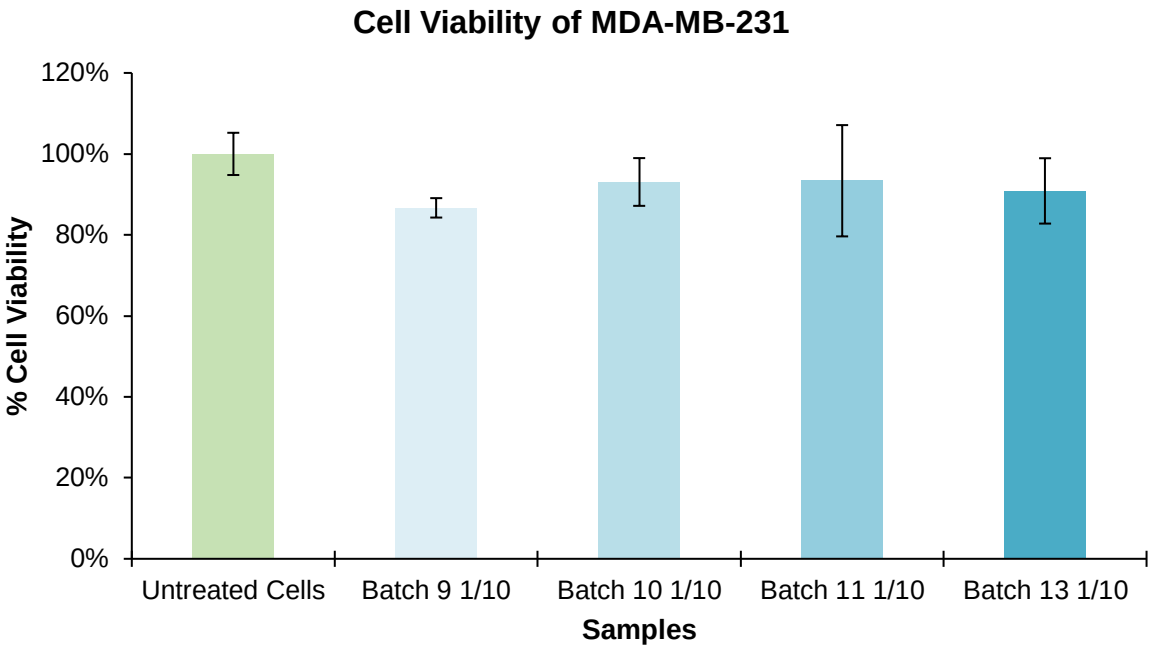

Figure 3.8 – Cytotoxic effect of HER2-specific VLPs on MDA-MB-231 cells. Batches 9, 10, 11 and 13 diluted at 1/10 were tested in triplicate on MDA-MB-231 cells, which lack HER2 overexpression. Error bars represent the 95% confidence interval for the mean.

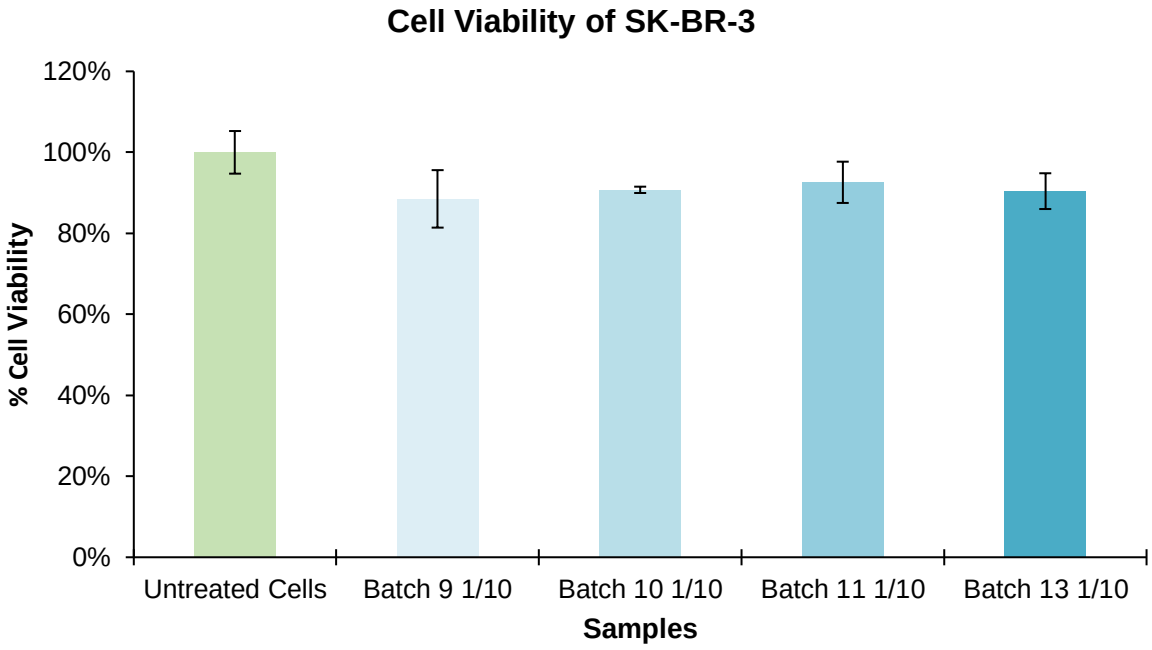

Figure 3.9 – Cytotoxic effect of HER2-specific VLPs on SK-BR-3 cells. Batches 9, 10, 11 and 13 diluted at 1/10 were tested in triplicate on SK-BR-3 cells, which display HER2 overexpression. Error bars represent the 95% confidence interval for the mean.

There is no significant difference between MDA-MB-231 and SK-BR-3 cells, and the cell viability of treated cells is not significantly lower than the cell viability of untreated cells. Furthermore, there is no significant difference between batches. These results seem to suggest that HER2-specific VLPs are not cytotoxic under the tested concentrations. The VLPs were originally suspended in spent medium from the transfection of HEK-293T cells. This medium could contain exosomes and proteins that could influence cell growth. This prompted the resuspension of VLPs in PBS, to eliminate extrinsic effects. Notwithstanding, given the small volumes of VLPs that were obtained, it was only possible to test a 1/10 dilution. Higher concentrations should be tested to evaluate whether the constructed VLPs are indeed not cytotoxic to the cells.

3.8 HIV-1-Based VLP Production and Quantification

One batch of HIV-1 Gag VLPs was produced as control through transient transfection of HEK-293T cells using pMDLg/RRE and pRSV-REV, at a 1:1 ratio (Section 2.6.1). Following production, the HIV-1-based VLPs were first concentrated through Amicon® Ultra centrifugal ultrafiltration (Section 2.7), but 1 mL of PBS was used to elute the retentate, instead of 5 mL. The protein concentration of the obtained HIV-1-based VLPs was evaluated through p24 ELISA (Section 2.8), and the attained concentration was 0. Amicon® Ultra centrifugal ultrafiltration can be used for the concentration of biological samples containing antibodies, antigens, enzymes, nucleic acids or viruses[132,133]. The protocol varies according to the sample, and it is possible that elution with PBS is not the most adequate method for HIV-1-based VLP concentration. VLPs could instead be recovered directly from the membrane or by reverse spinning, and then be re-suspended in PBS. It is also possible that the molecular weight cut-off of 50 kDa is not the most adequate for the size of HIV-1-based VLPs, and other molecular weight cut-offs could be tested.

The Lenti-X™ Concentrator was thus used to concentrate the remaining HIV-1-based VLPs (Section 2.7). The protein concentration of the obtained HIV-1-based VLPs was evaluated through p24 ELISA (Section 2.8), and the attained concentration was 3116.25 pg/mL. This concentration is due to the lack of pX1665, which implicates the use of higher quantities of both pMDLg/pRRE and pRSV-REV for transient transfection and consequent higher protein concentration of HIV-1-based VLPs. The condition of the cells employed for transient transfection, which had an adequate morphology and were confluent, also influenced production.

3.9 HER2-Specific VLP Production and Quantification for Radiolabelling

Five batches of HER2-specific VLPs were produced for radiolabelling using pX1665+His, together with pMDLg/RRE and pRSV-REV, at a 1:1:1 ratio (Section 2.6.3). All batches were then concentrated with the Lenti-X™ Concentrator (Section 2.7). The protein concentration of the obtained HER2-specific VLPs was determined through p24 ELISA (Section 2.8). The obtained concentrations are presented in Table 3.8.

Table 3.8 – Quantification of p24 protein of batches 15 to 19 of HER2-specific VLPs.

Batches	[VLP] (pg/mL)
15	1795.89
16	2082.91
17	1781.12
18	1665.00
19	1970.21

The concentrations for batches 15 to 19 following concentration with the Lenti-X™ Concentrator are considerably higher than the ones obtained for the other batches that were concentrated with the same method. When constructing the pX1665+His plasmid for radiolabelling, it was observed that the Myc-tag, a tag fused to the C-terminal of the scFv-HER2_gp41 sequence, was out of frame in the original pX1665 plasmid and was therefore not being expressed. Furthermore, it was adding an extra sequence of amino acids to the protein of interest. This was likely hindering the assembly of HER2-specific VLPs and therefore diminishing the obtained concentrations for the previous batches. This issue was corrected in the pX1665+His plasmid, which was used for the production of batches 15 to 19. This could explain the higher concentrations, although it is necessary to ascertain the incorporation of the protein of interest. Furthermore, the cells used for the production of these batches were in the same conditions as the cells used for the production of the control batch, which also influenced the process yield.

3.10 Characterization of HER2-Specific VLPs for Radiolabelling

3.10.1 Presence of the Anti-HER2 scFv in Novel HER2-Specific VLPs for Radiolabelling

Despite obtaining high concentrations, it was not possible to confirm the presence of the protein of interest in these batches (results not shown). This indicates that transfection with pX1665+His was not successful, which can be attributed to the inefficient DNA extraction of the pX1665+His plasmid. The ratios and concentration obtained following DNA extraction are depicted in Table 3.9. The previously constructed and extracted pX1665 plasmid was also tested for comparison.

Table 3.9 – Plasmid DNA quantification.

	Concentration (µg/mL)	Purity (A_{260}/A_{280})	Purity (A_{260}/A_{230})
pX1665+His	130.5	1.874	0.033
pX1665	606.3	2.058	2.099

The attained values indicate that pX1665+His was extracted at a lower concentration than the previously extracted pX1665 plasmid. The maximum absorbance of nucleic acids is 260 nm, whereas the maximum absorbance of proteins is 280 nm[134]. The ratio of these absorbances is typically used to assess the purity in both nucleic acid and protein extractions[134]. A ratio of around 1.8 is generally indicative of DNA purity[134]. Likewise, absorbance at 230 nm is associated with contamination, and therefore the ratio between the absorbance at 260 nm and the absorbance at 230 nm is also used as a purity measurement[134]. Values for pure nucleic acids are around 2[134]. The A_{260}/A_{230} ratio of pX1665+His is much lower than the one obtained for pX1665, indicating that the obtained DNA was not pure, likely because the bacterial pellet was too large for the extraction kit. Transfection of the pX1665+His was therefore unsuccessful and the constructed VLPs did not possess the anti-HER2 scFv.

3.11 Novel HER2-Specific VLP Production and Quantification for Radiolabelling

A novel DNA extraction was performed with a smaller bacterial pellet. pX1665+His was extracted at a concentration of 253.1 µg/mL, a A_{260}/A_{280} ratio of 2.049 and a A_{260}/A_{230} ratio of 1.564. These values are more similar to the ones described in literature for pure nucleic acids, and therefore a novel transfection protocol was performed with the extracted pX1665+His plasmid. Six new batches of HER2-specific VLPs were thus produced for radiolabelling, using pX1665+His, pMDLg/RRE and pRSV-REV, at a 1:1:1 ratio (Section 2.6.3). Batch 20 was first concentrated through Amicon® Ultra centrifugal ultrafiltration (Section 2.7) and the retentate was retrieved directly from the membrane, instead of being eluted by PBS. The protein concentration was determined through p24 ELISA (Section 2.8) and the obtained value was 241.8 pg/mL, which is significantly lower than the values obtained with the Lenti-X™ Concentrator and confirms that Amicon® Ultra centrifugal ultrafiltration with a molecular weight cut-off of 50 kDa is not adequate for HIV-1-based VLP concentration. The remaining volume of batch 20 and the other batches were thus concentrated with the Lenti-X™ Concentrator (Section 2.7). The protein concentration of the obtained HER2-specific VLPs was then determined through p24 ELISA (Section 2.8), and the attained values are depicted in Table 3.10.

Table 3.10 – Quantification of p24 protein of batches 20 to 25 of HER2-specific VLPs.

Batches	[VLP] (pg/mL)
20	1281.53
21	835.46
22	1477.08
23	1295.67
24	1474.61
25	927.63

The concentrations of batches 20 to 25 following concentration with the Lenti-X™ Concentrator are higher than the ones obtained for concentrated batches 9 to 14 but lower than the ones obtained for concentrated batches 15 to 19. This was expected, because the pX1665 plasmid, which was used for the production of batches 9 to 14, contained an extra amino acid sequence that could affect VLP assembly. Batches 15 to 19, on the other hand, did not incorporate the plasmid of interest, meaning that only HIV-1 Gag VLPs were formed, and assembly was likely easier to occur, which explains the attained values.

3.12 Characterization of Novel HER2-Specific VLPs for Radiolabelling

3.12.1 Presence of the Anti-HER2 scFv in Novel HER2-Specific VLPs for Radiolabelling

To confirm whether DNA extraction was successful, and the protein of interest is expressed, a Western Blot analysis was performed.

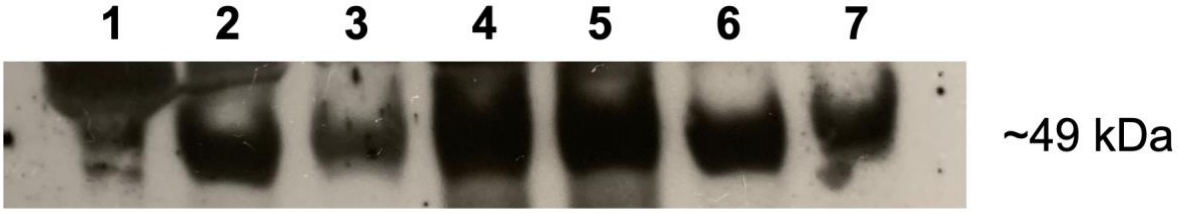

Figure 3.10 – Western Blot analysis of batches 20 to 25. Western Blot detection performed with an anti-HA monoclonal antibody (1:2000) and an anti-mouse secondary antibody (1:3000). Lane 1: positive control (batch 4); lane 2: batch 20; lane 3: batch 21; lane 4: batch 22; lane 5: batch 23; lane 6: batch 24; lane 7: batch 25. Visualization of the bands was performed with the ECL® reagent.

Western Blot analysis was first conducted with a HRP-conjugated anti-HA polyclonal antibody, but no bands were observed (results not shown). Notwithstanding, Western Blot analysis with the anti-HA monoclonal antibody revealed clear bands with a molecular weight of around 49 kDa (Figure 3.10). This value is in agreement with the previously described theoretical value[122], which indicates that the novel DNA extraction was successful and that the scFv-HER2_gp41 recombinant protein is present in the VLPs of batches 20 to 25. Batch 4, which had been previously evaluated through Western Blot with both anti-HA monoclonal and polyclonal antibodies, was employed as a positive control for comparison. As can be seen in Figure 3.3, it was possible to visualize a band for batch 4 with the HRP-conjugated anti-HA polyclonal antibody, which is not in accordance with the results obtained with the same antibody in this section. It is possible that the signal obtained with the HRP-conjugated anti-HA polyclonal antibody was lost due to repeated usage.

Despite the apparent presence of the anti-HER2 scFv in the constructed VLPs, it is important to confirm these results with another antibody, namely an antibody against the Myc-tag, or an antibody against gp41. The HA-tag derives from influenza virus A and is commonly used as a protein tag for Western Blot analysis and immunoprecipitation[135]. Notwithstanding, non-specific patterns were

observed in the performed Western Blot analysis, which can indicate that anti-HA antibodies lack specificity. It would thus be important to test other antibodies to observe whether the obtained bands overlap with the bands detected with the anti-HA antibodies and consequently validate the presence of the anti-HER2 scFv in the produced VLPs.

3.12.2 Morphological Characterization of Novel HER2-Specific VLPs for Radiolabelling

After producing different VLP batches for uptake and confirming that they possess the anti-HER2 scFv, a morphological characterization was performed. Batches 22 and 24 were selected for TEM analysis due to their concentrations (Table 3.10). The HIV-1 Gag VLP control batch was also chosen for TEM, with the aim of comparing the morphology of wild-type HIV-1 Gag VLPs and HER2-specific VLPs.

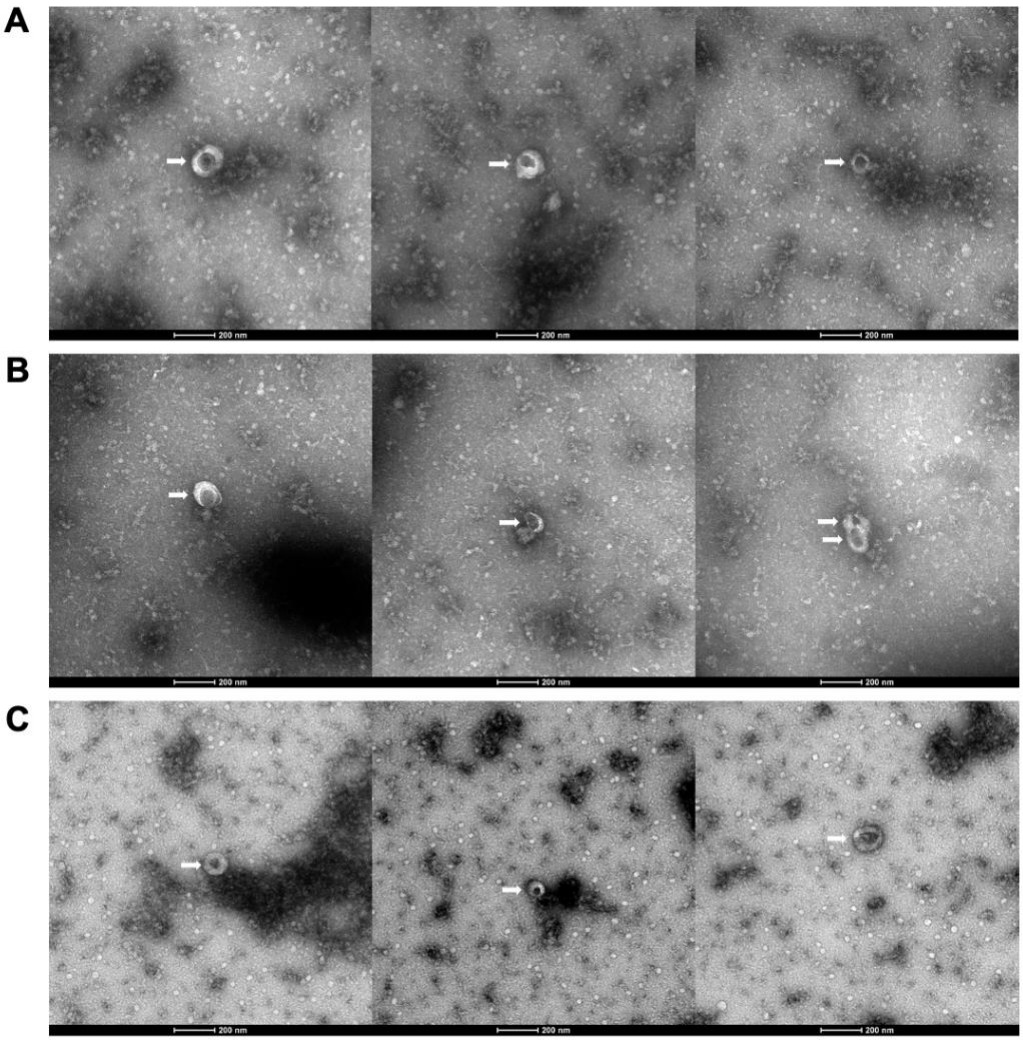

Figure 3.11 – TEM analysis of control batch and batches 22 and 24. (A) Control batch. Scale bar = 200 nm. (B) Batch 22. Scale bar = 200 nm. (C) Batch 24. Scale bar = 200 nm. Images taken at 60K.

The TEM images (Figure 3.11) reveal that VLP assembly occurred, with VLPs displaying the expected size[37,128] (Table 3.11). Furthermore, the morphology presented by HER2-specific VLPs (Figure 3.11 - B and C) does not differ from the morphology exhibited by HIV-1 Gag VLPs (Figure 3.11 - A). This suggests that the incorporation of a targeting moiety, like the anti-HER2 scFv, does not hamper VLP assembly. Negative staining is thus an adequate method to determine VLP morphology. Nevertheless, it would be important to perform immunogold labelling for TEM analysis, given that this technique relies on gold-labelled antibodies to localize specific proteins and consequently quantify their signals[136]. It would therefore be possible to observe the anti-HER2 scFv, determine its distribution and quantify its signal in the constructed VLPs, which would provide valuable information for downstream assays.

Table 3.11 – Size characterization of control batch and batches 22 and 24 of HER2-specific VLPs. SD stands for standard deviation. Size determined by ImageJ.

Batches	Size ± SD (nm)
Control	114.17 ± 20.36
22	121.08 ± 12.48
24	136.81 ± 9.83

3.13 Cytotoxic Evaluation of Novel HER2-Specific VLPs for Radiolabelling

The concentrations for batches 20, 22, 23 and 24 (Table 3.10) prompted the selection of these batches for the cytotoxicity assay. These batches were thus diluted at 1/10 in PBS and incubated with MDA-MB-231 and SK-BR-3 cells in triplicate. Cell proliferation of the cells treated with HER2-specific HIV-1-based VLPs for radiolabelling was compared with the cell proliferation of untreated cells. VLPs in PBS and cell culture medium were employed as controls.

Cell viability was obtained through Equation 2 and the results are depicted in Table 3.12.

Table 3.12 – Cell viability of MDA-MB-231 and SK-BR-3 cells treated with HER2-specific VLPs for radiolabelling.

Samples	% Cell viability	
	MDA-MB-231	**SK-BR-3**
Batch 20 1/10	113.488	116.281
Batch 22 1/10	119.205	119.000
Batch 23 1/10	111.511	105.247
Batch 24 1/10	132.496	106.497

The attained results for MDA-MB-231 cells are depicted in Figure 3.12 and the obtained results for SK-BR-3 cells are represented in Figure 3.13.

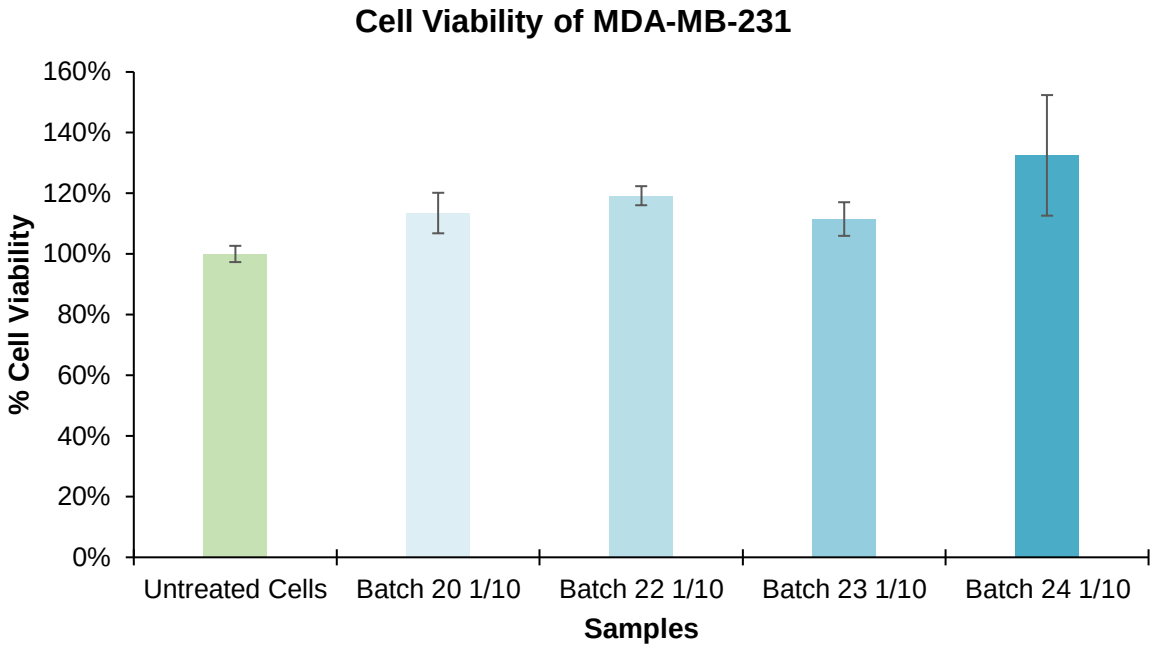

Figure 3.12 – Cytotoxic effect of HER2-specific VLPs for radiolabelling on MDA-MB-231 cells. Batches 20, 22, 23 and 24 diluted at 1/10 were tested in triplicate on MDA-MB-231 cells, which lack HER2 overexpression. Error bars represent the 95% confidence interval for the mean.

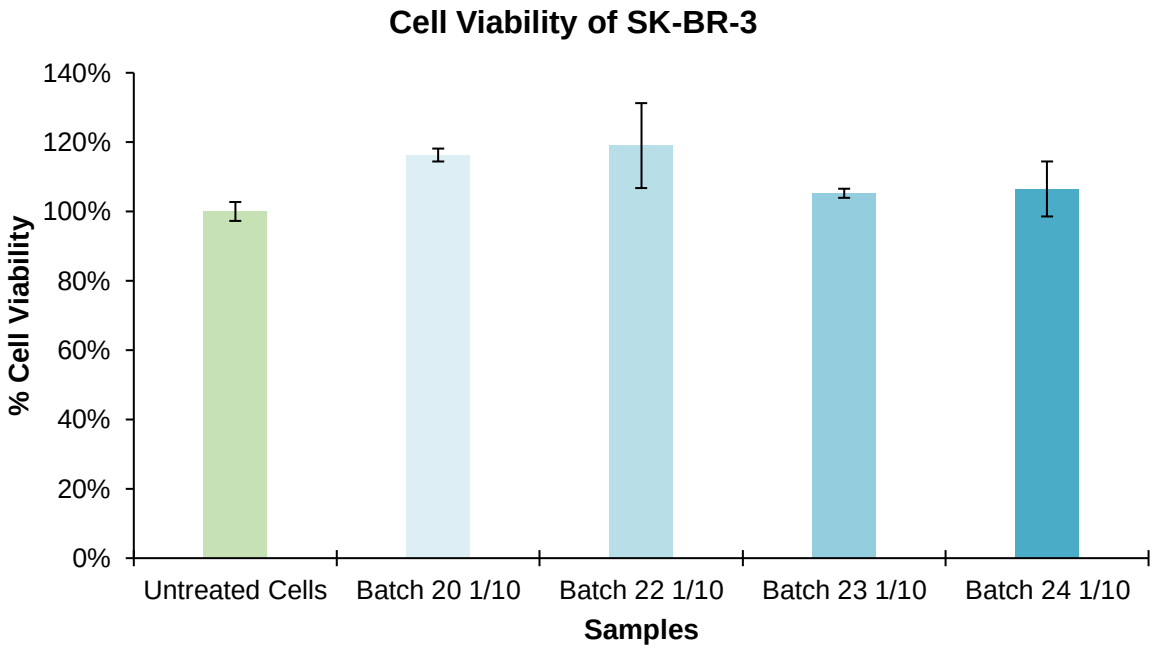

Figure 3.13 – Cytotoxic effect of HER2-specific VLPs for radiolabelling on SK-BR-3 cells. Batches 20, 22, 23 and 24 diluted at 1/10 were tested in triplicate on SK-BR-3 cells, which display HER2 overexpression. Error bars represent the 95% confidence interval for the mean.

Strikingly, the cell viability of both MDA-MB-231 and SK-BR-3 cells following treatment with the produced VLPs is higher than the cell viability of untreated cells. Furthermore, following statistical analysis, it was possible to observe a significant difference between batches. These results contrast with the previously obtained results for batches 9, 10, 11 and 13, and could be explained by experimental errors or the existence of proteins or exosomes in the collected samples, which could influence cell growth. As aforementioned, this prompts the production of further HER2-specific HIV-1-based VLPs and subsequent cytotoxicity assays with different dilutions to ascertain the effect that the designed VLPs have on the cells.

3.14 Radiolabelling of HER2-Specific VLPs with Technetium-99m

Technetium (Tc), number 43 on the periodic table, was the first element to be fabricated[137]. It was first produced through the bombardment of molybdenum (Mo) atoms with deuterons, and is currently manufactured via bombardment of Mo-98 with neutrons[137]. Mo-98 turns into Mo-99 after acquiring a neutron, which in turn decays to Tc-99[137]. Tc-99 is one of the three long lived isotopes of Tc, together with Tc-97 and Tc-98[137]. Tc-99m, or ^{99m}Tc, is a short lived version of Tc-99, with a half-life of around 6 h, and is widely explored in the medical field, namely for imaging and diagnosis[137-139]. It is attained through decay of molybdenum-99 and is employed for SPECT (Figure 3.14)[137,138]. More importantly, it can be used to label biologically active samples and consequently accompany their movement[137].

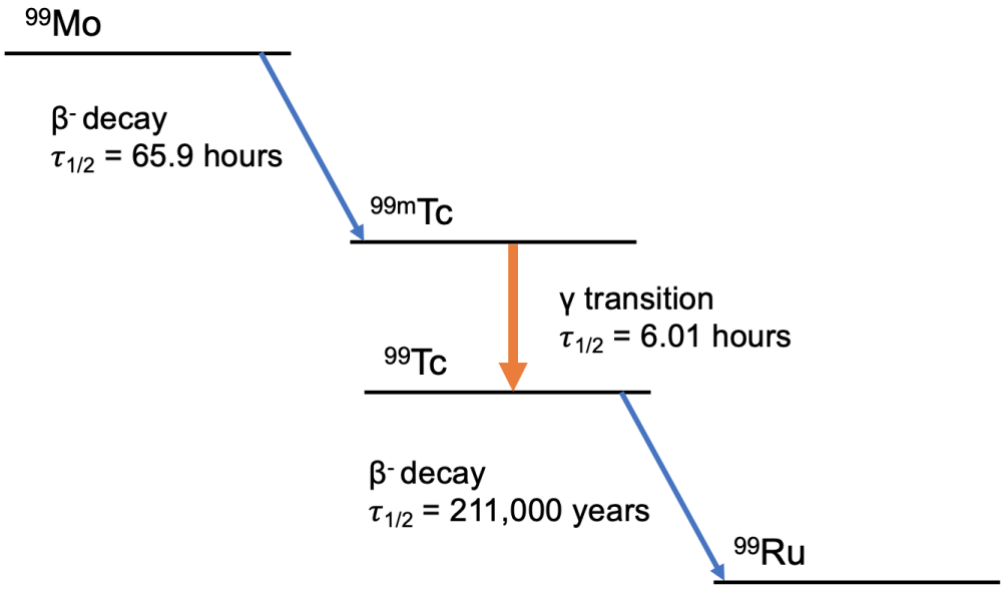

Figure 3.14 – Decay scheme of ^{99}Mo. Adapted from *Capogni, M. et al*.[140].

Tc complexes have typically relied on Tc in its +5 oxidation state[141,142]. Notwithstanding, ^{99m}Tc in the form of ^{99m}Tc-tricarbonyl ($[^{99m}Tc(CO)_3]^+$), with Tc in its +1 oxidation state, has proven to be more advantageous[142,143]. This organometallic compound is attained in its aqua-ion form *fac*-$[^{99m}Tc(CO)_3(H_2O)_3]^+$, following reduction of generator-eluted sodium pertechnetate ($[^{99m}TcO_4]^-$). A technetium labelling approach was developed through simple mixing of *fac*-$[^{99m}Tc(CO)_3]^+$ with His-tagged proteins, given that histidine has been described as the preferred *fac*-$[^{99m}Tc(CO)_3]^+$-binding ligand[142-144]. The pX1665 plasmid was thus altered, and a His-tag was incorporated into the scFv-HER2_gp41 sequence for radiolabelling with *fac*-$[^{99m}Tc(CO)_3]^+$.

Batch 21 was the His-tagged batch with the lowest concentration (Table 3.10), and was therefore chosen for the first radiolabelling assay, to ascertain whether it is possible to radiolabel the constructed VLPs. A small quantity of VLPs, 10.44 pg, was mixed with *fac*-$[^{99m}Tc(CO)_3]^+$ in a 1:1 ratio, incubated at 37 °C and analysed through ITLC at three different timeframes: 30, 60 and 90 min. $[^{99m}Tc(CO)_3]^+$ was also tested.

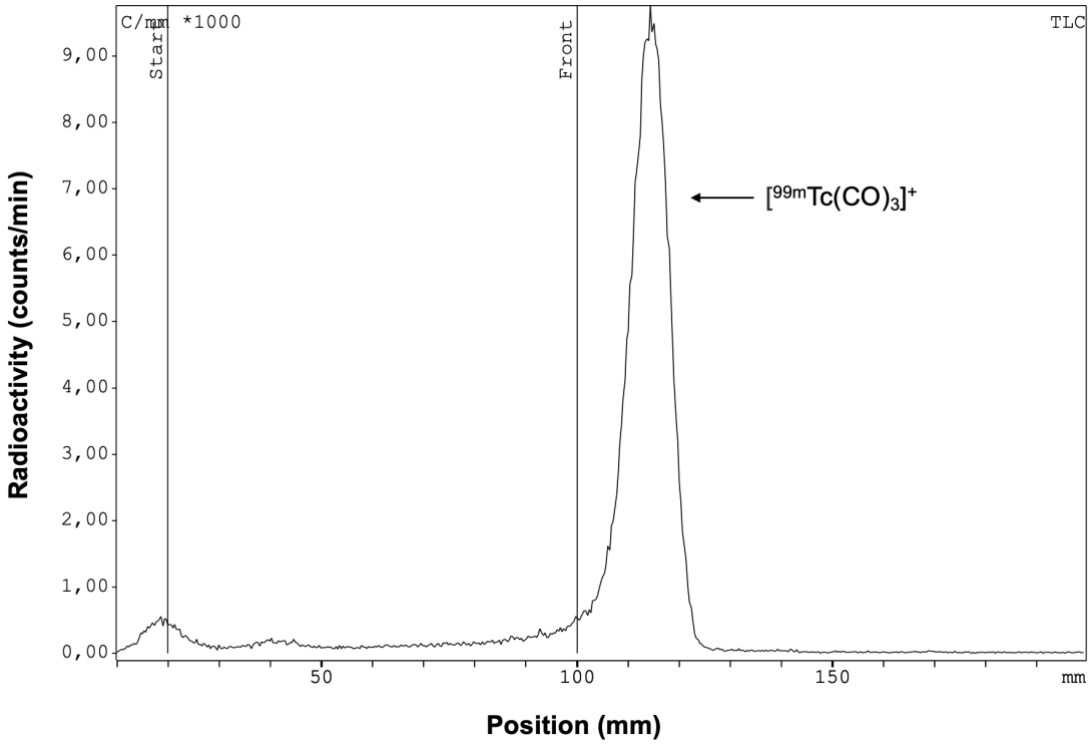

Figure 3.15 – ITLC chromatogram of $[^{99m}Tc(CO)_3]^+$. Sodium citrate buffer was used as a mobile phase.

$[^{99m}Tc(CO)_3]^+$ migrated with the solvent front, and no peak is observed at the application point (Figure 3.15), which suggests that *fac*-$[^{99m}Tc(CO)_3]^+$ was attained with high radiochemical purity (> 95%).

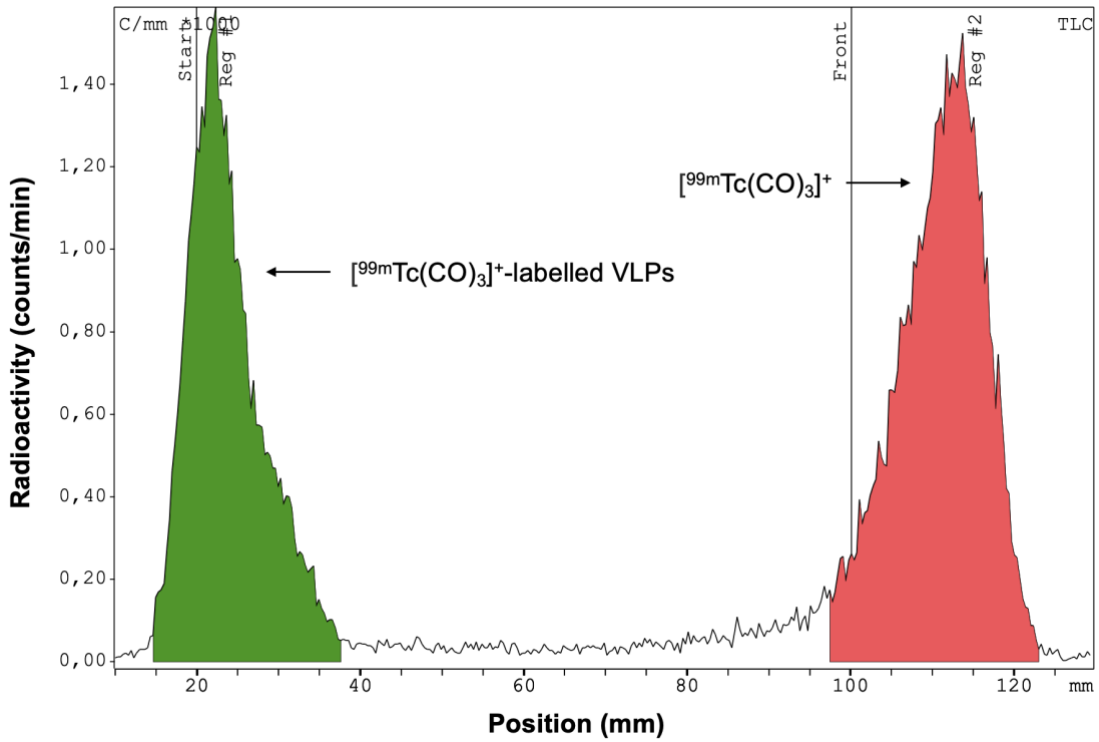

Figure 3.16 – ITLC chromatogram of $[^{99m}Tc(CO)_3]^+$-labelled VLPs. Incubation of VLPs with *fac*-$[^{99m}Tc(CO)_3]^+$ was carried out for 30 minutes. Sodium citrate buffer was used as eluent.

The first radiolabelling test was conducted at a timeframe of 30 minutes. Through the obtained chromatogram (Figure 3.16), it was possible to ascertain the radiolabelling efficiency, which was 44.23%. Other timeframes were tested, to assess whether time is a limiting factor for VLP radiolabelling. A radiolabelling efficiency of 49.9% was achieved following incubation for 60 min, whereas with the 90 min timeframe, 56.04% of the VLPs were radiolabelled. These preliminary results show that the incorporation of the His-tag permitted the radiolabelling of the constructed VLPs. Furthermore, the increase in radiolabelling efficiency with different timeframes was negligible, which indicates that the 30 min timeframe is sufficient for radiolabelling. It was only possible to efficiently label around half of the VLPs, which is attributable to the small quantity that was tested. Larger quantities should therefore be used in further tests for optimization. Moreover, purification with centrifugal filters could be performed. After establishing the optimal conditions for radiolabelling, stability of the labelled VLPs should be assessed in PBS and cell medium. Uptake studies with HER2-overexpressing cells and cells that lack HER2 overexpression could then be performed to determine whether the constructed VLPs can bind specifically to HER2. Affinity studies could also be conducted, after which imaging and therapeutic agents could be conjugated to the VLPs.

4

CONCLUSIONS

The aim of this project was to construct and characterize HIV-1-based VLPs that were modified with an anti-HER2 scFv, for targeted delivery to HER2-overexpressing cancer cells.

HER2-specific VLPs were successfully constructed in HEK-293T cells through transient transfection of the previously constructed pX1665 plasmid[122], together with pMDLg/pRRE, and pRSV-REV, using the Lipofectamine™ 3000 Transfection Reagent. Cell conditions, specifically confluence and morphology, were shown to be critical factors for transfection efficiency, and must be considered when assembling VLPs. HIV-1 Gag VLPs were also produced for morphological comparison with HER2-specific VLPs. A redesign of the pX1665 plasmid was then performed, with the addition of a His-tag to the scFv-HER2_gp41 sequence for radiolabelling purposes. VLPs constructed with this novel plasmid were also successfully assembled. All VLPs were quantified through p24 ELISA, and the obtained concentrations were in accordance with the literature[37].

Following production, the VLPs were characterized through Western Blot and TEM. Western Blot assays with anti-HA antibodies confirmed that the anti-HER2 scFv is present in the constructed VLPs. TEM analyses revealed that VLP assembly occurred and with the described size and morphology[37,96].

Cytotoxicity assays to measure cell viability upon treatment with the constructed VLPs were then conducted. The obtained results suggest that the constructed VLPs are not cytotoxic to cells, and no remarkable difference was observed between HER2-overexpressing cells (SK-BR-3) and cells that lack HER2 overexpression (MDA-MB-231).

Lastly, preliminary radiolabelling studies showed that His-tagged VLPs can be successfully radiolabelled with *fac*-$[^{99m}Tc(CO)_3]^+$.

Taken together, the findings hereby presented establish a protocol for the development of modified HIV-1-based VLPs. HER2 was chosen as a target due to its well-described role in cancer, a disease with ever-growing relevance that needs to be tackled. This work thus paves the way for the development of a novel targeted delivery tool that can be harnessed for different targets in numerous pathologies, namely cancer.

5

FUTURE PERSPECTIVES

Considering the results obtained in this thesis, it is necessary to confirm the presence of the anti-HER2 scFv in the constructed VLPs through Western Blot with other antibodies, given that anti-HA antibodies exhibit non-specific patterns. It would be important to repeat the Western Blot assays with antibodies against the Myc-tag or against gp41, both of which are present in the pX1665 plasmid. If the detected bands overlap with the bands obtained with anti-HA antibodies, then the expression of the anti-HER2 scFv in the produced VLPs will be validated. Immunogold labelling studies should also be carried out to observe the scFv in the VLPs and quantify its signal. Cytotoxicity assays should be repeated with higher VLP concentrations to uncover the cytotoxic effect of the developed VLPs. Lastly, optimization of the radiolabelling studies should be performed to achieve higher radiolabelling efficiency.

The next steps include cell uptake studies with radiolabelled VLPs to assess whether the VLPs bind specifically to the HER2 receptor, cell-binding assays with radiolabelled VLPs and trastuzumab to measure the equilibrium dissociation constant, incorporation of therapeutic and/or imaging agents and *in vivo* studies. These strategies would permit to set the designed VLP as a targeted delivery vessel with the ability to be employed in the clinical setting.

REFERENCES

1. Collaborators, G. B. D. D. (2020). Global Age-Sex-Specific Fertility, Mortality, Healthy Life Expectancy (HALE), and Population Estimates in 204 Countries and Territories, 1950-2019: A Comprehensive Demographic Analysis for the Global Burden of Disease Study 2019. *Lancet*, *396*(10258), 1160-1203. https://doi.org/10.1016/S0140-6736(20)30977-6

2. Zhang, X. (2015). Precision Medicine, Personalized Medicine, Omics and Big Data: Concepts and Relationships. *J Pharmacogenomics Pharmacoproteomics*, *6*(1), 1000e1144.

3. Collins, F. S. (1999). The Human Genome Project and the Future of Medicine. *Ann N Y Acad Sci*, *882*, 42-55; discussion 56-65. https://doi.org/10.1111/j.1749-6632.1999.tb08532.x

4. Konig, I. R., Fuchs, O., Hansen, G., von Mutius, E., & Kopp, M. V. (2017). What Is Precision Medicine? *Eur Respir J*, *50*(4). https://doi.org/10.1183/13993003.00391-2017

5. Collins, F. S., & Varmus, H. (2015). A New Initiative on Precision Medicine. *N Engl J Med*, *372*(9), 793-795. https://doi.org/10.1056/NEJMp1500523

6. Ho, D., Quake, S. R., McCabe, E. R. B., Chng, W. J., Chow, E. K., Ding, X., Gelb, B. D., Ginsburg, G. S., Hassenstab, J., Ho, C. M., Mobley, W. C., Nolan, G. P., Rosen, S. T., Tan, P., Yen, Y., & Zarrinpar, A. (2020). Enabling Technologies for Personalized and Precision Medicine. *Trends Biotechnol*, *38*(5), 497-518. https://doi.org/10.1016/j.tibtech.2019.12.021

7. Joyner, M. J., & Paneth, N. (2019). Promises, Promises, and Precision Medicine. *J Clin Invest*, *129*(3), 946-948. https://doi.org/10.1172/JCI126119

8. Bilkey, G. A., Burns, B. L., Coles, E. P., Mahede, T., Baynam, G., & Nowak, K. J. (2019). Optimizing Precision Medicine for Public Health. *Front Public Health*, *7*, 42. https://doi.org/10.3389/fpubh.2019.00042

9. Ashley, E. A. (2016). Towards Precision Medicine. *Nat Rev Genet*, *17*(9), 507-522. https://doi.org/10.1038/nrg.2016.86

10. Ashley, E. A. (2015). The Precision Medicine Initiative: A New National Effort. *JAMA*, *313*(21), 2119-2120. https://doi.org/10.1001/jama.2015.3595

11. Sung, H., Ferlay, J., Siegel, R. L., Laversanne, M., Soerjomataram, I., Jemal, A., & Bray, F. (2021). Global Cancer Statistics 2020: GLOBOCAN Estimates of Incidence and Mortality Worldwide for 36 Cancers in 185 Countries. *CA Cancer J Clin*, *71*(3), 209-249. https://doi.org/10.3322/caac.21660

12. Padma, V. V. (2015). An Overview of Targeted Cancer Therapy. *Biomedicine (Taipei)*, *5*(4), 19. https://doi.org/10.7603/s40681-015-0019-4

13. Zhong, L., Li, Y., Xiong, L., Wang, W., Wu, M., Yuan, T., Yang, W., Tian, C., Miao, Z., Wang, T., & Yang, S. (2021). Small Molecules in Targeted Cancer Therapy: Advances, Challenges, and Future Perspectives. *Signal Transduct Target Ther*, *6*(1), 201. https://doi.org/10.1038/s41392-021-00572-w

14. Institute, N. C. (2022). *Targeted Cancer Therapies*. Retrieved April 27, 2022 from https://www.cancer.gov/about-cancer/treatment/types/targeted-therapies/targeted-therapies-fact-sheet

15. American Cancer, S. (2021). *How Targeted Therapies Are Used to Treat Cancer*. Retrieved April 29, 2022 from https://www.cancer.org/treatment/treatments-and-side-effects/treatment-types/targeted-therapy/what-is.html

16. Lee, Y. T., Tan, Y. J., & Oon, C. E. (2018). Molecular Targeted Therapy: Treating Cancer with Specificity. *Eur J Pharmacol*, *834*, 188-196. https://doi.org/10.1016/j.ejphar.2018.07.034

17. Mitchell, M. J., Billingsley, M. M., Haley, R. M., Wechsler, M. E., Peppas, N. A., & Langer, R. (2021). Engineering Precision Nanoparticles for Drug Delivery. *Nat Rev Drug Discov*, *20*(2), 101-124. https://doi.org/10.1038/s41573-020-0090-8

18. Kim, B. Y., Rutka, J. T., & Chan, W. C. (2010). Nanomedicine. *N Engl J Med*, *363*(25), 2434-2443. https://doi.org/10.1056/NEJMra0912273

19. Chenthamara, D., Subramaniam, S., Ramakrishnan, S. G., Krishnaswamy, S., Essa, M. M., Lin, F. H., & Qoronfleh, M. W. (2019). Therapeutic Efficacy of Nanoparticles and Routes of Administration. *Biomater Res*, *23*, 20. https://doi.org/10.1186/s40824-019-0166-x

20. Chen, G., Roy, I., Yang, C., & Prasad, P. N. (2016). Nanochemistry and Nanomedicine for Nanoparticle-based Diagnostics and Therapy. *Chem Rev*, *116*(5), 2826-2885. https://doi.org/10.1021/acs.chemrev.5b00148

21. Pattni, B. S., Chupin, V. V., & Torchilin, V. P. (2015). New Developments in Liposomal Drug Delivery. *Chem Rev*, *115*(19), 10938-10966. https://doi.org/10.1021/acs.chemrev.5b00046

22. Allen, T. M., & Cullis, P. R. (2013). Liposomal Drug Delivery Systems: From Concept to Clinical Applications. *Adv Drug Deliv Rev*, *65*(1), 36-48. https://doi.org/10.1016/j.addr.2012.09.037

23. Elsabahy, M., & Wooley, K. L. (2012). Design of Polymeric Nanoparticles for Biomedical Delivery Applications. *Chem Soc Rev*, *41*(7), 2545-2561. https://doi.org/10.1039/c2cs15327k

24. Zielinska, A., Carreiro, F., Oliveira, A. M., Neves, A., Pires, B., Venkatesh, D. N., Durazzo, A., Lucarini, M., Eder, P., Silva, A. M., Santini, A., & Souto, E. B. (2020). Polymeric Nanoparticles: Production, Characterization, Toxicology and Ecotoxicology. *Molecules*, *25*(16). https://doi.org/10.3390/molecules25163731

25. Auffan, M., Rose, J., Bottero, J. Y., Lowry, G. V., Jolivet, J. P., & Wiesner, M. R. (2009). Towards a Definition of Inorganic Nanoparticles from an Environmental, Health and Safety Perspective. *Nat Nanotechnol*, *4*(10), 634-641. https://doi.org/10.1038/nnano.2009.242

26. Xu, Z. P., Zeng, Q. H., Lu, G. Q., & Yu, A. B. (2006). Inorganic Nanoparticles as Carriers for Efficient Cellular Delivery. *Chemical Engineering Science*, *61*(3), 1027-1040.

27. Gustafson, H. H., Holt-Casper, D., Grainger, D. W., & Ghandehari, H. (2015). Nanoparticle Uptake: The Phagocyte Problem. *Nano Today*, *10*(4), 487-510. https://doi.org/10.1016/j.nantod.2015.06.006

28. Nooraei, S., Bahrulolum, H., Hoseini, Z. S., Katalani, C., Hajizade, A., Easton, A. J., & Ahmadian, G. (2021). Virus-Like Particles: Preparation, Immunogenicity and Their Roles as Nanovaccines and Drug Nanocarriers. *J Nanobiotechnology*, *19*(1), 59. https://doi.org/10.1186/s12951-021-00806-7

29. Rohovie, M. J., Nagasawa, M., & Swartz, J. R. (2017). Virus-Like Particles: Next-Generation Nanoparticles for Targeted Therapeutic Delivery. *Bioeng Transl Med*, *2*(1), 43-57. https://doi.org/10.1002/btm2.10049

30. Zeltins, A. (2013). Construction and Characterization of Virus-Like Particles: A Review. *Mol Biotechnol*, *53*(1), 92-107. https://doi.org/10.1007/s12033-012-9598-4

31. Zdanowicz, M., & Chroboczek, J. (2016). Virus-Like Particles as Drug Delivery Vectors. *Acta Biochim Pol*, *63*(3), 469-473. https://doi.org/10.18388/abp.2016_1275

32. Mohsen, M. O., Zha, L., Cabral-Miranda, G., & Bachmann, M. F. (2017). Major Findings and Recent Advances in Virus-Like Particle (VLP)-Based Vaccines. *Semin Immunol*, *34*, 123-132. https://doi.org/10.1016/j.smim.2017.08.014

33. Bayer, M. E., Blumberg, B. S., & Werner, B. (1968). Particles Associated with Australia Antigen in the Sera of Patients with Leukaemia, Down's Syndrome and Hepatitis. *Nature*, *218*(5146), 1057-1059. https://doi.org/10.1038/2181057a0

34. Benjamin, C., Brohlin, O., Shahrivarkevishahi, A., & Gassensmith, J. J. (2020). Virus Like Particles: Fundamental Concepts, Biological Interactions, and Clinical Applications. *Nanoparticles for Biomedical Applications*, 153-174.

35. Lua, L. H., Connors, N. K., Sainsbury, F., Chuan, Y. P., Wibowo, N., & Middelberg, A. P. (2014). Bioengineering Virus-Like Particles as Vaccines. *Biotechnol Bioeng*, *111*(3), 425-440. https://doi.org/10.1002/bit.25159

36. Buffin, S., Peubez, I., Barriere, F., Nicolai, M. C., Tapia, T., Dhir, V., Forma, E., Seve, N., & Legastelois, I. (2019). Influenza A and B Virus-Like Particles Produced in Mammalian Cells Are Highly Immunogenic and Induce Functional Antibodies. *Vaccine*, *37*(46), 6857-6867. https://doi.org/10.1016/j.vaccine.2019.09.057

37. Gonelli, C. A., Khoury, G., Center, R. J., & Purcell, D. F. J. (2019). HIV-1-Based Virus-Like Particles that Morphologically Resemble Mature, Infectious HIV-1 Virions. *Viruses*, *11*(6). https://doi.org/10.3390/v11060507

38. Nanbo, A., Maruyama, J., Imai, M., Ujie, M., Fujioka, Y., Nishide, S., Takada, A., Ohba, Y., & Kawaoka, Y. (2018). Ebola Virus Requires a Host Scramblase for Externalization of Phosphatidylserine on the Surface of Viral Particles. *PLoS Pathog*, *14*(1), e1006848. https://doi.org/10.1371/journal.ppat.1006848

39. Sanchooli, A., Aghayipour, K., Naghlani, S. K., Samiee, Z., Kiasari, B. A., & Makvandi, M. (2020). Production of Human Papillomavirus Type-16 L1 VLP in *Pichia pastoris*. *Applied Biochemistry and Microbiology*, *56*(1), 51-57. https://doi.org/10.1134/S0003683820010147

40. Pogan, R., Weiss, V. U., Bond, K., Dulfer, J., Krisp, C., Lyktey, N., Muller-Guhl, J., Zoratto, S., Allmaier, G., Jarrold, M. F., Munoz-Fontela, C., Schluter, H., & Uetrecht, C. (2020). N-terminal VP1 Truncations Favor *T = 1* Norovirus-Like Particles. *Vaccines (Basel)*, *9*(1). https://doi.org/10.3390/vaccines9010008

41. Cerqueira, C., Pang, Y. Y., Day, P. M., Thompson, C. D., Buck, C. B., Lowy, D. R., & Schiller, J. T. (2016). A Cell-Free Assembly System for Generating Infectious Human Papillomavirus 16

Capsids Implicates a Size Discrimination Mechanism for Preferential Viral Genome Packaging. *J Virol*, *90*(2), 1096-1107. https://doi.org/10.1128/JVI.02497-15

42. Kurokawa, N., Lavoie, P. O., D'Aoust, M. A., Couture, M. M., Dargis, M., Trepanier, S., Hoshino, S., Koike, T., Arai, M., & Tsutsui, N. (2021). Development and Characterization of a Plant-Derived Rotavirus-Like Particle Vaccine. *Vaccine*, *39*(35), 4979-4987. https://doi.org/10.1016/j.vaccine.2021.07.039

43. Shirbaghaee, Z., & Bolhassani, A. (2016). Different Applications of Virus-Like Particles in Biology and Medicine: Vaccination and Delivery Systems. *Biopolymers*, *105*(3), 113-132. https://doi.org/10.1002/bip.22759

44. Kim, H. J., & Kim, H. J. (2017). Yeast as an Expression System for Producing Virus-Like Particles: What Factors Do We Need to Consider? *Lett Appl Microbiol*, *64*(2), 111-123. https://doi.org/10.1111/lam.12695

45. Einstein, M. H., Baron, M., Levin, M. J., Chatterjee, A., Edwards, R. P., Zepp, F., Carletti, I., Dessy, F. J., Trofa, A. F., Schuind, A., Dubin, G., & Group, H. P. V. S. (2009). Comparison of the Immunogenicity and Safety of *Cervarix*™ and *Gardasil*® Human Papillomavirus (HPV) Cervical Cancer Vaccines in Healthy Women Aged 18-45 Years. *Hum Vaccin*, *5*(10), 705-719. https://doi.org/10.4161/hv.5.10.9518

46. Lacson, E., Teng, M., Ong, J., Vienneau, L., Ofsthun, N., & Lazarus, J. M. (2005). Antibody Response to Engerix-B® and Recombivax-HB® Hepatitis B Vaccination in End-Stage Renal Disease. *Hemodial Int*, *9*(4), 367-375. https://doi.org/10.1111/j.1492-7535.2005.01155.x

47. Fernandes, B., Vidigal, J., Correia, R., Carrondo, M. J. T., Alves, P. M., Teixeira, A. P., & Roldao, A. (2020). Adaptive Laboratory Evolution of Stable Insect Cell Lines for Improved HIV-Gag VLPs Production. *J Biotechnol*, *307*, 139-147. https://doi.org/10.1016/j.jbiotec.2019.10.004

48. Chen, Q., & Lai, H. (2013). Plant-Derived Virus-Like Particles as Vaccines. *Hum Vaccin Immunother*, *9*(1), 26-49. https://doi.org/10.4161/hv.22218

49. Moon, K. B., Jeon, J. H., Choi, H., Park, J. S., Park, S. J., Lee, H. J., Park, J. M., Cho, H. S., Moon, J. S., Oh, H., Kang, S., Mason, H. S., Kwon, S. Y., & Kim, H. S. (2022). Construction of SARS-CoV-2 Virus-Like Particles in Plant. *Sci Rep*, *12*(1), 1005. https://doi.org/10.1038/s41598-022-04883-y

50. Makarkov, A. I., Golizeh, M., Ruiz-Lancheros, E., Gopal, A. A., Costas-Cancelas, I. N., Chierzi, S., Pillet, S., Charland, N., Landry, N., Rouiller, I., Wiseman, P. W., Ndao, M., & Ward, B. J. (2019). Plant-Derived Virus-Like Particle Vaccines Drive Cross-Presentation of Influenza A Hemagglutinin Peptides by Human Monocyte-Derived Macrophages. *NPJ Vaccines*, *4*, 17. https://doi.org/10.1038/s41541-019-0111-y

51. Le, D. T., & Muller, K. M. (2021). *In Vitro* Assembly of Virus-Like Particles and Their Applications. *Life (Basel)*, *11*(4). https://doi.org/10.3390/life11040334

52. Mohsen, M. O., Gomes, A. C., Vogel, M., & Bachmann, M. F. (2018). Interaction of Viral Capsid-Derived Virus-Like Particles (VLPs) with the Innate Immune System. *Vaccines (Basel)*, *6*(3). https://doi.org/10.3390/vaccines6030037

53. Naskalska, A., & Pyrc, K. (2015). Virus Like Particles as Immunogens and Universal Nanocarriers. *Pol J Microbiol*, *64*(1), 3-13. https://www.ncbi.nlm.nih.gov/pubmed/26094310

54. Zhang, X., Wei, M., Pan, H., Lin, Z., Wang, K., Weng, Z., Zhu, Y., Xin, L., Zhang, J., Li, S., Xia, N., & Zhao, Q. (2014). Robust Manufacturing and Comprehensive Characterization of

Recombinant Hepatitis E Virus-Like Particles in Hecolin®. *Vaccine*, *32*(32), 4039-4050. https://doi.org/10.1016/j.vaccine.2014.05.064

55. Laurens, M. B. (2020). RTS,S/AS01 Vaccine (Mosquirix™): An Overview. *Hum Vaccin Immunother*, *16*(3), 480-489. https://doi.org/10.1080/21645515.2019.1669415

56. Beltran-Pavez, C., Bontjer, I., Gonzalez, N., Pernas, M., Merino-Mansilla, A., Olvera, A., Miro, J. M., Brander, C., Alcami, J., Sanders, R. W., Sanchez-Merino, V., & Yuste, E. (2022). Potent Induction of Envelope-Specific Antibody Responses by Virus-Like Particle Immunogens Based on HIV-1 Envelopes from Patients with Early Broadly Neutralizing Responses. *J Virol*, *96*(1), e0134321. https://doi.org/10.1128/JVI.01343-21

57. Fries, L. F., Smith, G. E., & Glenn, G. M. (2013). A Recombinant Viruslike Particle Influenza A (H7N9) Vaccine. *N Engl J Med*, *369*(26), 2564-2566. https://doi.org/10.1056/NEJMc1313186

58. Lu, J., Lu, G., Tan, S., Xia, J., Xiong, H., Yu, X., Qi, Q., Yu, X., Li, L., Yu, H., Xia, N., Zhang, T., Xu, Y., & Lin, J. (2020). A COVID-19 mRNA Vaccine Encoding SARS-CoV-2 Virus-Like Particles Induces a Strong Antiviral-Like Immune Response in Mice. *Cell Res*, *30*(10), 936-939. https://doi.org/10.1038/s41422-020-00392-7

59. Mohsen, M. O., Vogel, M., Riether, C., Muller, J., Salatino, S., Ternette, N., Gomes, A. C., Cabral-Miranda, G., El-Turabi, A., Ruedl, C., Kundig, T. M., Dermime, S., Knuth, A., Speiser, D. E., & Bachmann, M. F. (2019). Targeting Mutated Plus Germline Epitopes Confers Pre-clinical Efficacy of an Instantly Formulated Cancer Nano-Vaccine. *Front Immunol*, *10*, 1015. https://doi.org/10.3389/fimmu.2019.01015

60. Chackerian, B., Rangel, M., Hunter, Z., & Peabody, D. S. (2006). Virus and Virus-Like Particle-Based Immunogens for Alzheimer's Disease Induce Antibody Responses Against Amyloid-Beta Without Concomitant T Cell Responses. *Vaccine*, *24*(37-39), 6321-6331. https://doi.org/10.1016/j.vaccine.2006.05.059

61. Rohn, T. A., Jennings, G. T., Hernandez, M., Grest, P., Beck, M., Zou, Y., Kopf, M., & Bachmann, M. F. (2006). Vaccination Against IL-17 Suppresses Autoimmune Arthritis and Encephalomyelitis. *Eur J Immunol*, *36*(11), 2857-2867. https://doi.org/10.1002/eji.200636658

62. Chung, Y. H., Cai, H., & Steinmetz, N. F. (2020). Viral Nanoparticles for Drug Delivery, Imaging, Immunotherapy, and Theranostic Applications. *Adv Drug Deliv Rev*, *156*, 214-235. https://doi.org/10.1016/j.addr.2020.06.024

63. Van Kan-Davelaar, H. E., Van Hest, J. C., Cornelissen, J. J., & Koay, M. S. (2014). Using Viruses as Nanomedicines. *Br J Pharmacol*, *171*(17), 4001-4009. https://doi.org/10.1111/bph.12662

64. Thong, Q. X., Biabanikhankahdani, R., Ho, K. L., Alitheen, N. B., & Tan, W. S. (2019). Thermally-Responsive Virus-Like Particle for Targeted Delivery of Cancer Drug. *Sci Rep*, *9*(1), 3945. https://doi.org/10.1038/s41598-019-40388-x

65. Hamilton, J. R., Tsuchida, C. A., Nguyen, D. N., Shy, B. R., McGarrigle, E. R., Sandoval Espinoza, C. R., Carr, D., Blaeschke, F., Marson, A., & Doudna, J. A. (2021). Targeted Delivery of CRISPR-Cas9 and Transgenes Enables Complex Immune Cell Engineering. *Cell Rep*, *35*(9), 109207. https://doi.org/10.1016/j.celrep.2021.109207

66. Kato, T., Yui, M., Deo, V. K., & Park, E. Y. (2015). Development of *Rous sarcoma* Virus-Like Particles Displaying hCC49 scFv for Specific Targeted Drug Delivery to Human Colon Carcinoma Cells. *Pharm Res*, *32*(11), 3699-3707. https://doi.org/10.1007/s11095-015-1730-2

67. Banskota, S., Raguram, A., Suh, S., Du, S. W., Davis, J. R., Choi, E. H., Wang, X., Nielsen, S. C., Newby, G. A., Randolph, P. B., Osborn, M. J., Musunuru, K., Palczewski, K., & Liu, D. R.

(2022). Engineered Virus-Like Particles for Efficient *In Vivo* Delivery of Therapeutic Proteins. *Cell*, *185*(2), 250-265 e216. https://doi.org/10.1016/j.cell.2021.12.021

68. Chao, C. N., Yang, Y. H., Wu, M. S., Chou, M. C., Fang, C. Y., Lin, M. C., Tai, C. K., Shen, C. H., Chen, P. L., Chang, D., & Wang, M. (2018). Gene Therapy for Human Glioblastoma Using Neurotropic JC Virus-Like Particles as a Gene Delivery Vector. *Sci Rep*, *8*(1), 2213. https://doi.org/10.1038/s41598-018-19825-w

69. Pysz, M. A., Gambhir, S. S., & Willmann, J. K. (2010). Molecular Imaging: Current Status and Emerging Strategies. *Clin Radiol*, *65*(7), 500-516. https://doi.org/10.1016/j.crad.2010.03.011

70. Min, X., Zhang, J., Li, R. H., Xia, F., Cheng, S. Q., Li, M., Zhu, W., Zhou, W., Li, F., & Sun, Y. (2021). Encapsulation of NIR-II AIEgens in Virus-like Particles for Bioimaging. *ACS Appl Mater Interfaces*, *13*(15), 17372-17379. https://doi.org/10.1021/acsami.1c02691

71. Shen, L., Zhou, J., Wang, Y., Kang, N., Ke, X., Bi, S., & Ren, L. (2015). Efficient Encapsulation of Fe_3O_4 Nanoparticles into Genetically Engineered Hepatitis B Core Virus-Like Particles Through a Specific Interaction for Potential Bioapplications. *Small*, *11*(9-10), 1190-1196. https://doi.org/10.1002/smll.201401952

72. Pang, H. H., Chen, P. Y., Wei, K. C., Huang, C. W., Shiue, Y. L., Huang, C. Y., & Yang, H. W. (2019). Convection-Enhanced Delivery of a Virus-Like Nanotherapeutic Agent with Dual-Modal Imaging for Besiegement and Eradication of Brain Tumors. *Theranostics*, *9*(6), 1752-1763. https://doi.org/10.7150/thno.30977

73. Cervera, L., Gòdia, F., Tarrés-Freixas, F., Aguilar-Gurrieri, C., Carrillo, J., Blanco, J., & Gutiérrez-Granados, S. (2019). Production of HIV-1-Based Virus-Like Particles for Vaccination: Achievements and Limits. *Appl Microbiol Biotechnol*, *103*(18), 7367-7384. https://doi.org/10.1007/s00253-019-10038-3

74. Martins, S. A., Santos, J., Silva, R. D., Rosa, C., Cabo Verde, S., Galamba Correia, J. D., & Melo, R. (2022). How Promising Are HIV-1-Based Virus-Like Particles for Medical Applications? *Frontiers in Cellular and Infection Microbiology*, 1526. https://doi.org/10.3389/fcimb.2022.997875

75. Deeks, S. G., Overbaugh, J., Phillips, A., & Buchbinder, S. (2015). HIV Infection. *Nat Rev Dis Primers*, *1*, 15035. https://doi.org/10.1038/nrdp.2015.35

76. Engelman, A., & Cherepanov, P. (2012). The Structural Biology of HIV-1: Mechanistic and Therapeutic Insights. *Nat Rev Microbiol*, *10*(4), 279-290. https://doi.org/10.1038/nrmicro2747

77. Lavado-García, J., Jorge, I., Boix-Besora, A., Vázquez, J., Gòdia, F., & Cervera, L. (2021). Characterization of HIV-1 Virus-Like Particles and Determination of Gag Stoichiometry for Different Production Platforms. *Biotechnol Bioeng*, *118*(7), 2660-2675. https://doi.org/10.1002/bit.27786

78. Deml, L., Speth, C., Dierich, M. P., Wolf, H., & Wagner, R. (2005). Recombinant HIV-1 Pr55gag Virus-Like Particles: Potent Stimulators of Innate and Acquired Immune Responses. *Mol Immunol*, *42*(2), 259-277. https://doi.org/10.1016/j.molimm.2004.06.028

79. Visciano, M. L., Diomede, L., Tagliamonte, M., Tornesello, M. L., Asti, V., Bomsel, M., Buonaguro, F. M., Lopalco, L., & Buonaguro, L. (2011). Generation of HIV-1 Virus-Like Particles Expressing Different HIV-1 Glycoproteins. *Vaccine*, *29*(31), 4903-4912. https://doi.org/10.1016/j.vaccine.2011.05.005

80. González-Dominguez, I., Puente-Massaguer, E., Cervera, L., & Gòdia, F. (2020). Quantification of the HIV-1 Virus-Like Particle Production Process by Super-Resolution Imaging: From VLP

Budding to Nanoparticle Analysis. *Biotechnol Bioeng*, *117*(7), 1929-1945. https://doi.org/10.1002/bit.27345

81. Meng, B., & Lever, A. M. (2013). Wrapping Up the Bad News: HIV Assembly and Release. *Retrovirology*, *10*, 5. https://doi.org/10.1186/1742-4690-10-5

82. Olson, E. D., & Musier-Forsyth, K. (2019). Retroviral Gag Protein-RNA Interactions: Implications for Specific Genomic RNA Packaging and Virion Assembly. *Semin Cell Dev Biol*, *86*, 129-139. https://doi.org/10.1016/j.semcdb.2018.03.015

83. Valley-Omar, Z., Meyers, A. E., Shephard, E. G., Williamson, A. L., & Rybicki, E. P. (2011). Abrogation of Contaminating RNA Activity in HIV-1 Gag VLPs. *Virol J*, *8*, 462. https://doi.org/10.1186/1743-422X-8-462

84. Zhang, Y., Qian, H., Love, Z., & Barklis, E. (1998). Analysis of the Assembly Function of the Human Immunodeficiency Virus Type 1 Gag Protein Nucleocapsid Domain. *J Virol*, *72*(3), 1782-1789. https://doi.org/10.1128/JVI.72.3.1782-1789.1998

85. Tedbury, P. R., & Freed, E. O. (2014). The Role of Matrix in HIV-1 Envelope Glycoprotein Incorporation. *Trends Microbiol*, *22*(7), 372-378. https://doi.org/10.1016/j.tim.2014.04.012

86. Qi, M., Williams, J. A., Chu, H., Chen, X., Wang, J. J., Ding, L., Akhirome, E., Wen, X., Lapierre, L. A., Goldenring, J. R., & Spearman, P. (2013). Rab11-FIP1C and Rab14 Direct Plasma Membrane Sorting and Particle Incorporation of the HIV-1 Envelope Glycoprotein Complex. *PLoS Pathog*, *9*(4), e1003278. https://doi.org/10.1371/journal.ppat.1003278

87. Lavado-Garcia, J., Zhang, T., Cervera, L., Godia, F., & Wuhrer, M. (2022). Differential *N*- and *O*-Glycosylation Signatures of HIV-1 Gag Virus-Like Particles and Coproduced Extracellular Vesicles. *Biotechnol Bioeng*, *119*(5), 1207-1221. https://doi.org/10.1002/bit.28051

88. Lancaster, C., Pristatsky, P., Hoang, V. M., Casimiro, D. R., Schwartz, R. M., Rustandi, R., & Ha, S. (2016). Characterization of N-glycosylation Profiles from Mammalian and Insect Cell Derived Chikungunya VLP. *J Chromatogr B Analyt Technol Biomed Life Sci*, *1032*, 218-223. https://doi.org/10.1016/j.jchromb.2016.04.025

89. Lavado-Garcia, J., Diaz-Maneh, A., Canal-Pauli, N., Perez-Rubio, P., Godia, F., & Cervera, L. (2021). Metabolic Engineering of HEK293 Cells to Improve Transient Transfection and Cell Budding of HIV-1 Virus-Like Particles. *Biotechnol Bioeng*, *118*(4), 1649-1663. https://doi.org/10.1002/bit.27679

90. Fuenmayor, J., Cervera, L., Rigau, C., & Godia, F. (2018). Enhancement of HIV-1 VLP Production Using Gene Inhibition Strategies. *Appl Microbiol Biotechnol*, *102*(10), 4477-4487. https://doi.org/10.1007/s00253-018-8930-8

91. Gutiérrez-Granados, S., Cervera, L., Segura Mde, L., Wölfel, J., & Gòdia, F. (2016). Optimized Production of HIV-1 Virus-Like Particles by Transient Transfection in CAP-T Cells. *Appl Microbiol Biotechnol*, *100*(9), 3935-3947. https://doi.org/10.1007/s00253-015-7213-x

92. Gutiérrez-Granados, S., Farràs, Q., Hein, K., Fuenmayor, J., Félez, P., Segura, M., & Gòdia, F. (2017). Production of HIV Virus-Like Particles by Transient Transfection of CAP-T Cells at Bioreactor Scale Avoiding Medium Replacement. *J Biotechnol*, *263*, 11-20. https://doi.org/10.1016/j.jbiotec.2017.09.019

93. Cervera, L., Gutierrez-Granados, S., Martinez, M., Blanco, J., Godia, F., & Segura, M. M. (2013). Generation of HIV-1 Gag VLPs by Transient Transfection of HEK 293 Suspension Cell Cultures Using an Optimized Animal-Derived Component Free Medium. *J Biotechnol*, *166*(4), 152-165. https://doi.org/10.1016/j.jbiotec.2013.05.001

94. Boix-Besora, A., Lorenzo, E., Lavado-Garcia, J., Godia, F., & Cervera, L. (2022). Optimization, Production, Purification and Characterization of HIV-1 GAG-Based Virus-like Particles Functionalized with SARS-CoV-2. *Vaccines (Basel)*, *10*(2). https://doi.org/10.3390/vaccines10020250

95. Chojnacki, J., Staudt, T., Glass, B., Bingen, P., Engelhardt, J., Anders, M., Schneider, J., Muller, B., Hell, S. W., & Krausslich, H. G. (2012). Maturation-Dependent HIV-1 Surface Protein Redistribution Revealed by Fluorescence Nanoscopy. *Science*, *338*(6106), 524-528. https://doi.org/10.1126/science.1226359

96. Steppert, P., Burgstaller, D., Klausberger, M., Berger, E., Aguilar, P. P., Schneider, T. A., Kramberger, P., Tover, A., Nobauer, K., Razzazi-Fazeli, E., & Jungbauer, A. (2016). Purification of HIV-1 Gag Virus-Like Particles and Separation of Other Extracellular Particles. *J Chromatogr A*, *1455*, 93-101. https://doi.org/10.1016/j.chroma.2016.05.053

97. Chen, C. W., Saubi, N., & Joseph-Munne, J. (2020). Design Concepts of Virus-Like Particle-Based HIV-1 Vaccines. *Front Immunol*, *11*, 573157. https://doi.org/10.3389/fimmu.2020.573157

98. Hargrave, A., Mustafa, A. S., Hanif, A., Tunio, J. H., & Hanif, S. N. M. (2021). Current Status of HIV-1 Vaccines. *Vaccines (Basel)*, *9*(9). https://doi.org/10.3390/vaccines9091026

99. Weber, J., Cheinsong-Popov, R., Callow, D., Adams, S., Patou, G., Hodgkin, K., Martin, S., Gotch, F., & Kingsman, A. (1995). Immunogenicity of the Yeast Recombinant p17/p24:Ty Virus-Like Particles (p24-VLP) in Healthy Volunteers. *Vaccine*, *13*(9), 831-834. https://doi.org/10.1016/0264-410x(94)00061-q

100. Veenstra, J., Williams, I. G., Colebunders, R., Dorrell, L., Tchamouroff, S. E., Patou, G., Lange, J. M., Weller, I. V., Goeman, J., Uthayakumar, S., Gow, I. R., Weber, J. N., & Coutinho, R. A. (1996). Immunization with Recombinant p17/p24:Ty Virus-Like Particles in Human Immunodeficiency Virus-Infected Persons. *J Infect Dis*, *174*(4), 862-866. https://doi.org/10.1093/infdis/174.4.862

101. Tagliamonte, M., Visciano, M. L., Tornesello, M. L., De Stradis, A., Buonaguro, F. M., & Buonaguro, L. (2010). Constitutive Expression of HIV-VLPs in Stably Transfected Insect Cell Line for Efficient Delivery System. *Vaccine*, *28*(39), 6417-6424. https://doi.org/10.1016/j.vaccine.2010.07.054

102. Franco, D., Liu, W., Gardiner, D. F., Hahn, B. H., & Ho, D. D. (2011). CD40L-Containing Virus-Like Particle as a Candidate HIV-1 Vaccine Targeting Dendritic Cells. *J Acquir Immune Defic Syndr*, *56*(5), 393-400. https://doi.org/10.1097/QAI.0b013e31820b844e

103. Ao, Z., Wang, L., Mendoza, E. J., Cheng, K., Zhu, W., Cohen, E. A., Fowke, K., Qiu, X., Kobinger, G., & Yao, X. (2019). Incorporation of Ebola Glycoprotein into HIV Particles Facilitates Dendritic Cell and Macrophage Targeting and Enhances HIV-Specific Immune Responses. *PLoS ONE*, *14*(5), e0216949. https://doi.org/10.1371/journal.pone.0216949

104. Chua, A. J., Vituret, C., Tan, M. L., Gonzalez, G., Boulanger, P., Ng, M. L., & Hong, S. S. (2013). A Novel Platform for Virus-Like Particle-Display of Flaviviral Envelope Domain III: Induction of Dengue and West Nile Virus Neutralizing Antibodies. *Virol J*, *10*, 129. https://doi.org/10.1186/1743-422X-10-129

105. Venereo-Sanchez, A., Gilbert, R., Simoneau, M., Caron, A., Chahal, P., Chen, W., Ansorge, S., Li, X., Henry, O., & Kamen, A. (2016). Hemagglutinin and Neuraminidase Containing Virus-Like Particles Produced in HEK-293 Suspension Culture: An Effective Influenza Vaccine Candidate. *Vaccine*, *34*(29), 3371-3380. https://doi.org/10.1016/j.vaccine.2016.04.089

106. Fontana, D., Garay, E., Cervera, L., Kratje, R., Prieto, C., & Godia, F. (2021). Chimeric VLPs Based on HIV-1 Gag and a Fusion Rabies Glycoprotein Induce Specific Antibodies against Rabies and Foot-and-Mouth Disease Virus. *Vaccines (Basel)*, *9*(3). https://doi.org/10.3390/vaccines9030251

107. Lambricht, L., Vanvarenberg, K., De Beuckelaer, A., Van Hoecke, L., Grooten, J., Ucakar, B., Lipnik, P., Sanders, N. N., Lienenklaus, S., Preat, V., & Vandermeulen, G. (2016). Coadministration of a Plasmid Encoding HIV-1 Gag Enhances the Efficacy of Cancer DNA Vaccines. *Mol Ther*, *24*(9), 1686-1696. https://doi.org/10.1038/mt.2016.122

108. Robert, M. A., Lytvyn, V., Deforet, F., Gilbert, R., & Gaillet, B. (2017). Virus-Like Particles Derived from HIV-1 for Delivery of Nuclear Proteins: Improvement of Production and Activity by Protein Engineering. *Mol Biotechnol*, *59*(1), 9-23. https://doi.org/10.1007/s12033-016-9987-1

109. Indikova, I., & Indik, S. (2020). Highly Efficient 'Hit-and-Run' Genome Editing with Unconcentrated Lentivectors Carrying Vpr.Prot.Cas9 Protein Produced from RRE-Containing Transcripts. *Nucleic Acids Res*, *48*(14), 8178-8187. https://doi.org/10.1093/nar/gkaa561

110. Lyu, P., Javidi-Parsijani, P., Atala, A., & Lu, B. (2019). Delivering Cas9/sgRNA Ribonucleoprotein (RNP) by Lentiviral Capsid-Based Bionanoparticles for Efficient 'Hit-and-Run' Genome Editing. *Nucleic Acids Res*, *47*(17), e99. https://doi.org/10.1093/nar/gkz605

111. Iqbal, N., & Iqbal, N. (2014). Human Epidermal Growth Factor Receptor 2 (HER2) in Cancers: Overexpression and Therapeutic Implications. *Mol Biol Int*, *2014*, 852748. https://doi.org/10.1155/2014/852748

112. Wang, J., & Xu, B. (2019). Targeted Therapeutic Options and Future Perspectives for HER2-Positive Breast Cancer. *Signal Transduct Target Ther*, *4*, 34. https://doi.org/10.1038/s41392-019-0069-2

113. Montemurro, F., Di Cosimo, S., & Arpino, G. (2013). Human Epidermal Growth Factor Receptor 2 (HER2)-Positive and Hormone Receptor-Positive Breast Cancer: New Insights Into Molecular Interactions and Clinical Implications. *Ann Oncol*, *24*(11), 2715-2724. https://doi.org/10.1093/annonc/mdt287

114. Boku, N. (2014). HER2-Positive Gastric Cancer. *Gastric Cancer*, *17*(1), 1-12. https://doi.org/10.1007/s10120-013-0252-z

115. Zhao, D., Klempner, S. J., & Chao, J. (2019). Progress and Challenges in HER2-Positive Gastroesophageal Adenocarcinoma. *J Hematol Oncol*, *12*(1), 50. https://doi.org/10.1186/s13045-019-0737-2

116. Diver, E. J., Foster, R., Rueda, B. R., & Growdon, W. B. (2015). The Therapeutic Challenge of Targeting HER2 in Endometrial Cancer. *Oncologist*, *20*(9), 1058-1068. https://doi.org/10.1634/theoncologist.2015-0149

117. Tai, W., Mahato, R., & Cheng, K. (2010). The Role of HER2 in Cancer Therapy and Targeted Drug Delivery. *J Control Release*, *146*(3), 264-275. https://doi.org/10.1016/j.jconrel.2010.04.009

118. Xu, B., Yan, M., Ma, F., Hu, X., Feng, J., Ouyang, Q., Tong, Z., Li, H., Zhang, Q., Sun, T., Wang, X., Yin, Y., Cheng, Y., Li, W., Gu, Y., Chen, Q., Liu, J., Cheng, J., Geng, C., . . . Investigators, P. (2021). Pyrotinib Plus Capecitabine Versus Lapatinib Plus Capecitabine for the Treatment of HER2-Positive Metastatic Breast Cancer (PHOEBE): A Multicentre, Open-Label, Randomised, Controlled, Phase 3 Trial. *Lancet Oncol*, *22*(3), 351-360. https://doi.org/10.1016/S1470-2045(20)30702-6

119. Yan, M., Ouyang, Q., Sun, T., Niu, L., Yang, J., Li, L., Song, Y., Hao, C., Chen, Z., Orlandi, A., Ishii, N., Takabe, K., Franceschini, G., Ricci, F., Verschraegen, C., Liu, Z., Zhang, M., Lv, H., Liu, L., . . . Zhang, G. (2022). Pyrotinib Plus Capecitabine for Patients with Human Epidermal Growth Factor Receptor 2-Positive Breast Cancer and Brain Metastases (PERMEATE): A Multicentre, Single-Arm, Two-Cohort, Phase 2 Trial. *Lancet Oncol*, *23*(3), 353-361. https://doi.org/10.1016/S1470-2045(21)00716-6

120. Crivianu-Gaita, V., & Thompson, M. (2016). Aptamers, Antibody scFv, and Antibody Fab' Fragments: An Overview and Comparison of Three of the Most Versatile Biosensor Biorecognition Elements. *Biosens Bioelectron*, *85*, 32-45. https://doi.org/10.1016/j.bios.2016.04.091

121. Bates, A., & Power, C. A. (2019). David vs. Goliath: The Structure, Function, and Clinical Prospects of Antibody Fragments. *Antibodies (Basel)*, *8*(2). https://doi.org/10.3390/antib8020028

122. Santos, J., Cardoso, M., Moreira, I. S., Goncalves, J., Correia, J. D. G., Verde, S. C., & Melo, R. (2021). Integrated In Silico and Experimental Approach Towards the Design of A Novel Recombinant Protein Containing an Anti-HER2 scFv. *Int J Mol Sci*, *22*(7). https://doi.org/10.3390/ijms22073547

123. Schneider, C. A., Rasband, W. S., & Eliceiri, K. W. (2012). NIH Image to ImageJ: 25 Years of Image Analysis. *Nat Methods*, *9*(7), 671-675. https://doi.org/10.1038/nmeth.2089

124. Lin, Y. C., Boone, M., Meuris, L., Lemmens, I., Van Roy, N., Soete, A., Reumers, J., Moisse, M., Plaisance, S., Drmanac, R., Chen, J., Speleman, F., Lambrechts, D., Van de Peer, Y., Tavernier, J., & Callewaert, N. (2014). Genome Dynamics of the Human Embryonic Kidney 293 Lineage in Response to Cell Biology Manipulations. *Nat Commun*, *5*, 4767. https://doi.org/10.1038/ncomms5767

125. Liao, W. H., Huang, K. J., Chang, Y. F., Wang, S. M., Tseng, Y. T., Chiang, C. C., Wang, J. J., & Wang, C. T. (2007). Incorporation of Human Immunodeficiency Virus Type 1 Reverse Transcriptase into Virus-Like Particles. *J Virol*, *81*(10), 5155-5165. https://doi.org/10.1128/JVI.01796-06

126. Gonzalez-Dominguez, I., Puente-Massaguer, E., Cervera, L., & Godia, F. (2020). Quality Assessment of Virus-Like Particles at Single Particle Level: A Comparative Study. *Viruses*, *12*(2). https://doi.org/10.3390/v12020223

127. Dokland, T. (2009). Back to the Basics: The Fundamentals of Cryo-Electron Microscopy. *Microscopy and Microanalysis*, *15*(S2), 1538-1539.

128. Hanne, J., Zila, V., Heilemann, M., Muller, B., & Krausslich, H. G. (2016). Super-Resolved Insights into Human Immunodeficiency Virus Biology. *FEBS Lett*, *590*(13), 1858-1876. https://doi.org/10.1002/1873-3468.12186

129. Berridge, M. V., Herst, P. M., & Tan, A. S. (2005). Tetrazolium Dyes as Tools in Cell Biology: New Insights Into Their Cellular Reduction. *Biotechnol Annu Rev*, *11*, 127-152. https://doi.org/10.1016/S1387-2656(05)11004-7

130. Chavez, K. J., Garimella, S. V., & Lipkowitz, S. (2010). Triple Negative Breast Cancer Cell Lines: One Tool in the Search for Better Treatment of Triple Negative Breast Cancer. *Breast Dis*, *32*(1-2), 35-48. https://doi.org/10.3233/BD-2010-0307

131. Brockhoff, G., Heckel, B., Schmidt-Bruecken, E., Plander, M., Hofstaedter, F., Vollmann, A., & Diermeier, S. (2007). Differential Impact of Cetuximab, Pertuzumab and Trastuzumab on BT474 and SK-BR-3 Breast Cancer Cell Proliferation. *Cell Prolif*, *40*(4), 488-507. https://doi.org/10.1111/j.1365-2184.2007.00449.x

132. Merck. (2022). *Amicon® Devices*. Retrieved September 14, 2022 from https://www.sigmaaldrich.com/PT/en/products/protein-biology/protein-sample-prep/amicon-centrifugals

133. Merck. (2022). *Virus Concentration by Ultrafiltration*. Retrieved September 14, 2022 from https://www.sigmaaldrich.com/PT/en/technical-documents/technical-article/analytical-chemistry/filtration/viral-concentration-amicon-ultrafiltration

134. Desjardins, P., & Conklin, D. (2010). NanoDrop Microvolume Quantitation of Nucleic Acids. *J Vis Exp*(45). https://doi.org/10.3791/2565

135. Schembri, L., Dalibart, R., Tomasello, F., Legembre, P., Ichas, F., & De Giorgi, F. (2007). The HA Tag is Cleaved and Loses Immunoreactivity During Apoptosis. *Nat Methods*, *4*(2), 107-108. https://doi.org/10.1038/nmeth0207-107

136. Tao-Cheng, J. H., Crocker, V., Moreira, S. L., & Azzam, R. (2021). Optimization of Protocols for Pre-Embedding Immunogold Electron Microscopy of Neurons in Cell Cultures and Brains. *Mol Brain*, *14*(1), 86. https://doi.org/10.1186/s13041-021-00799-2

137. Information, N. C. f. B. (2022). *PubChem Element Summary for AtomicNumber 43, Technetium*. Retrieved October 8, 2022 from https://pubchem.ncbi.nlm.nih.gov/element/Technetium

138. Kane, S. M., & Davis, D. D. (2022). Technetium-99m. In *StatPearls*. https://www.ncbi.nlm.nih.gov/pubmed/32644439

139. Papagiannopoulou, D. (2017). Technetium-99m Radiochemistry for Pharmaceutical Applications. *J Labelled Comp Radiopharm*, *60*(11), 502-520. https://doi.org/10.1002/jlcr.3531

140. Capogni, M., Pietropaolo, A., Quintieri, L., Angelone, M., Boschi, A., Capone, M., Cherubini, N., De Felice, P., Dodaro, A., Duatti, A., Fazio, A., Loreti, S., Martini, P., Pagano, G., Pasquali, M., Pillon, M., Uccelli, L., & Pizzuto, A. (2018). 14 MeV Neutrons for (99)Mo/(99m)Tc Production: Experiments, Simulations and Perspectives. *Molecules*, *23*(8). https://doi.org/10.3390/molecules23081872

141. Lipowska, M., He, H., Malveaux, E., Xu, X., Marzilli, L. G., & Taylor, A. (2006). First Evaluation of a ^{99m}Tc-Tricarbonyl Complex, $^{99m}Tc(CO)_3$(LAN), as a New Renal Radiopharmaceutical in Humans. *J Nucl Med*, *47*(6), 1032-1040. https://www.ncbi.nlm.nih.gov/pubmed/16741314

142. Badar, A., Williams, J., de Rosales, R. T., Tavare, R., Kampmeier, F., Blower, P. J., & Mullen, G. E. (2014). Optimising the Radiolabelling Properties of Technetium Tricarbonyl and His-Tagged Proteins. *EJNMMI Res*, *4*(1), 14. https://doi.org/10.1186/2191-219X-4-14

143. Waibel, R., Alberto, R., Willuda, J., Finnern, R., Schibli, R., Stichelberger, A., Egli, A., Abram, U., Mach, J. P., Pluckthun, A., & Schubiger, P. A. (1999). Stable One-Step Technetium-99m Labeling of His-Tagged Recombinant Proteins with a Novel Tc(I)-Carbonyl Complex. *Nat Biotechnol*, *17*(9), 897-901. https://doi.org/10.1038/12890

144. Tait, J. F., Smith, C., & Gibson, D. F. (2002). Development of Annexin V Mutants Suitable for Labeling with Tc(I)-Carbonyl Complex. *Bioconjug Chem*, *13*(5), 1119-1123. https://doi.org/10.1021/bc025545s

A

APPENDIX

A.1 Plasmid Maps

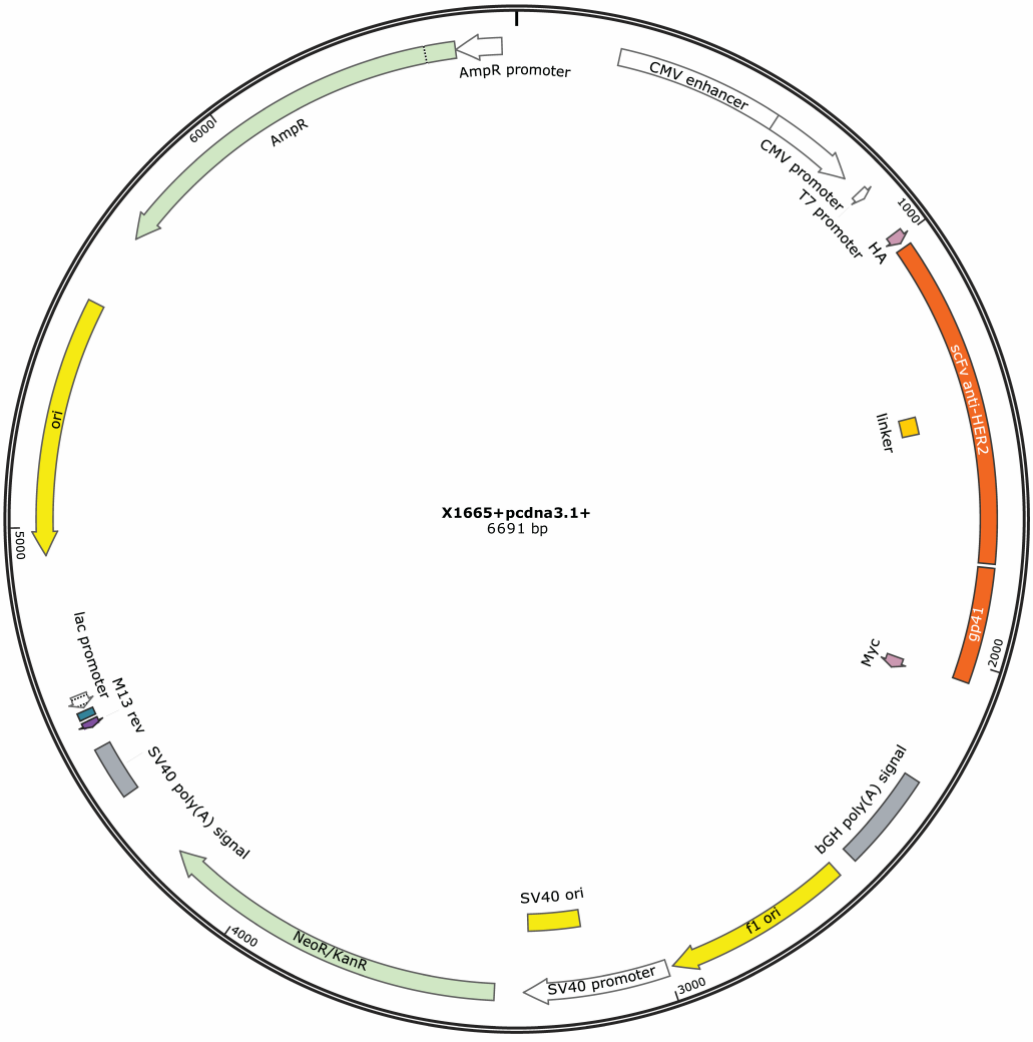

Figure A.1 – Plasmid map of X1665+pcDNA3.1+.

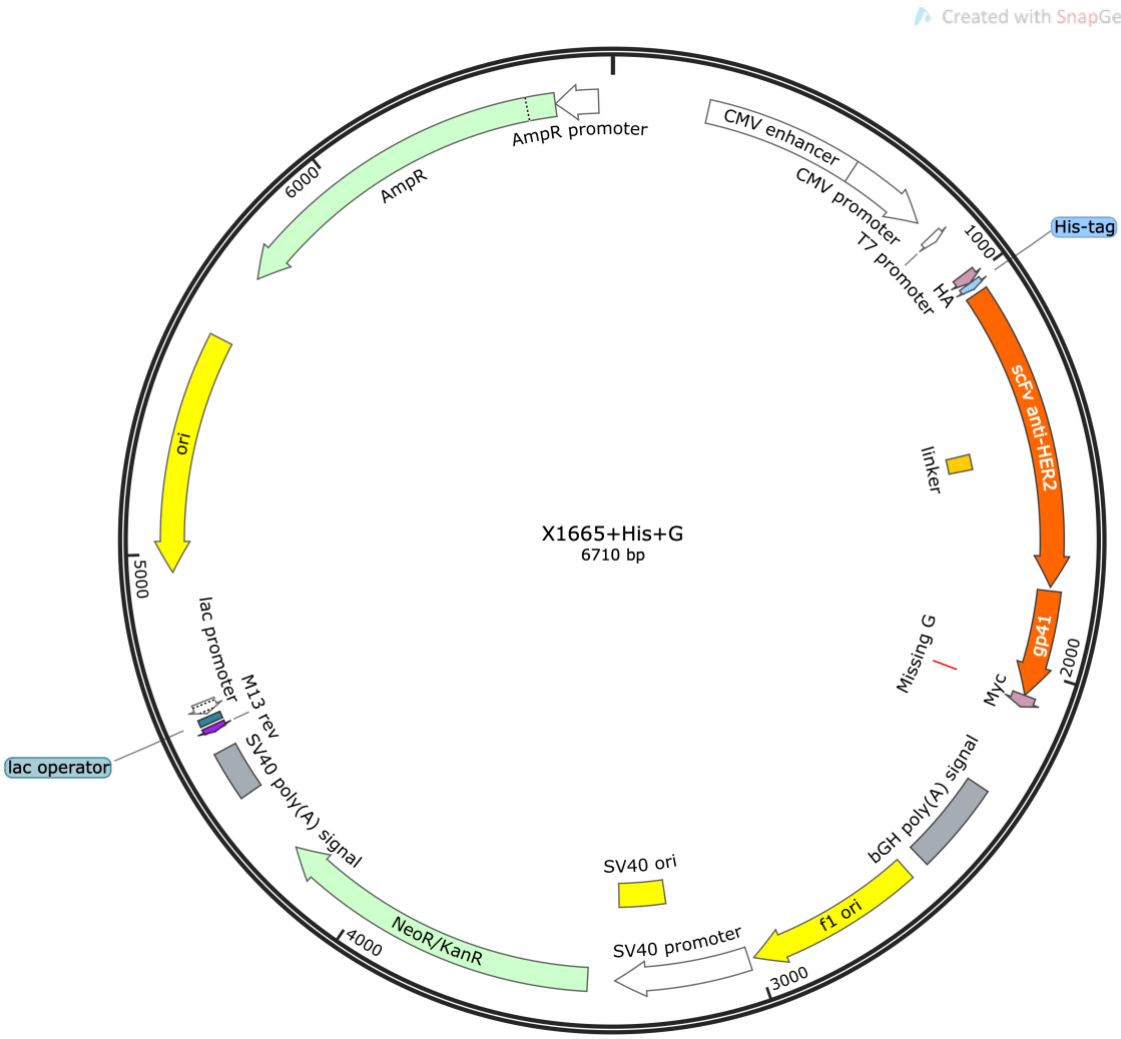

Figure A.2 – Plasmid map of X1665+His+G.

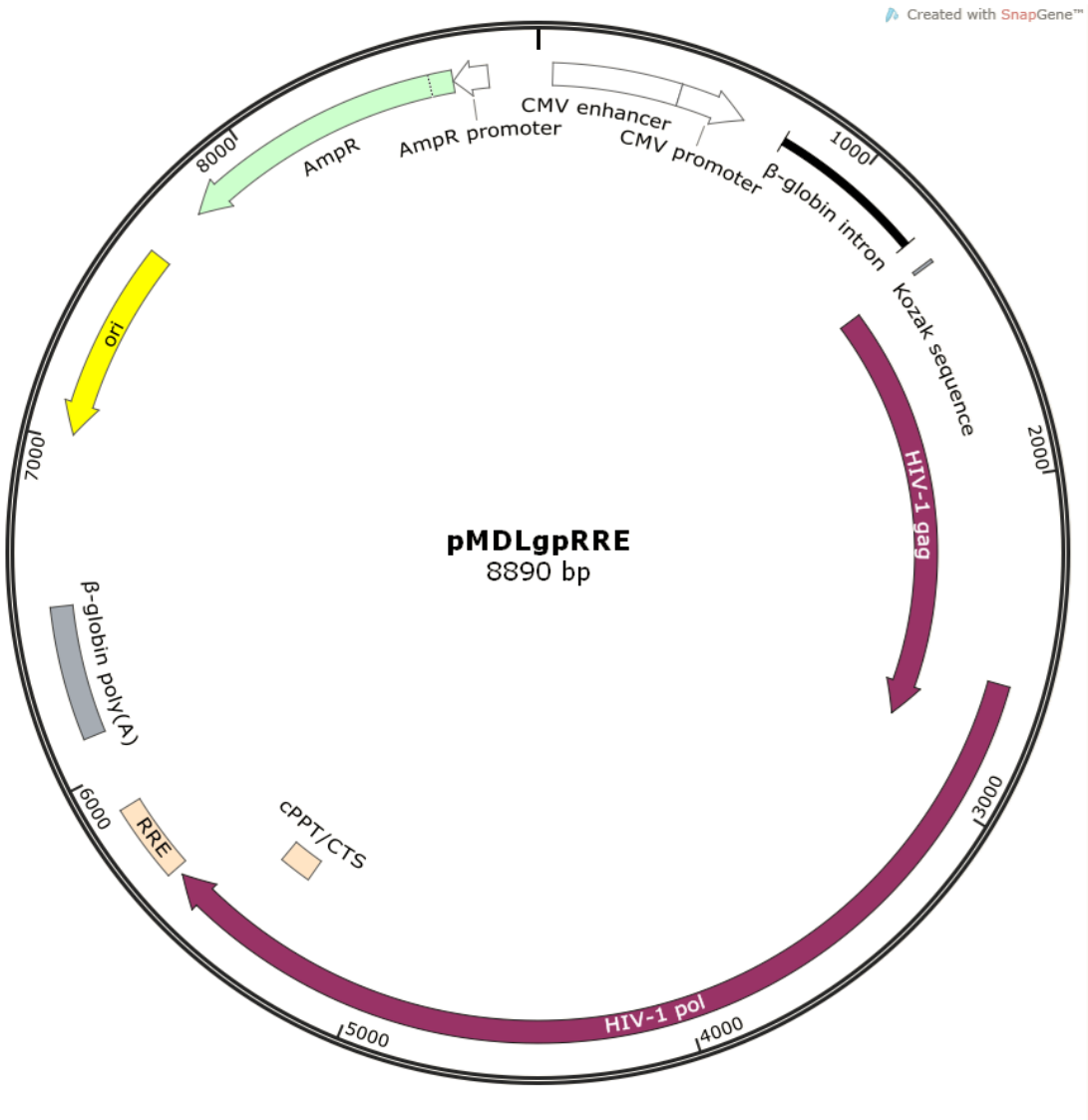

Figure A.3 – Plasmid map of pMDLg/pRRE.

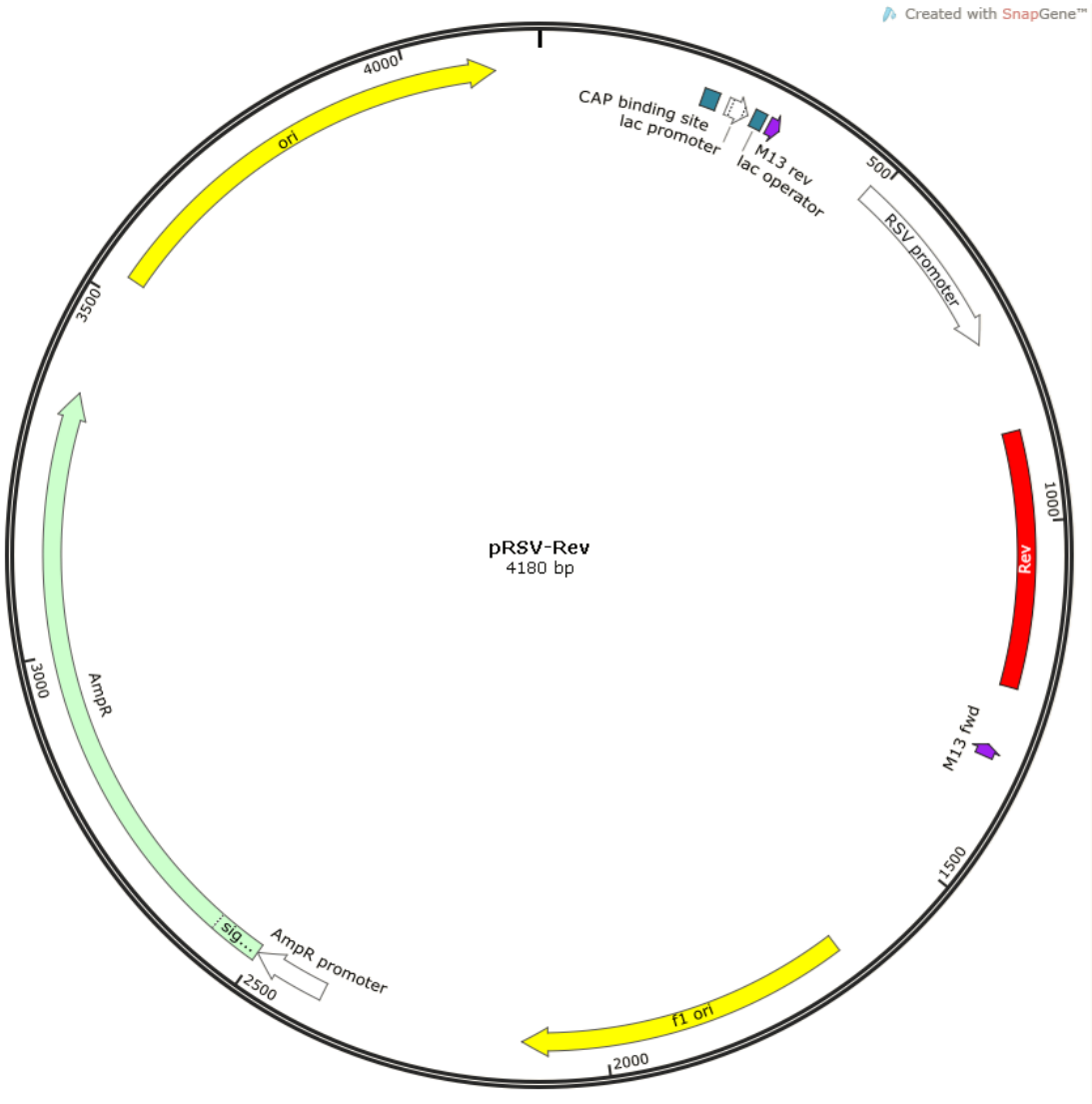

Figure A.4 – Plasmid map of pRSV-REV.